Model-Based Validation of Fuel Cell Hybrid Vehicle Control Systems

By

Erik Wilhelm

A thesis
presented to the University of Waterloo
in fulfillment of the
thesis requirement for the degree of
Master of Applied Science
in
Chemical Engineering

Waterloo, Ontario, Canada, 2007

I hereby declare that I am the sole author of this thesis. This is a true copy of the thesis, including any required final revisions, as accepted by my examiners.

I understand that my thesis may be made electronically available to the public.

Abstract

Hydrogen fuel cell technology has emerged as an efficient and clean alternative to internal combustion engines for powering vehicles, and hydrogen powertrains will aid in addressing key environmental issues such as urban air quality and global warming. This work demonstrates the effectiveness of a ‘hardware-in-loop’ (HIL) simulation system for validating the safety and effectiveness of control algorithms for a hydrogen fuel cell hybrid passenger vehicle.

A significant amount of the work completed in conjunction with the thesis topic was the design and construction of the fuel cell vehicle for competition. Producing a ‘rolling test bench’ that generates data to be used to create HIL simulation models required nearly two years of work before an acceptable level of reliability was reached to produce usable data. Some detail will be given in this thesis regarding the infrastructure modifications required to safely build a hydrogen fuel cell vehicle, as well as the design challenges faced in the integration of a fuel cell power module, two electric drive motors, a nickel metal hydride battery, and required power electronics into a small sport utility vehicle originally designed for an internal combustion powertrain.

The virtual control validation performed involved designing dynamic models of the systems of interest and performing real-time simulation to ensure that the appropriate controller response is observed. For this thesis, emphasis was placed on several key vehicle control topics. Communication robustness was evaluated to ensure that the complicated vehicle communication network could effectively handle traffic from the six powertrain sub-controllers. Safety algorithms were tested for appropriate response to fault conditions. Control systems were developed and tuned offline reducing the amount of time required for in-vehicle development and testing. Software-in-the-loop simulation was used to check initial code integrity and to validate the hardware-in-the-loop vehicle models. The methodology presented in this work was found to be sufficient for a thorough safety and rationality evaluation of control strategies for hybrid fuel cell vehicles.

Acknowledgements

I would like to thank Dr. M.W. Fowler for his kind and generous support, his confidence in my ability, and for the patience that he showed as my faculty advisor during the process of writing this thesis. He encouraged my development in innumerable ways and I will always be grateful.

I would also like to acknowledge the mentoring and assistance that Dr. R.A. Fraser, the faculty advisor for the Alternative Fuels Team, provided during this work and throughout the ChallengeX project. His insight and experience is the foundation upon which all of the UWAFT advanced vehicle developments rested.

The University of Waterloo Alternative Fuels Team is an interesting, dedicated, and motivated group of people. We had some fun, we learned a great deal, and we got the job done. Christin Strong was always there for me during the good times and the bad, and does a great job wiring vehicles. Mike ‘Wally’ Wahlstrom and I were co-leaders of this boat, and it was a privilege to work with someone so talented. Chris Lawrence set an incredible example for being able to work effectively on two hours of sleep. Matt Stevens was a great source of inspiration and a co-leader of the UWAFT T-bone sub-team. Sumit Kundu brought perspective to this work and, as the ‘godfather’ of the green energy group, had to deal with UWAFT absconding with his lab equipment. Ryan Huizing made it ok to stay late because he was always there from sunset until sunrise anyway. Jeff Gostick (with Sumit’s help) made a great thing happen on the hydrogen system, and installed the best-looking exhaust tip at competition on our vehicle. Charles Hua, the new co-leader of the team, picked up a lot of responsibility and bore it with grace. Filip Spacek made the Bluetooth/CAN device code work, and made sure I made it to the Duke. And for that I am infinitely grateful.

The National Science and Engineering Research Council of Canada supported this work financially through the PGS-M scholarship program. I am very grateful for the funding that enabled me to perform this work and to help design and build a fuel cell Equinox.

Dedication

This work is dedicated to my parents, Diane and Jim, and to my brother Roland. My family prepared me for these years of work and gave me the ability to persevere through difficult moments.

Table of Contents

List of Tables

List of Figures

Nomenclature and Abbreviations

UWAFT: University of Waterloo Alternative Fuels Team

HIL: Hardware-in-the-loop

SIL: Software-in-the-loop

PEM: Polymer electrolyte membrane

kW: Kilowatt

A: Ampere

V: Volt. Also depicted as E.

kph: kilometers per hour

CAD: Canadian dollars

°C: degree Celcius

Psi: pounds per square inch

NiMH: nickel metal hydride

SMR: steam methane reforming

FCPM: fuel cell power module

MEA: membrane electrolyte assembly

Ω: ohm

ECU: Engine control unit

CAN: controller area network

ms: millisecond

I/O: input / output

ABS: anti-lock braking

GM: General Motors

PSAT: Powertrain systems analysis toolkit

Nm: Newton-meter

Ah: Amp-hour

DC: direct current

AC: alternating current

BCM: body control module

slpm: standard liter per minute

SIT: simulation interface toolkit

RPM: revolutions per minute

PWM: pulse width modulation

TCS: torque control strategy

HCS: hybrid control strategy

TPS: throttle position sensor

MCU: motor control unit

RMS: root mean squared

SOC: state of charge

DFMEA: design failure modes and effects analysis

GUI: graphical user interface

Chapter 1: Introduction

1.1 Problem Statement

The environmental and economic motivation to reduce greenhouse gas emission and energy use in transportation has resulted in the introduction of fuel cells as an alternative to internal combustion propulsion, and thereby caused an increase in vehicle powertrain complexity.

To ensure that the control hardware and algorithms for a complex fuel cell hybrid vehicle respond safely and as-intended, extensive off-line testing must be performed before the control systems are implemented on the road.

1.2 Objectives

This work outlines the development of “hardware-in-the-loop” (HIL) and “software-in-the-loop” (SIL) controls validation methodologies for an advanced fuel cell / battery hybrid vehicle powertrain. The work was performed in parallel with the design and construction of a fuel cell hybrid Chevrolet Equinox which was the target of the control system simulation.

A challenge specific to the Waterloo vehicle development team was based on an inherent limitation of current fuel cell powered vehicles. The fuel cell technology used for the Equinox cannot be operated in temperatures below 10°C, which resulted in a significantly reduced development and testing window relative to teams located in more temperate regions of North America. By basing a significant portion of the vehicle control development on software-in-the-loop and hardware-in-the-loop techniques outlined in this thesis, the development and refinement of control algorithms was able to take place year round. Additionally, this thesis demonstrates how SIL and HIL techniques can be applied to offer significant time reduction in development by allowing for the rapid establishment and execution of tests. Finally, with an expensive powertrain technology such as a fuel cell power module, it is prudent to ensure that the controller will be able to safely operate the vehicle before the algorithms are loaded and the key is turned. The intent of this work is to advance the field of real time vehicle simulation and hardware-in-the-loop controller validation as a design engineering tool.

1.3 Problem Background

Transportation technology has captured the global imagination and has been the subject of intense research and development for the past century and a half. Throughout the history of powered transportation, society has sought out higher performance, increased comfort, and additional functions for their passenger vehicles. It is a critical point in civilization's history where consideration must now not only be made for vehicle performance, but must now also for how traveling impacts the environment. The threat that our near-exclusive use of fossil fuels for transportation energy poses to the environment is considerable. The fact that the combustion of fossil fuels has caused a significant increase in atmospheric greenhouse gas concentration and that this increase due to human activity has had a warming effect on our climate is widely accepted in the scientific community [1]. The detrimental effects that global warming will have on the global ecosystem and economy have been extensively modeled and are predicted to be severe, including increased tropical storms, droughts, and floods [2]. Poor air quality in urban areas caused by vehicle emissions has a significant negative impact on human health [3]. In addition to the negative effects that fossil fuel use in transportation has on the environment, the dependence on energy from foreign sources has destabilized political relations between nations leading to wars and famine. The 20th century's adoption of oil as a transportation energy source was due in most part to its ease of extraction and use. The short-term simplicity of burning oil to provide power for transportation has, however, created the above-mentioned long-term problems which must be addressed [3].

While there are at least three viable alternative fuels competing to replace petroleum for transportation energy, hydrogen shows the most promise. It also presents the greatest challenges as a new energy carrier, when compared with liquid alternative fuels such as ethanol or biodiesel. There are many uncertainties surrounding hydrogen as a fuel, such the current lack of adequate production and distribution infrastructure, the difficulty of safe storage in vehicles at suitable energy densities, and the high cost per kilowatt of fuel cell power systems. The large initial capital outlay to finance the construction of a vehicle fueling infrastructure is one of the major impediments to the adoption of hydrogen as a fuel. Without stations which offer hydrogen fuel, consumers are reluctant to purchase fuel cell vehicles. Without a consumer market for hydrogen-powered vehicles, energy companies are reluctant to build stations.   On-board storage density has been improving for hydrogen, but it is still far from where it needs to be to offer drivers the range that they can enjoy from liquid fuels. Figure 1 highlights the current state of hydrogen storage and the improvements needed in order for it to become competitive without requiring consumers to change their driving habits [5].

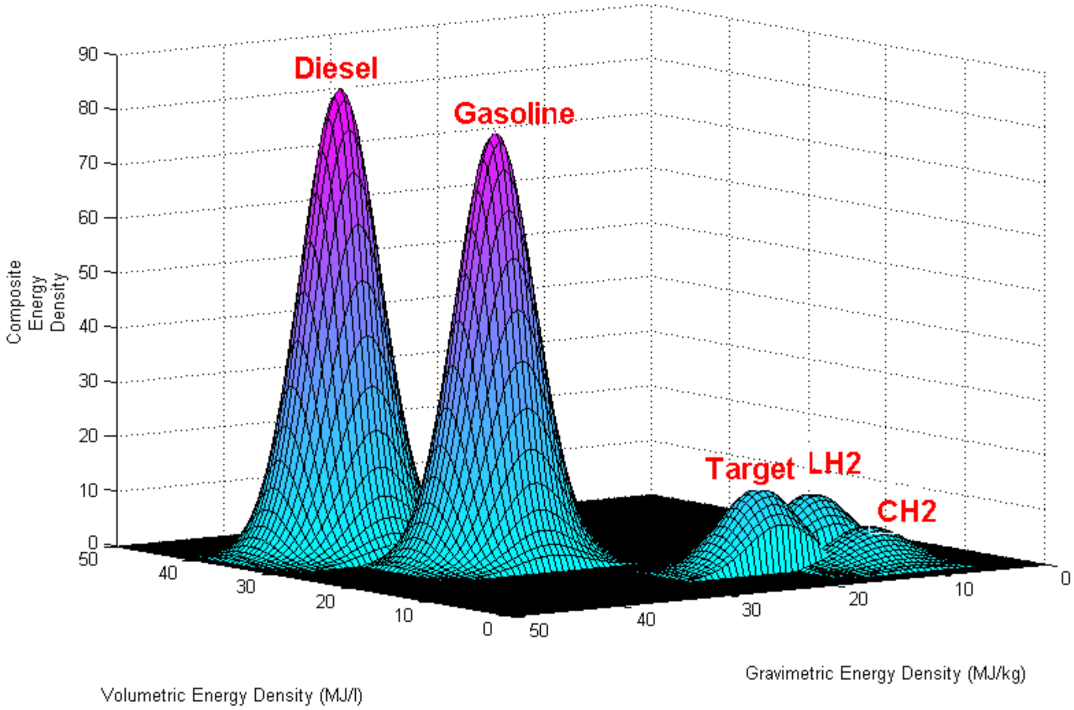

Figure 1: Hydrogen storage technology state-of-the-art and targets

The cost of fuel cell vehicle technology is also a barrier to its widespread adoption. Current prototype and one-off fuel cell engine technology costs a prohibitive $8,000-$10,000 CAD/kW in 2005 dollars, which does not compare favorably with internal combustion engine technology that costs around $50 USD/kW [6]. Carlson et al present a convincing estimate of the mass production reduction in price per kilowatt for fuel cell technology, suggesting that it should reach $108 USD/kW [7] in 2005 dollars. The technological advancements required to further reduce this price are the reduction in the use of rare earth metal catalysts to promote the fuel cell reaction and improvements in stack plate manufacturability.

The production and distribution cost of hydrogen as a transportation fuel is also currently higher than that of petroleum fuels. Granovskii et al determined in a comparison of hydrogen production methods with gasoline that, as the impact of the fuel air pollution and greenhouse gas emissions decreases, so does the economic efficiency for the production process [8]. This disparity must be corrected by factoring the environmental remediation cost of fossil fuel consumption into its production and distribution cost to ensure that future generations do not bear the burden of these costs. It is also important to consider the impending fossil fuel shortages as ‘easy oil’ is depleted and energy companies experience more difficulties in extracting reserves such as oil sands and deep-ocean wells, which carry an inherently higher risk and environmental impact.

The public image of hydrogen has suffered as a result of several high profile accidents such as the Hindenburg disaster of 1937. Despite the damaging publicity of the Hindenburg legacy, the reality remains that hydrogen as a fuel can be stored and handled as safely as gasoline or any other transportation fuel [9]. It merely has a different set of safe handling requirements than that of conventional liquid fuels. For example, it is important to have adequate detection systems in place to monitor for leaks because hydrogen is odourless and colourless. On the other hand, if a minor leak occurs, hydrogen is less likely than gasoline to pose a flammability risk in an enclosed space such as a garage due to hydrogen’s diffusivity and buoyancy properties [10].

While the technical challenges surrounding hydrogen fuel such as its storage, production, and distribution are significant, the potential that it has to improve the human condition justifies the efforts required to overcome them and to move towards a hydrogen economy. In particular, the use of renewable energy sources such as wind, solar, and hydro to generate hydrogen represents an attractive closed-loop energy path that does not release greenhouse gasses such as carbon dioxide, and that therefore mitigates the human impact on global warming [2]. Figure 2 shows a typical carbon cycle before and after the implementation of a renewable hydrogen transportation fuel system.

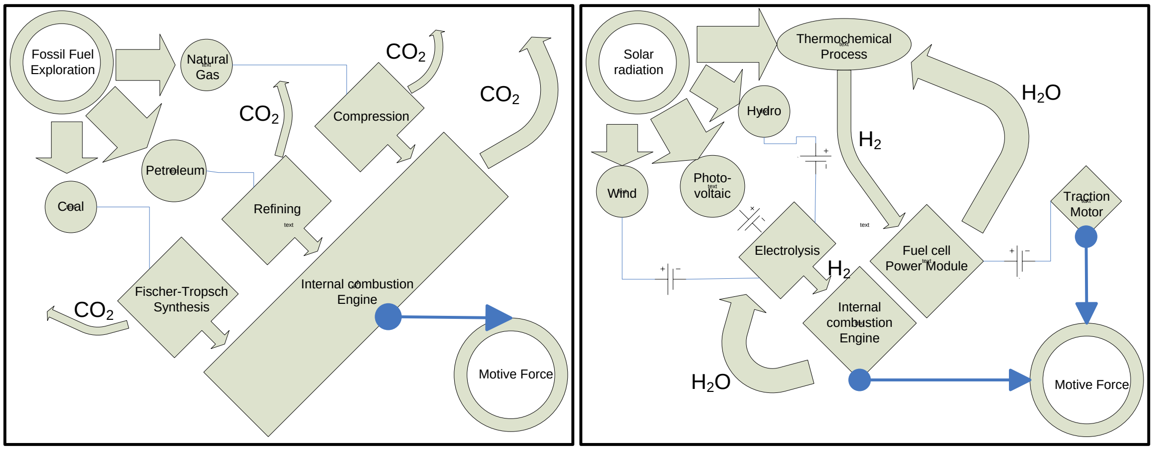

Figure 2: Panel 1: Current energy cycle **Panel 2: Hydrogen energy cycle**

The human health effects of vehicle emissions are well-documented. A study by the Ontario government in 2005 found that vehicle emissions were responsible for approximately 5000 deaths in that year [3]. In addition to reducing or eliminating well-to-wheels greenhouse gas emissions, hydrogen fuel also eliminates almost every criteria of vehicle tailpipe emission with the exception of nitrous oxides. By producing hydrogen from fossil fuels in central rural plants and transporting it into urban areas, it is possible to reduce the volatile organic, particulate, and ground level ozone pollutants that are created by all internal combustion vehicles and thereby create a healthier environment in our cities.

A significant portion of the world's petroleum reserves are located in countries where political instabilities often disrupt production and distribution. Geopolitical instability could be mitigated by the adoption of a fuel with production diversity such as hydrogen, as an energy pathway selection can be made from the myriad of sources available. Countries with large supplies of bio-wastes such as sugar cane stalk in the case of Brazil or pulp and paper waste in the case of the United States can convert their waste stock into valuable fuel [11]. Countries with significant hydroelectric and nuclear generating capacity that is typically underutilized during off-peak hours can use their plants more effectively to generate hydrogen. Equatorial countries are well-positioned to use solar energy to produce hydrogen for export to their neighbors. Figure 3 shows the current distribution of transportation fuel resources as well as how global solar resources are distributed. It is clear that if solar energy were used to produce hydrogen, the global energy supply would be much more evenly distributed.

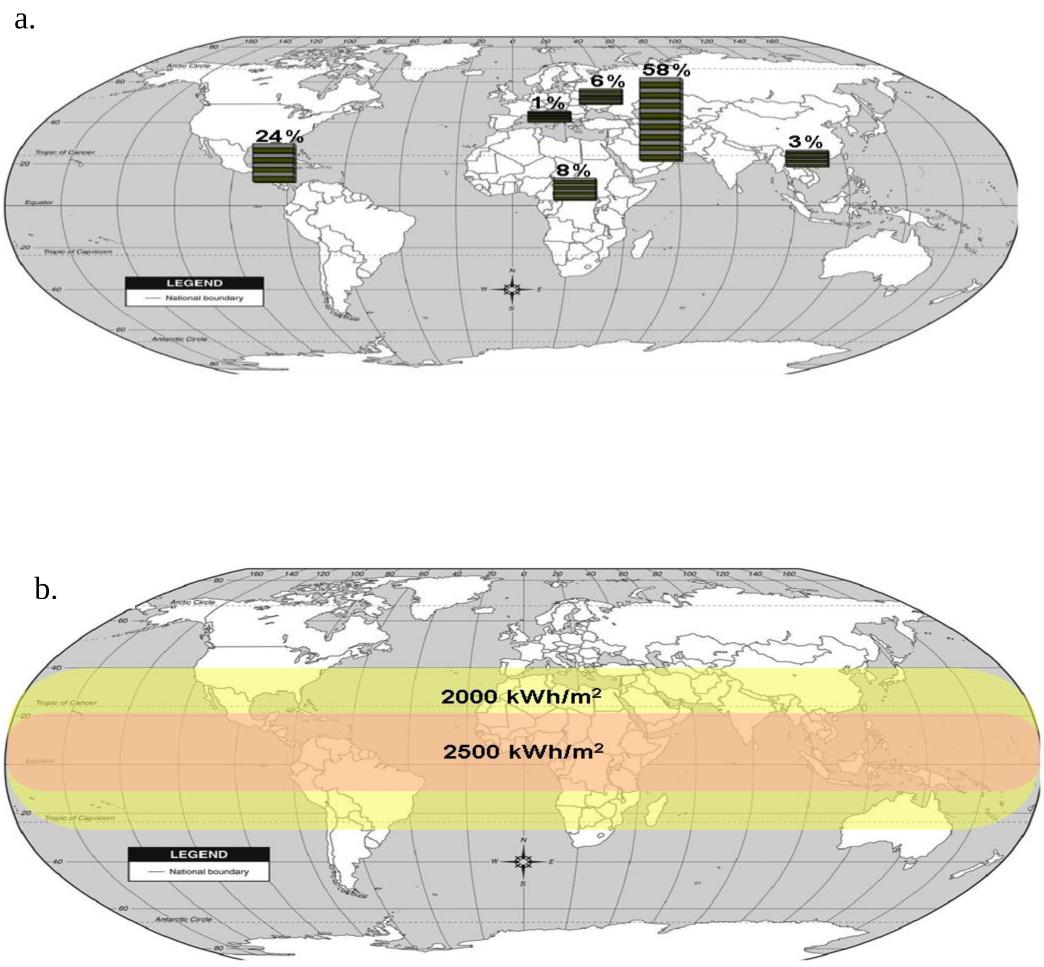

Figure 3: Distribution of transportation fuel resources. Fossil[12] (a) and solar[13] (b)

The life cycle assessments of different well-to-wheel hydrogen fuel production pathways can aid in gaining a perspective on the relative merits of each and how they compare to our present day transportation energy system. An extensive life cycle analysis has been performed on the efficiency and loss associated with all available feed stocks for hydrogen production by Granovski, et al. Selected production pathways are shown in Figure 4.

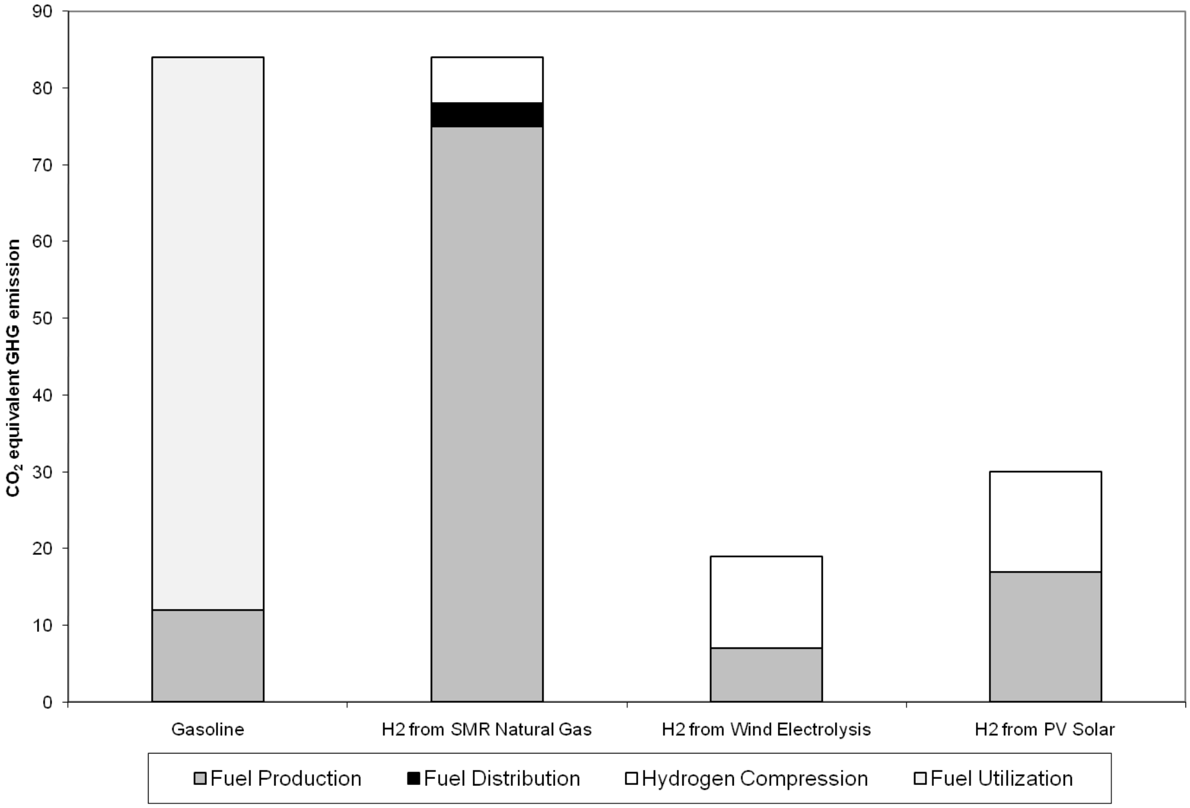

Figure 4: Lifecycle analysis of promising hydrogen production methods [14]

In the life cycle analysis on greenhouse gas emissions during hydrogen production, most often wind and solar production methods compare favorably with fossil fuel production methods such as the steam methane reforming (SMR) of natural gas, the most common method of production at present [14]. Renewable methods of production are one of the key ways that hydrogen technology can reduce the environmental cost of transportation energy utilization.

At the end of the 19th century and the beginning of the 20th century, there was no dominant transportation fuel; gasoline, electric, and steam-powered vehicles were all competing for the market. Society finds itself in a similar situation at the end of the 20th century and the beginning of the 21st century. A representation of the last two hundred years and a reasonable projection of the transportation energy system that can be expected in the coming decades [15] are outlined in Figure 5.

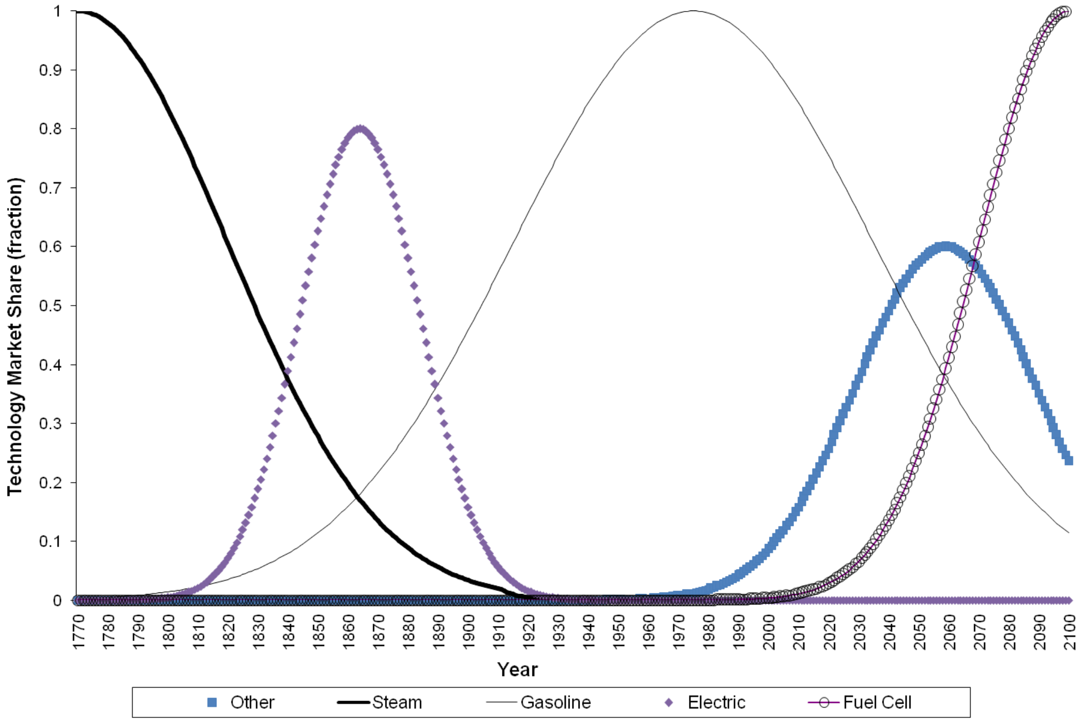

Figure 5: Projected 21st century transportation energy system [15]

A primary challenge for the transition from the incumbent transportation technology is a near-term perspective that places limited value in avoiding environmental and economic impact. In the next decade, hydrogen produced from fossil fuels for transportation use will improve our urban air quality and reduce our dependency on foreign oil. In the coming quarter century, hydrogen produced in a sustainable fashion will reduce anthropogenic carbon dioxide emission significantly and help to mitigate global warming. The challenges and opportunities that lie ahead are easy to compare to the ones that faced the fathers of the automotive industry at the turn of the 19th century. Efforts should be made to ensure that, as the future of mobility for succeeding generations is reinvented, the lessons of the past are considered and not forgotten.

1.4 Hybrid Vehicle Powertrains

Hybrid electric vehicles use in-vehicle energy storage devices such as batteries or ultracapacitors with electric motors in addition to their primary drive engines in order to recapture braking energy and to drive the wheels using the most efficient energy pathway. Most vehicle manufacturers have made significant progress in the past five years in developing hybrid vehicles to add to their product lines, with consumer demand for hybrid technology increasing significantly in the past years. Figure 6 shows the sale of hybrid vehicles in the US from 2004 until 2007 [16]. The correlation between consumer preference for vehicles that save fuel and the price of fuel at any given time is clear.

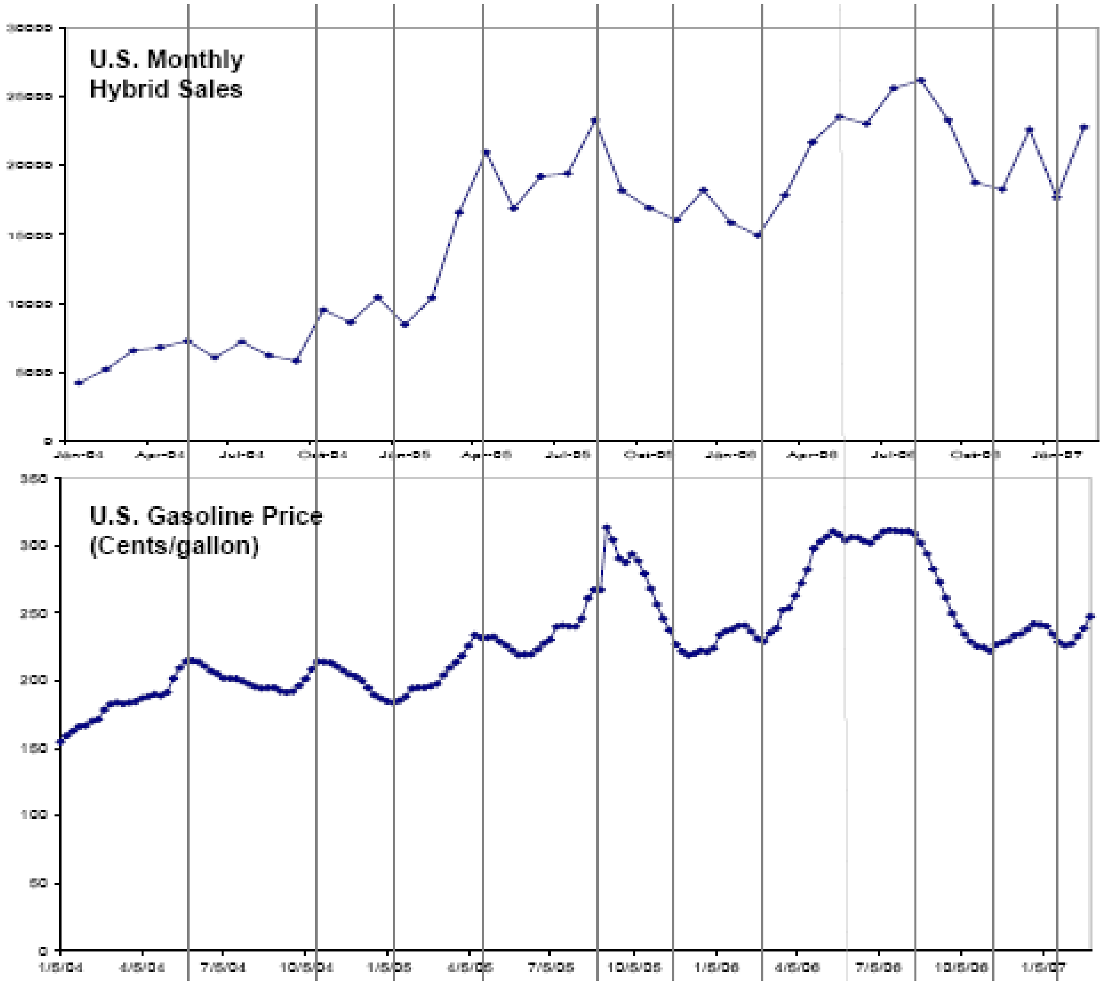

Figure 6: US hybrid sales in 2004-2007 [16]

1.3.1 Parallel Hybrids

In the parallel hybrid architecture, the motor and the engine are both able to deliver power to the wheels. This allows the motor to assist the engine on hard acceleration, as well as to take over completely during low speed driving. During braking, the motor becomes a generator that recharges the battery with the mechanical energy required for stopping. The disadvantage of the architecture shown in Figure 7 is that the internal combustion engine cannot be constantly operated in its most efficient operating range because it is mechanically linked to the wheels.

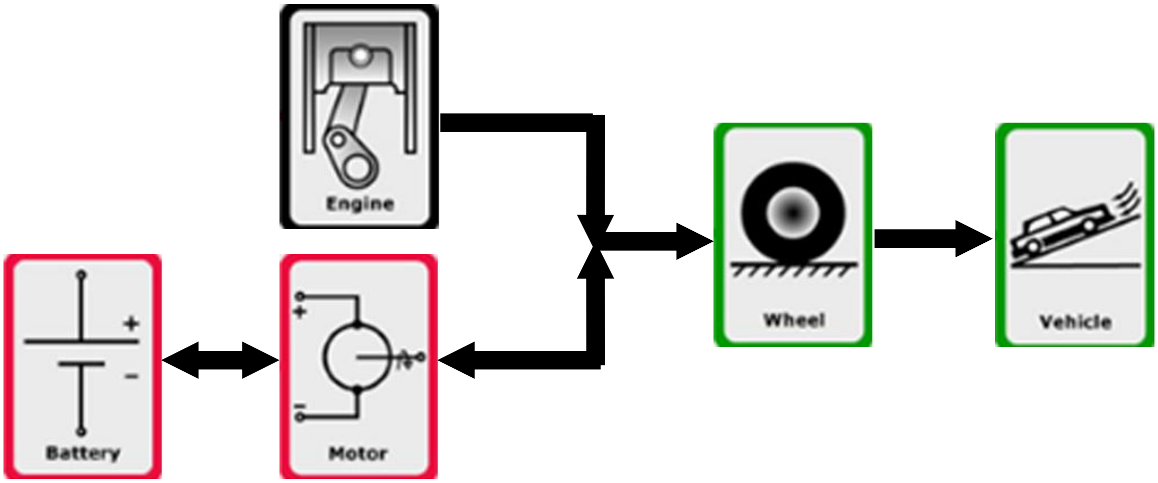

Figure 7: Parallel hybrid vehicle configuration [44]

1.3.2 Series Hybrids

Series hybrid vehicles seek to operate an optimally sized internal combustion engine at the engine's most efficient operating range. Then engine generates electricity which is then either used at the wheels, or to charge the battery, depending on the driver request. The wheels are driven by the electric motor alone and regenerative braking is still possible, as shown in Figure 8. The disadvantages of this architecture is that the power must flow through all of the powertrain components, so they must all be sized large enough to handle the vehicle's torque requirements and the efficiency losses in energy conversion are significant.

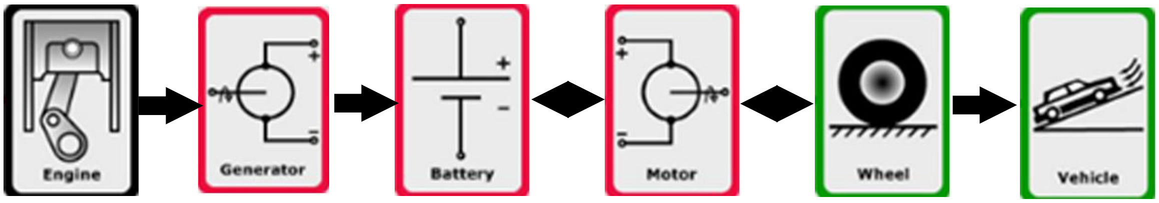

Figure 8: Series hybrid vehicle configuration [44]

1.3.3 Series Parallel Hybrids

The series parallel configuration shown in Figure 9 takes allows the greatest flexibility in power delivery, and can therefore select the most efficient operating point while maintaining the ability to provide sufficient power to the wheels during heavy acceleration. The major drawbacks of this architecture are its weight, cost, and complexity. The Toyota Prius employs a series-parallel powertrain configuration, and has established itself as the flagship for hybrid vehicles [17].

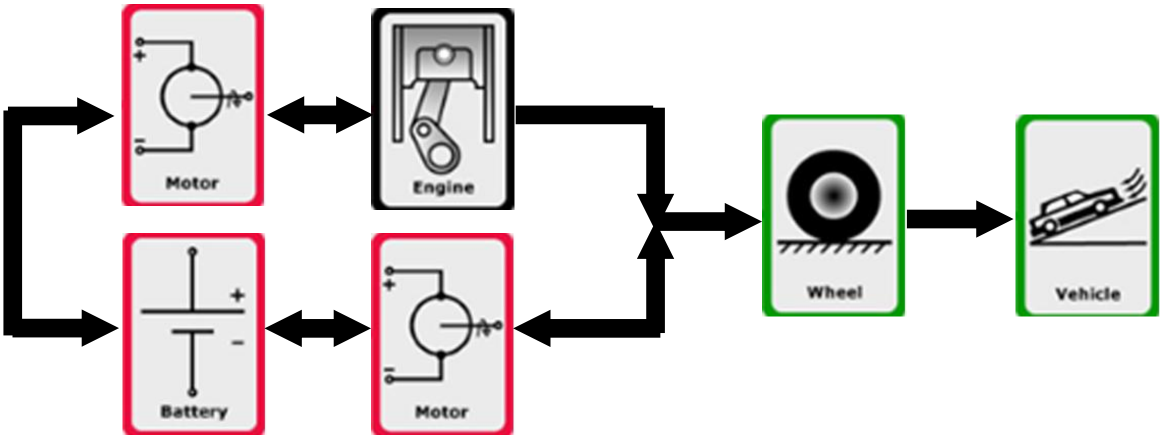

Figure 9: Series-parallel hybrid vehicle configuration [44]

1.4 Transportation Fuel Cell Technology

One key enabling technology for the transition to a hydrogen energy economy is the fuel cell engine. Fuel cell power modules (FCPM's) are able to transform chemical fuel energy into electrical energy with 50-60% practical efficiencies. Fuel cells have been researched for over 150 years [18], since the first demonstration of the principle by Sir William Grove in 1839. In the last 20 years, significant progress has been made towards developing transportation fuel cell applications, particularly with the development of stable ion conducting membrane polymers.   The first successful vehicular fuel cell integration was performed on a tractor for Allis-Chalmers that used potassium hydroxide as an electrolyte in 1959 [19]. Since that early effort, the fuel cell technology that has been broadly accepted as the most promising for transportation application is the polymer electrolyte membrane (PEM) fuel cell.   In addition to requiring robust and durable fuel cell stacks, the balance of plant that every fuel cell engine requires to meter and condition the reactant feed streams has required significant development, particularly to ensure reliable cold starting and operation. Today, all major vehicle manufacturers are involved to some degree in fuel cell research and development. General Motors is a leader in the drive towards transportation fuel cells and plans to have commercial products by 2010 [20].

Fuel cells share many of the physical and electrochemical characteristics of batteries. The primary difference is that fuel cells receive a constant reactant feed, whereas batteries must be charged to return their reactants to the electrodes. A single polymer electrolyte fuel cell is pictured in Figure 10 with its salient physical features labeled [18].   Polymer electrolyte fuel cells are low temperature fuel cells and do not require caustic or acidic liquid electrolytes and are therefore well-suited for transportation applications. In addition, they operate at low temperatures of around 65°C and are therefore inherently safer than higher temperature fuel cells.

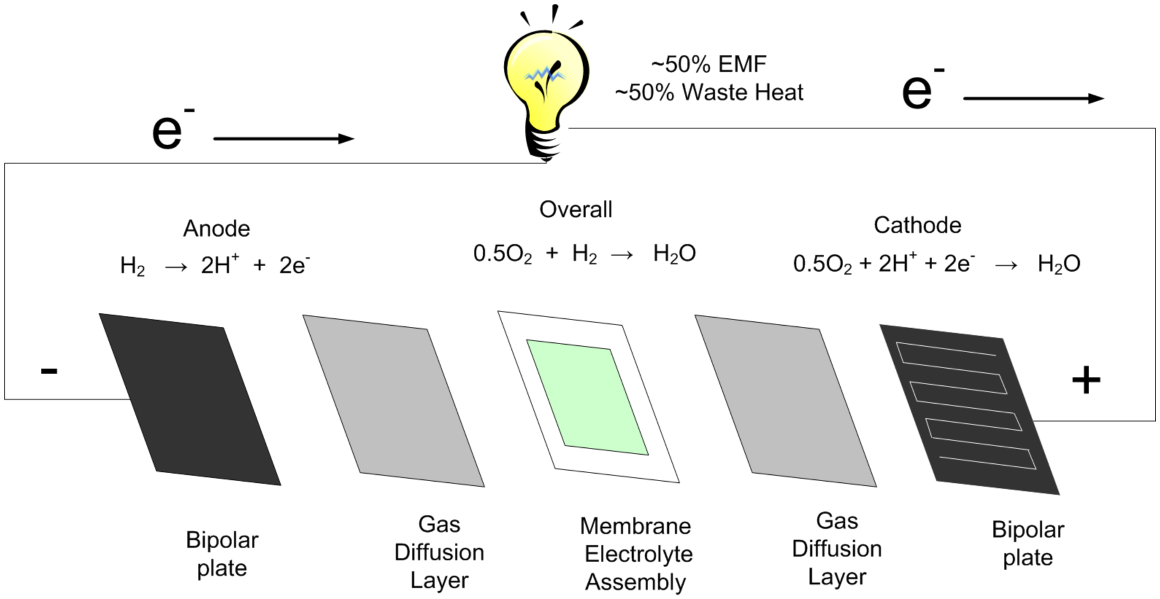
~50% EMF
~50% Waste Heat
e-
e-
Anode
$H_2 \rightarrow 2H^+ + 2e^-$
Overall
$0.5O_2 + H_2 \rightarrow H_2O$
Cathode
$0.5O_2 + 2H^+ + 2e^- \rightarrow H_2O$
-
+
Bipolar plate
Gas Diffusion Layer
Membrane Electrolyte Assembly
Gas Diffusion Layer
Bipolar plate

Figure 10: Single polymer electrolyte fuel cell

The bipolar plate in Figure 10 acts as a current carrier and provides physical structural rigidity to the cell. It also plays a key role in reactant gas delivery and product water removal. Modern fuel cell bipolar plate design reduces or eliminates reactant gas humidification requirements by wicking water to dry areas of the membrane and removing water from saturated areas of the gas diffusion layer [21]. Bipolar plates were originally produced from machined graphite, but are now most often either stamped and anodized metal or molded conductive polymer. The gas diffusion layer distributes gases to the reaction sites on the catalyst layer and wicks water from the membrane to the flow channels in the bipolar plate. It is composed of carbon cloth with water permeability and physical characteristics that maximize performance [22]. The polymer electrolyte membrane and catalyst layer are manufactured as a single unit, known as a membrane electrolyte assembly (MEA). The MEA facilitates the fuel cell reaction in Figure 10. It allows protons to travel from the anode to the cathode during the reaction, but is an electronic insulator forcing the electrons produced to travel through an external circuit and do work. The reaction on both the anode and cathode is catalyzed primarily by platinum, but this area is the focus of research to develop new catalysts and doping compounds to reduce cost and increase functionality such as catalyst regeneration [23]. The sulfate group shown in the simplified chemical representation of a PEM shown in

Figure 11 is required in order to facilitate proton transfer by creating an acidic membrane condition in the presence of water [18]. The structure of the polymer electrolyte membrane is the reason that proper water management and hydration is critical to efficient fuel cell operation.

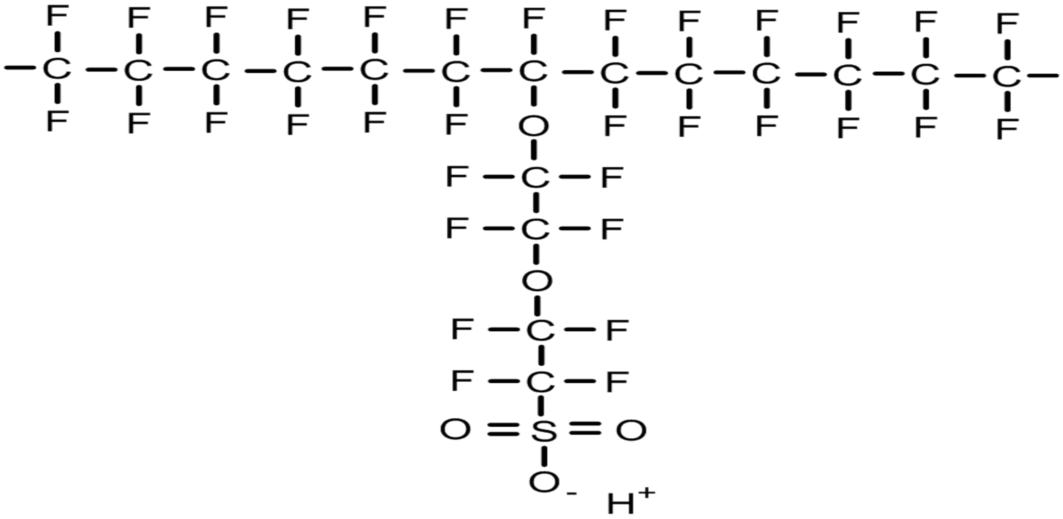

Figure 11: Polymer electrolyte membrane structure: sulphonated flouroethylene

PEM fuel cells obey the same electrochemical laws that batteries do. Their performance characteristics differ significantly, however, because of their unique solid electrolyte. The discharge characteristics of a fuel cell are shown in Figure 12.

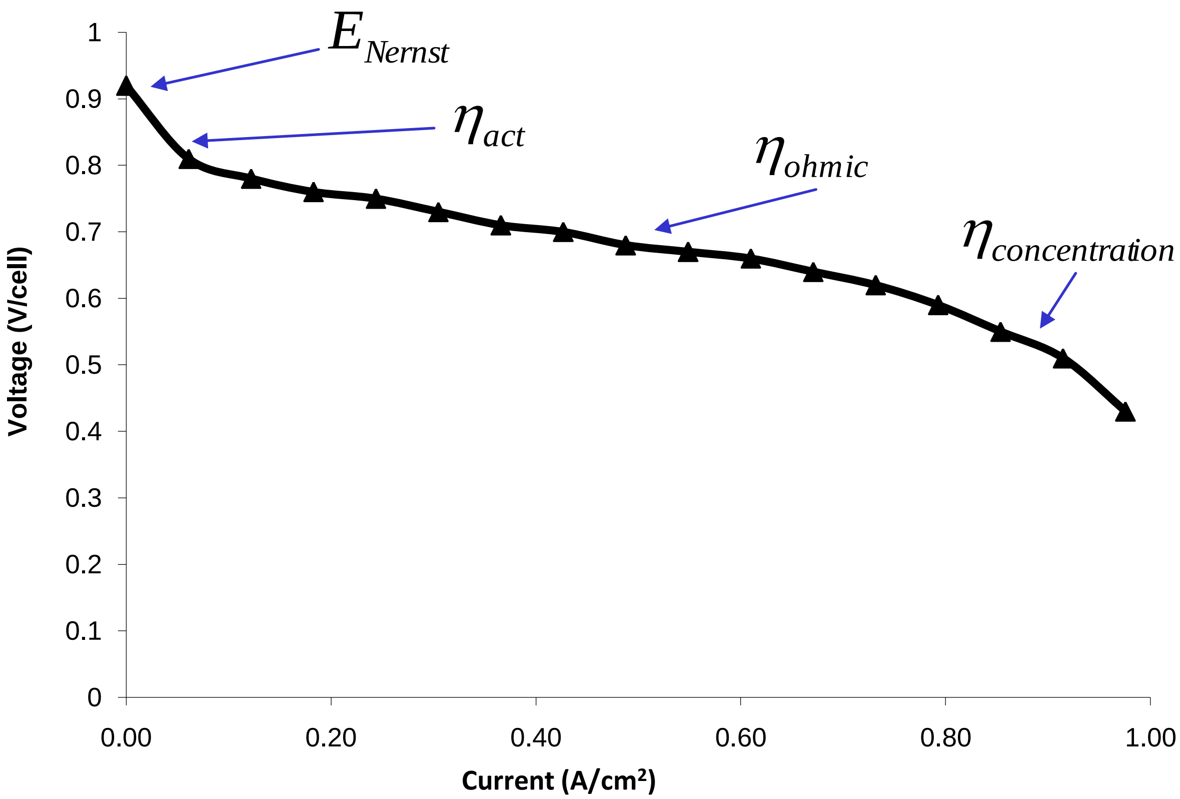

Figure 12: Polarization curve showing the operating characteristics of a fuel cell

The loss regions highlighted in the sample discharge (polarization) curve of the fuel cell shown in Figure 12 are the activation losses (η_{act}) , the ohmic losses (η_{ohmic}), and the concentration losses ($\eta_{concentration}$). Activation loss is the highly non-linear voltage drop that is representative of the energy used to drive the chemical reaction that transfers electrons to or from the electrodes at the catalyst surface, and is characteristic of the fuel cell reaction kinetics. It is directly related to the effective catalytic surface area. Ohmic loss is the linear voltage drop that is caused by resistance in the electrical connections of the system as well as the resistance to proton transport through the electrolyte. Concentration overpotential is the loss caused by the slow mass transport of reactants from the bulk fluid to the reaction sites and is non-linear according to mass transfer relationships. The Nearnst law defines the thermodynamic voltage limitation (or E) of the system by Equation 1. This equation relates the concentration of reactant gasses to reversible fuel cell potential, giving the maximum possible voltage at a given temperature and pressure[18].

$$E = E^{o} + \frac{RT}{2F}\ln\left(\frac{a_{H_2} \cdot a_{O_2}^{\frac{1}{2}}}{a_{H_2O}}\right) \qquad 1$$

To achieve useful operation voltages for use in vehicle or power applications, single fuel cells must be combined into stacks of multiple cells such as the stack shown in Figure 13. The stack shown in this figure has 18 cells, and is considered a low voltage stack at ~16V with no load. Typical vehicle fuel cells have between 200 and 400 cells (180V – 360V), and have an active area of 300 to 600 cm^2.

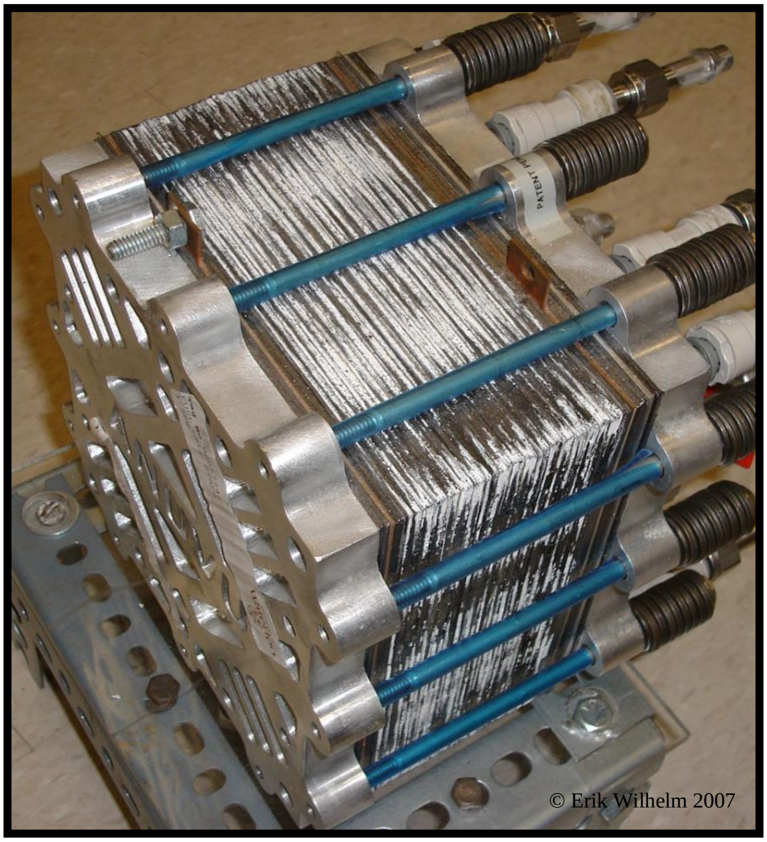
© Erik Wilhelm 2007

Figure 13: Fuel cell stack comprised of 18 cells in series

The fuel cell stack must then be supplied with reactants at the proper temperature, pressure, and levels of humidity. In order to do so, a balance of plant must be established around the stack and is commonly called a fuel cell power module (FCPM). The fuel cell power module also controls the system to ensure that it operates in the most efficient manner at a given load, monitors system performance and safety, and interfaces with the vehicle controller. Table 1 outlines the common elements of a fuel cell balance of plant.

Table 1: High power fuel cell power module components

Component	Function	Power Draw
Fuel cell stack	Perform the electrochemical fuel cell reaction	N/A
Air compressor	Deliver oxidant in required quantities to the stack	2 ~ 3 kW
Hydrogen recirculation pump	Ensure even humidification and reactant delivery	50 ~100 W
Water pump	Circulate cooling fluid through stack to remove heat	500 ~600 W
Heat exchanger	Dissipate waste heat produced in the reaction	N/A
Controller	Meter reactant flow and ensure safe operation	1~5 W
Anode humidification	Ensure anode reactant stream is adequately humidified	N/A
Cathode humidification	Ensure cathode reactant stream is adequately humidified	30 ~ 90 W
Purge and vent valves	Regulate hydrogen exhaust and prevent overpressure	20 ~ 40 W

Integrating fuel cell power module technology into current vehicle architectures presents challenges as well as opportunities. The volumetric power density of fuel cell engines, currently 1.5 kW/L [24], does not compare favorably to the power density of internal combustion engines which are typically around 50 kW/L. Similarly, the gravimetric energy density of fuel cell power modules, typically 0.07 kW/kg, is still less than the gravimetric energy density of internal combustion engines, which is around 0.5 kW/kg. When the fuel storage system is considered, petroleum and diesel-fuelled vehicles require even less volume and weight than their fuel cell counterparts.   On the other hand, fuel cells and their hydrogen storage technologies have a greater degree of flexibility in their packaging location. The transmission of power in fuel cell vehicles is electromechanical, so the fuel cell engine can be effectively packaged in a low-profile manner in-line with the chassis of the vehicle. This lowers the vehicle's center of mass and improves handling. The hydrogen storage may also be packaged in many configurations on the vehicle and piped to the required fuel cell inlet ports. For example, the Michelin fuel cell vehicle uses the hydrogen storage as its structural members which allows for a very rigid body structure and thus improved handling [25]. The state of the art fuel cell hybrid vehicles that have been developed by the automotive industry are outlined in Table 2.

Table 2: The state of the art of fuel cell vehicle technology

Manufacturer	Vehicle	Hybrid Features
DaimlerChrysler	Modified Mercedes-Benz A-Class "F-Cell"	65kW drive motor, 350 bar storage, 150 km range
Ford Motor	Modified Ford Focus "FCV"	85 kW fuel cell, NiMH battery, 300 km range
General Motors	Modified Chevrolet Equinox "Equinox Fuel Cell"	93 kW fuel cell, 35kW NiMH battery, 320 km range
Honda	Custom Honda "FCX"	80 kW drive motors, ultracapacitors, 430 km range
Hyundai	Modified Hyundai Tucson "FCEV"	80 kW drive motors, NiMH battery, 300 km range
Nissan	Modified Nissan X-TRAIL "FCV"	85 kW drive motors, Lion battery, 350 km range
Toyota	Modified Toyota Highlander "FCV"	82 kW drive motors, NiMH battery, 330 km range

Fuel cell hybrid technology is at an advanced stage of development, and the barriers to commercialization are primarily related to cost reduction, fueling infrastructure, and hydrogen storage (range). Although several technical and political challenges remain unsolved, the economic and environmental benefits of introducing fuel cell vehicles as an alternative to internal combustion technology are understood to outweigh the costs. It is widely acknowledged in the automotive industry that hydrogen will be a viable transportation fuel in the coming decades [17].

1.5 Hardware-in-the-loop Control Validation

Hardware-in-the-loop simulation (HIL) is an increasingly valuable tool for rapid prototyping, system modeling, and validation. This simulation methodology was first implemented in aviation and guided missile control tuning and validation where physical control testing is at best difficult and, at worst, dangerous or impossible. HIL has since found widespread use in vehicle control design, where emphasis on safe and economical testing has made HIL an industry standard. The definition of HIL, which was originally the validation of an engine control unit (ECU) in a virtual vehicle simulation environment, has been expanded to include hardware from almost all vehicle subsystems. Often when designing a model, feedback from either the physical subsystem or the virtual subsystem can be neglected with little effect on fidelity. Figure 14 illustrates examples of this assumption. The effect that a wind turbine will have on a hurricane’s wind speed can be neglected in simulation, as can the effect of a chassis on a road profile in a unidirectional simulation methodology. This allows the simulation to be run offline, with data from the driver system (hurricane, road profile) used in the driven (wind turbine, vehicle) system. Hardware-in-the-loop simulation, however, captures a control and feedback loop allowing bidirectional interaction between the virtual and physical components to be observed and tested [26].

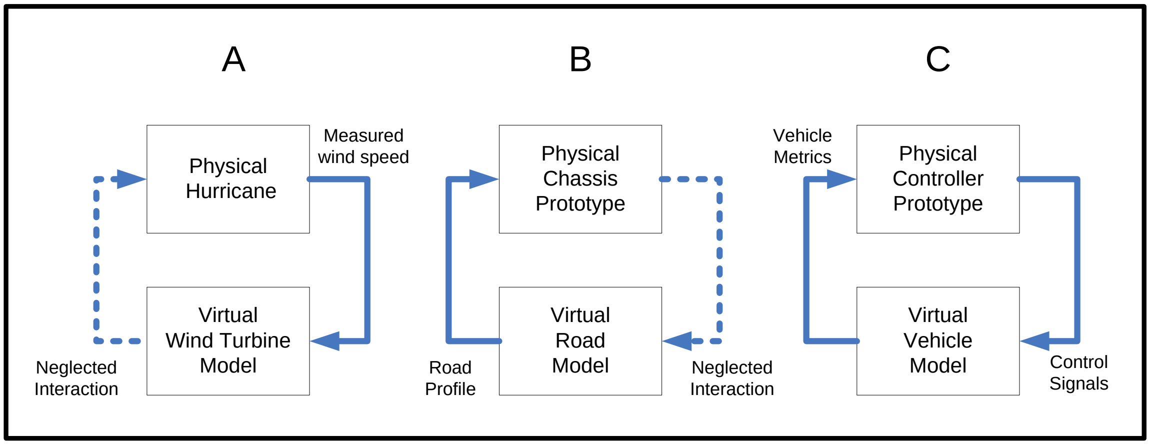

Figure 14: Examples of uni- and bidirectional simulation [26]

The definition of hardware-in-the-loop simulation that will be used in this thesis is “the use of comprehensive virtual vehicle and road profiles in real-time simulation environments to validate and tune multiple engine control units” and is shown in panel C of Figure 14.

The advantages that HIL simulation offers to the automotive industry are outlined in Table 3 [26]. The ability to test vehicle subsystems in a safe and repeatable fashion, as well as the time and cost savings associated with HIL testing should be highlighted as major benefits of performing the validation in a vehicle design cycle.

Table 3: Utility of HIL simulation in the automotive industry

Advantage	Description	Example
Cost Effectiveness	Less hardware required	Simulation of subsystems before hardware selection
Rapid Prototyping	Reduced setup time	Engine control performed without dynamometer test
Fidelity/Verisimilitude	Can resolve focus on individual subsystems	Isolating pump dynamics is easier to simulate
Simulation Speed	Complex physical phenomena runs faster	Empirical nature of models allows shorter testing time
Repeatability	Boundary conditions controllable	Suspension systems can be loaded in simulation
Virtual environment	HIL allows simulation of destructive events	Airbag deployment can be tested
Comprehensiveness	Broad range of physical conditions simulated	Temperature variation from a mountain ascent testing
Safety	Vehicle safety systems can be validated	Ensuring appropriate torque requests for throttle signals
Parallelism	Subsystems can be developed in parallel	Hybrid control strategy tuned parallel to development

The burgeoning hybrid vehicle market has prompted vehicle manufacturers to accelerate the development of hybrid vehicles, necessitating the rapid prototyping capability offered by HIL simulation. Hybrid vehicle powertrain complexity also requires more complicated control hardware and algorithms, which presents an opportunity to use HIL simulation to test fail-safe functionality and rationality in the increasingly complex hybrid control systems.

There are several important considerations when establishing hardware-in-the-loop simulation systems above and beyond what is required for unidirectional modeled systems. In addition to model accuracy and fidelity, determinism and interconnectivity between hardware and software components must be designed for in HIL test apparatus.

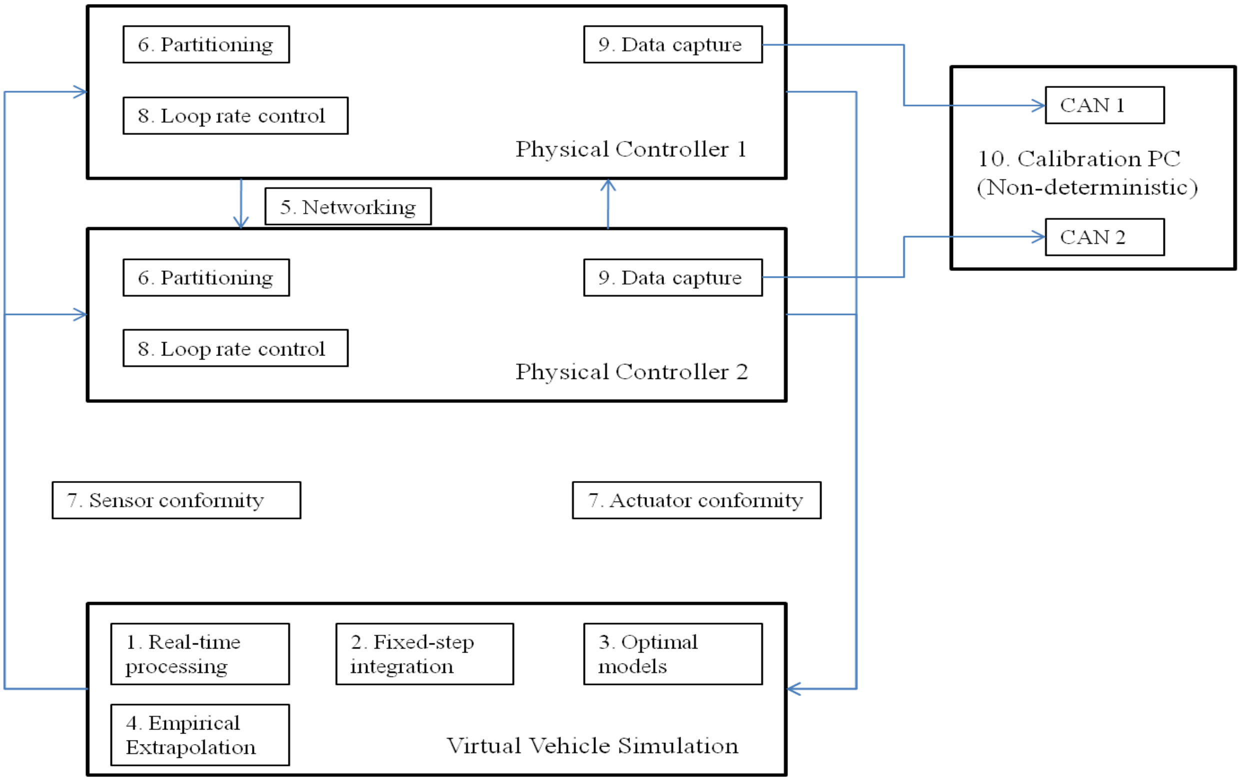

Figure 15: Hardware-in-the-loop system considerations

Some of the important characteristics of HIL simulators are shown in Figure 15 and require elaboration in the list below [27].

1. The processor that is running the virtual vehicle simulator must be able to operate deterministically in order to ensure system transient characteristics are captured and simulated. This requires a **real-time** operating system that executes integration steps at regular intervals signaled by clock interrupts. Event stream processing must often be employed to attain the sampling rate requirements of 1ms or less required by automotive control systems [28].
2. To ensure that each integration step occurs within the specified simulation time, **fixed step** solvers must be used for HIL systems. This introduces modeling challenges when state changes such as gear shifting occur between simulation steps and necessitates a hybrid discreet/continuous state model to be developed to handle these events [26].
3. In order to accurately represent the physical vehicle systems being simulated, the HIL models must be sufficiently complex. Increasing model complexity requires

increasing simulation step time, which conflicts with the system's real-time operating requirements. An **optimal** balance must be struck between model accuracy and simplicity to correctly represent the physical systems while ensuring that transient dynamics are captured during simulation [29].

4. **Empirical** models are often chosen to ensure sufficient accuracy balanced with deterministic execution. It is important to ensure that models constructed from fitted data perform in a rational way outside of the data collection range. Amplification of error can occur at data boundaries, particularly during start-up transients, for example.
5. The controller area **network** (CAN) protocol that is used in the vehicle system must be rigorously emulated on the HIL simulation system. This network must also be tested for bus utilization, error handling, and network management capabilities which requires the ability to externally monitor and load the network.
6. Designing the vehicle control system must include careful analysis of the method of splitting control functionality between control hardware. Time critical and non-time critical tasks should be split between loops and assigned to the appropriate vehicle controllers. **Partitioning** the control in this fashion allows independent processing paths to be used to check control rationality and ensure safety through redundancy.
7. Sensor and actuator **conformity** must be tested by comparing vehicle sensor performance metrics to HIL real-time simulator I/O performance metrics. In order to ensure appropriate controller response, the HIL hardware must be able to accept inputs and set outputs with the same time factor, range, and sensitivity that the vehicle controller expects and delivers.
8. Controller **loop rate** can be tuned if the HIL simulation timing is sufficiently fast to simulate the quickest vehicle system response. For example, anti-lock braking systems require a physical model running integration steps every 4 ms in order to ensure that the vehicle controller can be tuned to perform its function properly in real time [30].
9. The overall HIL simulation system should be monitored by an external computer to **capture data**, provide non-deterministic system status updates, program new

code to both the simulator and controller, and control simulation runs. This computer also allows disturbances to the communication and I/O bus to be performed to test controller response under repeatable failure conditions.

The types of tests and applications of hardware-in-the-loop simulation for vehicle control validation are many, and the list is growing with the increasing popularity of exotic hybrid and fuel cell vehicle powertrains. Table 4 is a short list of some of the ways that HIL has been applied. Note that some of the applications define HIL to include hardware such as engines, air compressors, or brake actuators that interface with real-time simulation [31]. This departs from the definition of a vehicle controller coupled with a real-time controller used in this thesis.

Table 4: Hardware-in-the-loop automotive application (individually referenced)

Hardware	Institute	Application
ABS controller [31]	KERI	14 degree of freedom vehicle simulation for ABS tuning and validation
Generic control [45]	DaimlerChrysler	Automatic comparison of time-dependent signals and responses
Compressor and controller [46]	VKA	Characterization of compressor dynamics decoupled from fuel cell
Powertrain controller [47]	Ford	Testing signal I/O faults for short to ground, short to battery, and float
Engine Control Unit [32]	Delphi	Robust software design and testing practices on an encoder reader
Diesel Engine controller [48]	ANL	Full powertrain coupled with PSAT vehicle dynamics and control package

Literature that has been published since the advent of hardware-in-the-loop simulation in the early 1980’s has documented applications such as communication bus validation, jitter and determinism characterization, algebraic loop troubleshooting, executed command and data lag identification, fail-safe testing, response variable tuning, and system variability determination through stochastic simulation [32].

This thesis will outline the development HIL simulation models and how control systems for a fuel cell hybrid vehicle can be safely and effectively tested. As the complexity of future vehicle powertrains increases, so does the utility of virtual control system validation. The novel HIL and SIL simulation techniques presented here are intended to guide future fuel cell vehicle control system validation efforts, particularly in the areas of communication validation and fail-safe testing.

Chapter 2: Fuel Cell Hybrid Chevrolet Equinox

2.1 ChallengeX

This thesis was closely integrated with the development of a fuel cell vehicle at the University of Waterloo in the period from 2005 to 2007. In 2007, it was one of only 6 passenger fuel cell vehicles on the road in Canada and the only such vehicle to be built by students. While the thesis focused on the HIL control system development, significant work was also performed on fuel cell power train design and integration. The graduate studies activities also extended to overall team leadership, hydrogen fueling system design, safe facility infrastructure development, and participation in outreach events.

The University of Waterloo Alternative Fuels team was selected from over 300 universities that applied to participate in the ChallengeX competition. This advanced vehicle design competition is part of a series organized by Argonne National Labs since 1989 and is sponsored by General Motors (GM), the US Department of Energy, and Natural Resources Canada.

Figure 16: 17 ChallengeX teams at GM's Milford Proving Grounds [33]

The ChallengeX competition is a four-year competition with three phases that parallels GM's Global Vehicle Development Process [33]. Figure 16 shows the seventeen competing schools with their 2005 Chevrolet Equinox vehicles. The first year of the competition focused on model-based design, simulation, and market analysis with the goal of developing vehicle technical specifications to drive the development in the second and third phases. The vehicle technical specifications for the second and third year of the competition, as well as the base Equinox performance specifications are found in Table 5. The UWAFT team captured first place honours in the design phase of the ChallengeX competition, as well as securing eight first place awards and two third place awards. The second phase of the competition required that the design from the first phase be implemented into a "mule vehicle" which met the vehicle performance specifications. Phase three of the competition required the Equinox be brought to a "99% buy-off" level of production readiness. This level of production readiness can only be reached when the vehicles' appearance, drive quality, performance, reliability, safety, and control systems pass stringent quality checks.

Table 5: University of Waterloo Fuel Cell Equinox: Technical Specifications [35]

Metric	Base Vehicle	Waterloo Y2 VTS	Waterloo Y3 VTS
Fuel Economy - combined EPA [l/100km]	≤10.1	≤6.96	≤7.35
Mass [kg]	≤1818	≤2227	≤2000
Acceleration: 0-100kph [s]	≤8.9	≤9.9	≤9.0
Acceleration: 80-110kph [s]	≤6.8	≤9.4	≤6.8
Range – highway [km]	≥512	≥224	≥220
Start Time [s]	<2.0	≤5.0	≤5.0
Passenger Capacity	5	2	5
Emissions [Tier, bin]	Tier 2, Bin 5	Tier 2, Bin 1	Tier 2, Bin 1
Trailering Grade-ability 7% gr. – 90kph – 0.4km [kg]	1591	1136	1136
Trailering Grade-ability 4% gr. – 90kph – 10km [kg]	1591	1136	1136

The approach that was taken to achieving a 99% buy-off level of production readiness for the third year of the competition involved a significant amount of control development and optimization. Hardware-in-the-loop simulation was used extensively to meet the Year Three development targets. Augmenting basic powertrain control with full diagnostic capability, adding redundancy and fail safe measures, and analyzing control response to unexpected inputs are examples of how hardware-in-the-loop control validation played a large role in 99% buy-off development.

2.2 Vehicle Architecture Description

The University of Waterloo Alternative Fuels Team made extensive use of Powertrain Systems Analysis Toolkit (PSAT) as a design tool during the first phase of the ChallengeX competition. The results of running a series of over 400 powertrain models on standard drive cycles were used in selecting and optimizing the fuel cell hybrid vehicle powertrain outlined in Table 6.

Table 6: University of Waterloo fuel cell hybrid vehicle powertrain components [35]

Device	Make/Model	Specifications
Fuel Cell Power Module	Hydrogenics/HYPM 65kW	Max Power: 65kW Voltage Range: 190-300V Current Range: 0-300A Mass: 350kg
Hydrogen Storage	Dynetek/ZM180	Max Pressure: 5000 psi Tank Capacity: 4.31kg H2 Tank Weight: 92kg Tank Volume: 178L
DC/DC Converter	Custom UWAFT design and construction	Input Voltage Range: 190-310V Output Voltage Range: 300-385V Converter Type: Boost Mass: 30 kg
Motors (2 units)	Ballard/312V67	Peak Power: 67kW Continuous Power: 32kW Max Torque: 190Nm Mass: 84kg
Motor Controllers (2 units)	Ballard/312V67	Continuous Power: 67kW Input Voltage: 260-385V Output Current: 280A RMS
Battery Pack	Cobasys/NiMHax288-60	Voltage Range: 220-360V Capacity: 8.5Ah Energy: 2.4kWh Mass: 88kg

The second year of the ChallengeX competition focused on the mechanical integration of all of the specified mechanical powertrain elements. The Equinox has a unibody construction, which necessitated many structural modifications to package all the required fuel cell powertrain elements. The overall powertrain layout is shown in Figure 17.

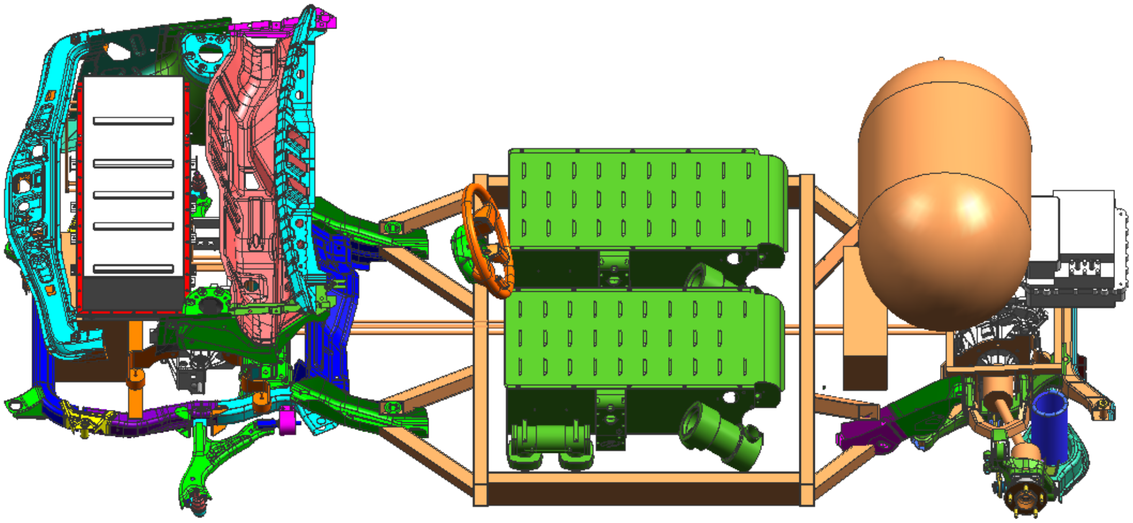

Figure 17: Powertrain packaging for the fuel cell Chevrolet Equinox

A nickel metal hydride battery, a three phase induction traction motor, a high DC/DC converter, and power distribution are housed underhood. The fuel cell power module is packaged in the floor of the vehicle to allow for five passenger seating. This required the redesign of the main structural frame rails, which provide the Equinox chassis with most of its stiffness [34]. The rear cradle and vehicle sub-frame required significant modification to accept a drive motor and hydrogen tank supports. Most of the powertrain component mounting solutions were implemented using aluminum to ensure that vehicle weight restrictions were met [35].

2.2.1 Vehicle Electrical Systems

The UWAFT fuel cell Equinox has a high voltage bus (220-360V), a 24V bus, and a 12V bus, in addition to control system and communication bus wiring. The complexity of these electrical systems was managed by developing comprehensive wiring diagrams for the various vehicle systems. Figure 18 is a schematic of the wiring runs that were implemented on the vehicle. A and B are fuel cell high power conduit. D, E, H, and I represent motor high power conduit. G and C connect the battery and the fuel cells through the DC/DC converter respectively to the high power bus. F ensures that high voltage parasitic loads are powered.

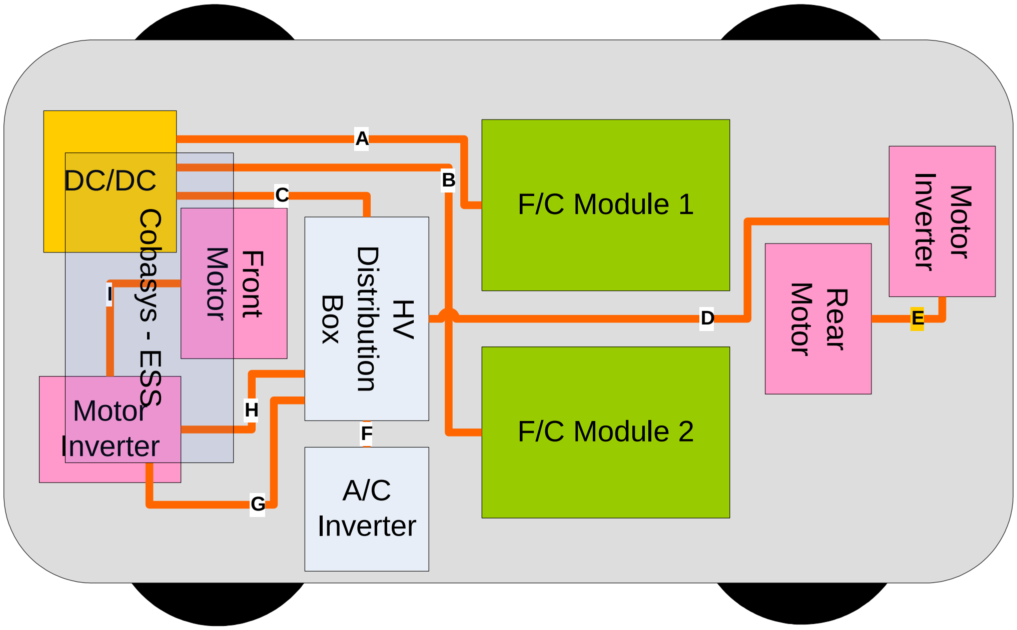

Figure 18: Major wiring conduits on the fuel cell Equinox

Connector labels corresponding to wiring diagrams ensured that troubleshooting of circuits could be easily accomplished and added to the 99% buy-off production readiness for the third year Equinox implementation [36].

2.2.2 Vehicle Control Architecture

The Equinox control architecture consists of a supervisory controller, a secondary controller, and a body controller. The body controller (BCM) is stock and is programmed by GM. The supervisory and secondary controllers are both UWAFT programmed controllers and have the specifications shown in Table 7.

Table 7: Vehicle controller technology

	Supervisory controller	**Secondary controller**
Controller:	Mototron ECU565-128	Mototron ECU555-80
Processor:	Motorola MPC565	Motorola MPC555
Clock Frequency:	56 MHz	40 MHz
Internal Flash:	1M	448K
External Flash:	NIL	2M (optional)
EEPROM	8K serial/optional 64K x 8 (parallel)	8K serial/optional 128k (parallel)
Internal SRAM:	36K	32K
Supply Voltage:	6-32VDC	8-16V
Analog In/Out Used	24	7
Digita In/Out Used	8	6
PWM Used	8	16
CAN Used	2	2

The number of powertrain elements and their specific control requirements necessitated a complex communication bus to be implemented in the vehicle. There are three controller area network (CAN) busses on-board and almost every available signal connection to both controllers is used. Figure 19 shows the control hardware architecture in the vehicle, as well as the elements requiring control.

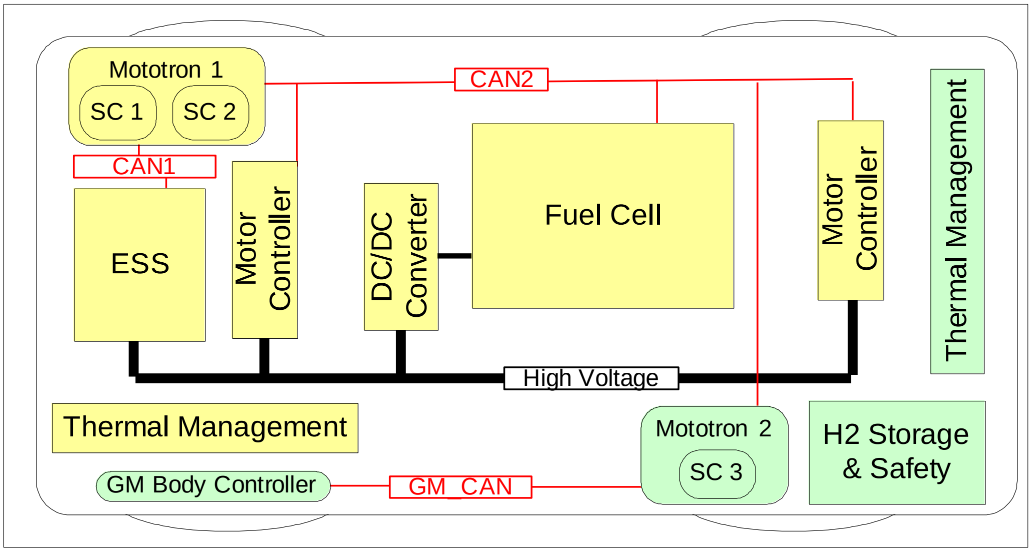

Figure 19: Fuel cell Equinox control architecture

The high degree of complexity in the control architecture stems from the number of independent powertrain subsystems. The integration of six major powertrain elements from four independent manufacturers posed communication compliance challenges in addition to the inherent difficulty of physically controlling the powertrain elements. To solve these challenges, the communication bus was divided into three sections, and more reliance on analog signal bus communication was required. The benefit of a complicated hybrid architecture, however, is the ability to optimize the powertrain efficiency by controlling which energy source provides power to the wheels for a given operational mode [43].

2.2.3 Vehicle Hydrogen Storage System

The hydrogen storage system for the fuel cell Equinox was designed by Enviromech Industries for the Alternative Fuels Team[37]. The ZM180 tank used in the system stores 4.31 kg of hydrogen at its service pressure of 5075psi and is a carbon-fiber wound type 3 tank. The fuel system was designed to comply with the most current codes and standards for in-vehicle hydrogen storage, detailed in Table 8.

Table 8: Safety standards applicable to vehicular hydrogen storage

Code	Description
CGA G-5.5	Hydrogen Vent Systems
NFPA 52	Vehicular Fuel Systems Code
CSA B109-01	Natural Gas for Vehicles Installation Code
CSA B51 Part 2	High Pressure Cylinders for the On-Board Storage of Natural Gas as a Fuel for Automotive Vehicles
B51S1-05	Supplement No. 1 to B51-03, Boiler, Pressure Vessel and Pressure Piping Code
ANSI/AGA NGV 3.1/CGA 12.3 and NGV 12.3-M95	Fuel System Components for natural gas powered vehicles
Dynetek Cylinder And Component Operations Manual	Vehicle Applications

In order to validate the safety of the on-board hydrogen systems in collision events, the stress and strain performance of the tank mounting solution was simulated using a finite element analysis (FEA). The results from the FEA are shown in Figure 20, and were compared with dynamic FEA results as well as real crash data for validation [38].

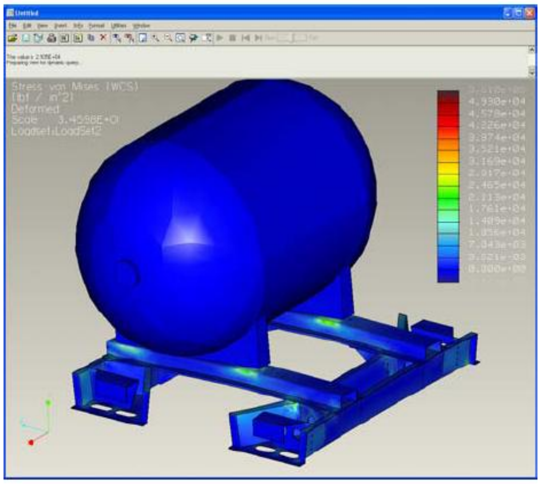

Figure 20: Finite Element Analysis on hydrogen tank mounting structure

The tank fills most of the vehicle's cargo space, highlighting the challenge of storing sufficient quantities of hydrogen on board fuel cell vehicles, as discussed in the introduction. Figure 21 shows the final hydrogen tank packaging.

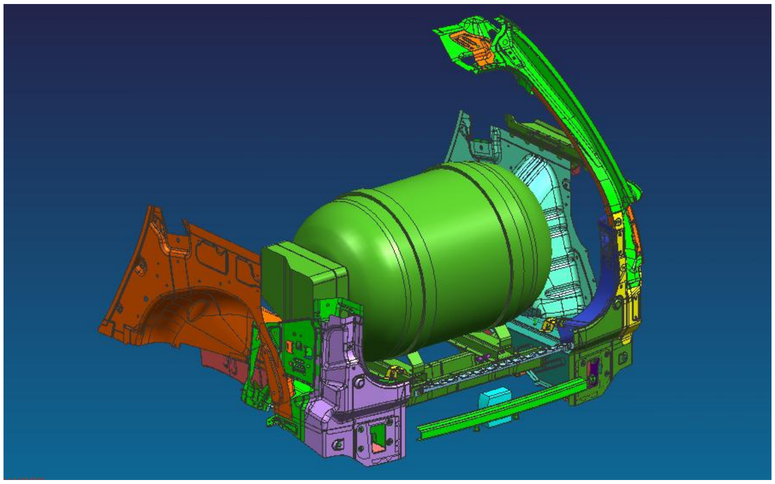

Figure 21: Hydrogen tank location on the Chevrolet Equinox vehicle

2.2.4 Fuel Cell Power Module

The fuel cell power module selected for the Equinox was designed and built by Hydrogenics Corporation, and is capable of producing 65kW nominally at approximately 50% thermodynamic system efficiency. The power module consists of two units, with a total of four individual fuel cell stacks and is shown in Figure 22.

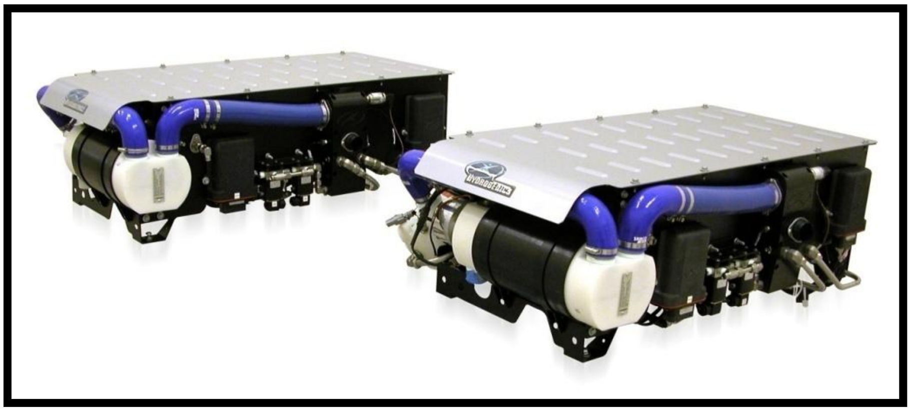

Figure 22: 65kW HyPM fuel cell power module

The power module’s physical, mechanical, and electrical characteristics are summarized in Table 9.

Table 9: Fuel cell power module performance characteristics

	Minimum	Maximum	Unit
Voltage	190	300	V
Current	0	350	A
Power	0	65	kW
System Efficiency	45	56	%
Coolant Temperature	59	68	C
Weight	-	300	kg
Volume	-	543	L

The system has a single compressor which delivers 4200 slpm of air divided between the master and slave modules [39]. It is important to ensure even air flow between the two modules. The compressor is located where the fuel tank was packaged on the stock Equinox and has uneven lengths of piping into the fuel cell power module. To create even flow distribution to each stack module, fluid dynamic simulation (CFD) was used to estimate the difference in airflow. Designs developed using CFD were then tested and tuned to balance the oxidant delivery to each side of the power module. Figure 23 shows the simulation graphics, and an expanded view is found in Appendix F. A restriction was ultimately introduced in the shorter line in order to ensure even airflow between the system halves.

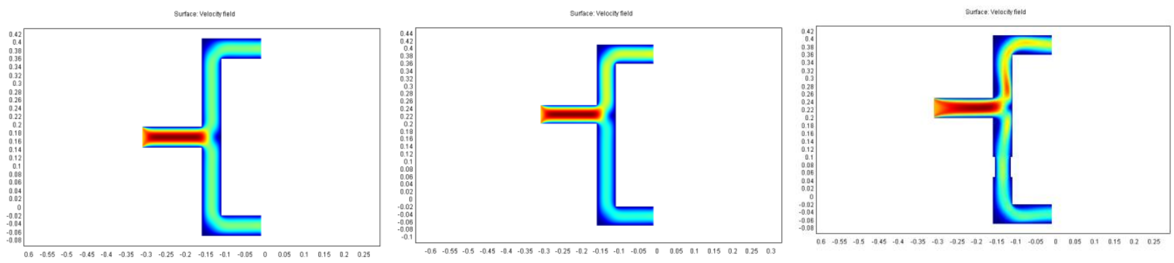

Equal length, 1:1 distribution	Actual length, 1:0.82 distribution	Constriction, 1:0.69 distribution

Figure 23: Computational fluid dynamics on the fuel cell air delivery system [50]

2.2.5 Thermal systems

There are four component cooling loops on the Equinox. Each loop consists of one or more radiator, pump, and fan. The coolant for the battery and motor loops is a 50/50 mixture of water and glycol. The fuel cell power module requires de-ionized water as a coolant to ensure that no current leak occurs between the cells in series. The characteristics of each of the cooling loops are described in Table 10.

Table 10: Fuel cell Equinox thermal system operating characteristics

Loop	Components	Flow (LPM)	Delta P (psi)	Max T (C)	Required Heat Rejection (kW)
Fuel Cell	FCPM	120	6.5	80	80
Battery	Battery, AC Inverter	12	6	45	3
Front Motor	Motor, Inverter, DC/DC	9.5	9	50	4.5
Rear Motor	Motor, Inverter, Blower	8	10	40	3.7

To ensure that each cooling loop would integrate seamlessly into the vehicle, extensive solid models were built. An example of the solid modeling performed is shown in Figure 24 for the fuel cell power module de-ionized water cooling loop.

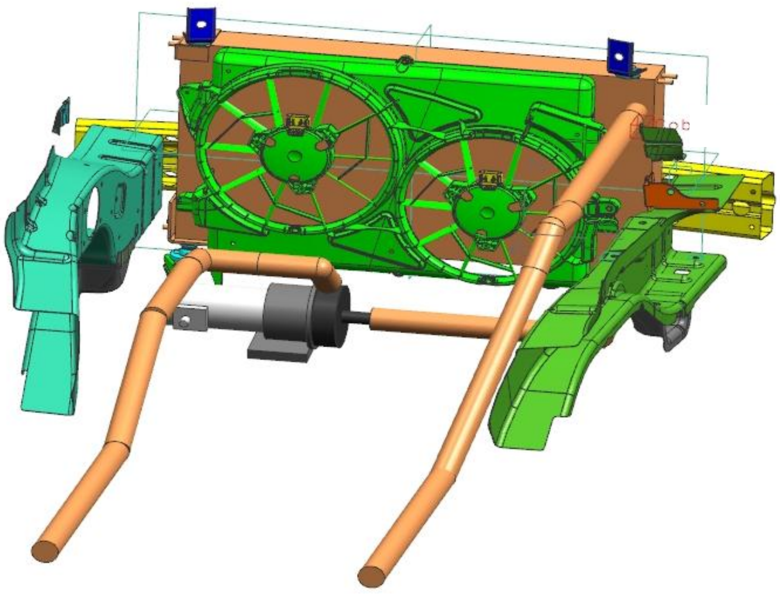

Figure 24: Fuel cell heat rejection system packaging solid model

2.3 Infrastructure Modification

In order to safely handle hydrogen in the Alternative Fuels Team facility, a safety certification process was undertaken. Codes and standards that needed to be adhered to during the design of the hydrogen safe test facility were [51]:

1. NFPA 30A Automotive and Marine Service Station Code
2. NFPA 50A Standard for Gaseous Hydrogen Systems at Consumer Systems
3. NFPA 50B Standard for Liquefied Hydrogen Systems at Consumer Sites
4. NFPA 52 Compressed Natural Gas (CNG) Vehicular Fuel Systems Code
5. NFPA 70 National Electric Code (NEC)
6. NFPA 88A Standard for Parking Structures (Facility Related)
7. NFPA 88B Standard for Repair Garages (Facility Related)
8. NFPA 68 Venting of Deflagrations (Station and Facility Related)
9. California Fire Code

Ventilation systems were added to the UWAFT facility to increase the number of air changes per hour in the test cell during power module operation. A programmable logic controller supervises the ambient hydrogen level, the power supply to devices above 2m, the main door level, and the emergency stop shut off switches. In an emergency state, the hydrogen supply to the facility is isolated, visual and auditory signals warn that an alarm is present, and the ventilation system increases its speed.

Chapter 3: HIL modeling methodology

An overview of the ‘Hardware-in-the-loop’ (HIL) simulation system is shown below in Figure 25, and an expanded view is shown in Appendix F. The PXI real time controller and data acquisition boards, the Mototron controllers, and the interface pad are shown in an expanded view in the figure. The HIL simulation system was constructed and programmed specifically for this thesis. To remain accurate to the physical vehicle control system, identical controller hardware and wiring methods were used.

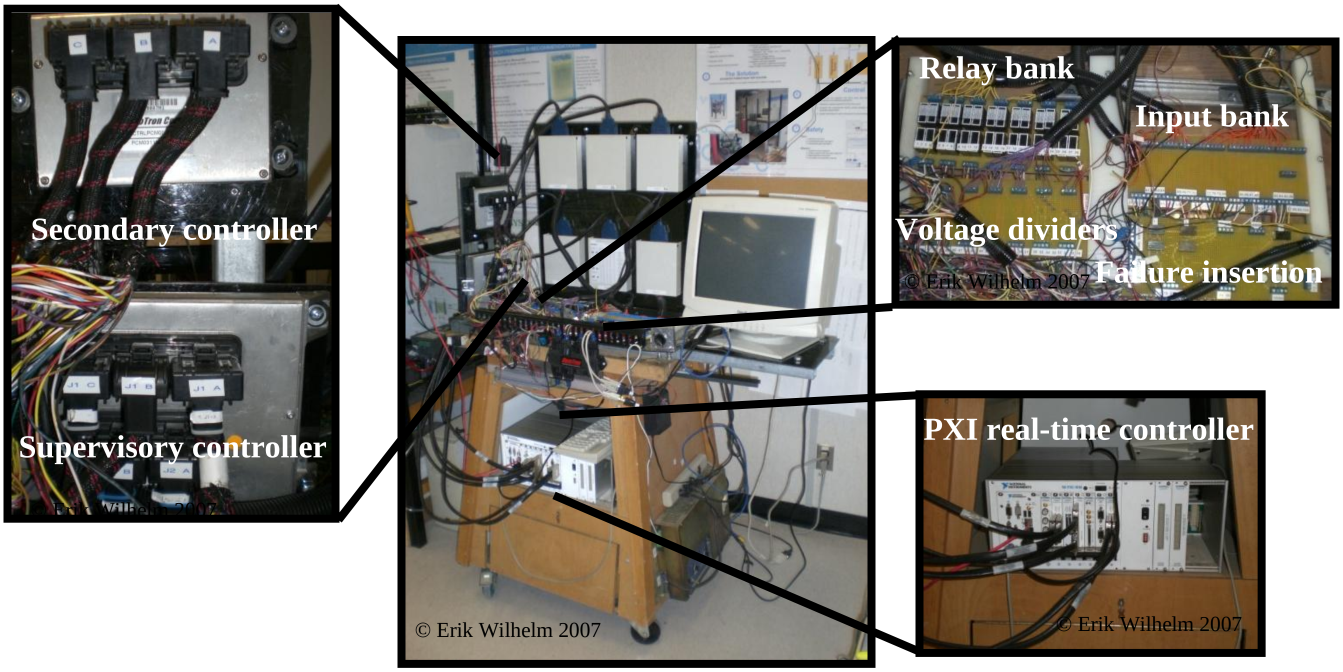

Figure 25: A Hardware-in-the-loop simulation system for a fuel cell Chevy Equinox

A close-up of the interface pad is shown in Figure 25, showing the four circuit boards used to pass the signals between the real time simulator and the controllers. To simulate vehicle low voltage (12 and 24V) controller wiring more accurately, relays similar in size and performance to the vehicle’s relays were wired to the HIL controller’s low side drivers. These relays perform vehicle functions such as switching pumps and fans, controlling lights and contactors. By having these elements in the system, the switching time can be more accurately simulated. The low side driver circuit as well as the circuit for the failure insertion is shown in Figure 26. All other circuits are either pull-down resistors or are pass-through connections. Please see Appendix B for full simulation system connection summary.

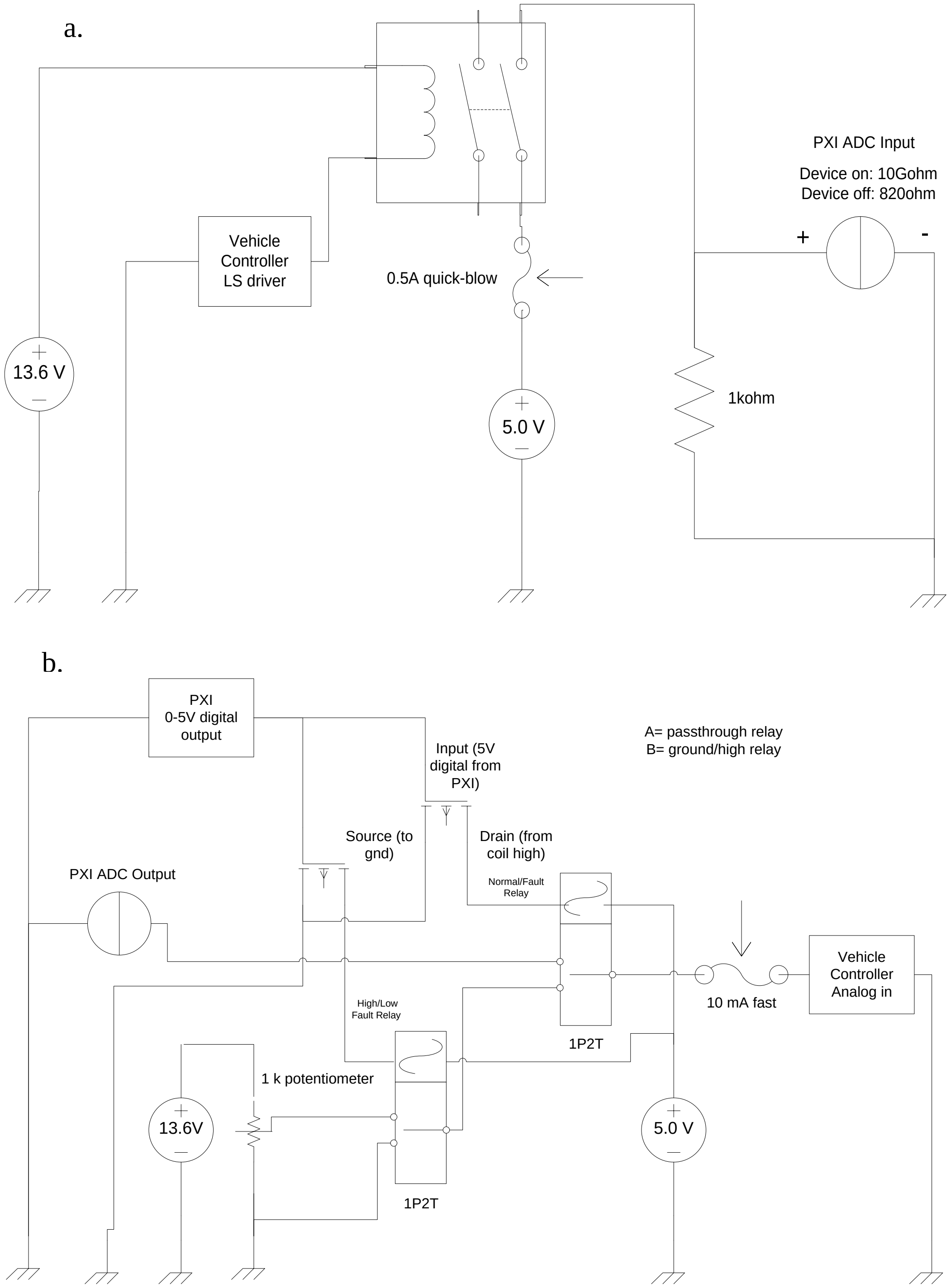

Figure 26: HIL system circuits. Low-side relay driver (a) Failure insertion (b)

The speed with which the HIL simulation system can be reconfigured to run a new test scenario simulation dictates the method used to validate vehicle controls. Iteratively solving control challenges is a valid approach to overall control system development on the HIL system due to the significantly reduced turnaround time for each trial in a virtual environment. Conversely, iteratively solving controls challenges cannot happen as quickly during in-vehicle testing due to safety concerns, prototype powertrain repair cost, and length of trials. Most of the work performed on the HIL system involves a 'guess and check' style of iteration, with initial guesses being arrived at based on engineering analysis and judgment.

3.1 Vehicle Communication Validation

3.1.1 Communication Lag Testing

The objective of this test was to quantify the jitter inherent in the vehicle control hardware. Control system 'jitter' is the failure of the control loop to execute within the predefined loop time. By not performing deterministically (having jitter), a control system poses a risk to vehicle hardware by not being able to accurately and predictably perform its control tasks. The first step was determining the limits of the real-time capabilities on the PXI real-time controller used as the virtual vehicle. The ability of the PXI to deterministically run the vehicle plant model was theoretically confirmed [49] and the next step was then to determine the lag inherent in both signal and data communication busses on the hardware-in-the-loop simulation system. The final step was the extrapolation of the results of the hardware-in-the-loop simulation to the vehicle to evaluate the ability of the control hardware to accurately perform its control tasks over all of its operation modes.

The PXI 8187 real time controller has an Intel P4 processor at 2.5 GHz with 1 GB of RAM. The LabVIEW real time operating system on the controller ensures that the model loop rates are fast enough to ensure that the simulation/control loop stays stable. Using LabVIEW shared variable or RT-FIFO communication protocols to exchange data between time critical and non-time critical loops according to National Instrument's best practice recommendations increased confidence in the ability of the PXI to perform the tasks required for the Hardware-in-the-loop simulation system [40]. The application of these techniques may be found in the sample code in Appendix C. In particular, the methods described below were applied to all code written for the HIL simulator, including:

1. RT-FIFO functions were used to pass data between time critical and non-time critical loops;
2. 'Sleep' time was added to the highest priority control loops to ensure that lower priority loops would have an opportunity to execute;
3. Continuous sample timing was used as opposed to discrete sampling to allow the RT system to pull data from the acquisition board as soon as new data was available;
4. No TCP/IP communication was used in medium or high priority code to ensure that communication lag to the host computer did not impinge on real time operation; and
5. As many code optimization features as possible were allowed when the Simulink real time workshop was building code.

The I/O requirements for the vehicle controller are shown in Table 11. A significant number of the channels available on the Mototron controller could not be used for fuel cell hybrid vehicle control because they were configured for internal combustion engine monitoring and control applications. For example, four inputs are designed to be wired to oxygen sensors which is a critical application in a combustion engine but renders the inputs unusable in a fuel cell vehicle operation. The full control electrical connection schematic for the HIL simulation stand can be found in Appendix B and outlines all connections, including power, ground, and other physical interface pad connections.

Table 11: Hardware-in-the-loop simulation system input/output requirement summary

Signal Type	Channels
Analog In (0-5V)	44
Analog Out (Relay Drivers)	22
Analog Out (PWM)	14
CAN	3
Serial	1
Total I/O	**84**

The controller area network (CAN) communication on the vehicle takes place at 500 kbit/s and all PWM signals are transmitted at 10 kHz.

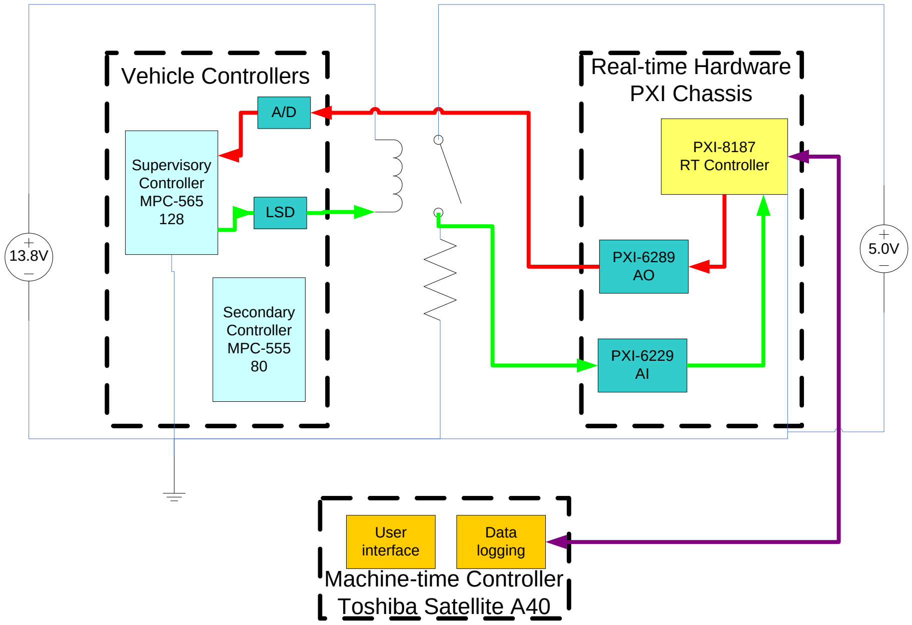

Figure 27: Communication lag test data flow: Begins red, ends green

The communication lag test involves two channels on each of the PXI and the Mototron controllers. The PXI generates an output signal, the Mototron controller reads the signal in and passes it directly to a low side driver which induces 12V across the pull down resistor read by the PXI. The outgoing pulse is shown in Figure 27 as a red line and the echoed signal is shown in the Figure as a green line. This setup passes signals as closely as possible to the way that they are actually passed during vehicle operation.

The determinism check algorithm was designed to run continuously in the background while other code is running to ensure that the system remains stable when more complicated control algorithms are developed and deployed on the controller. Figure 28 shows the algorithm, which relies on triggered subsystems to execute timing shifts when the pulse is sent and received to determine the lag in the signal.

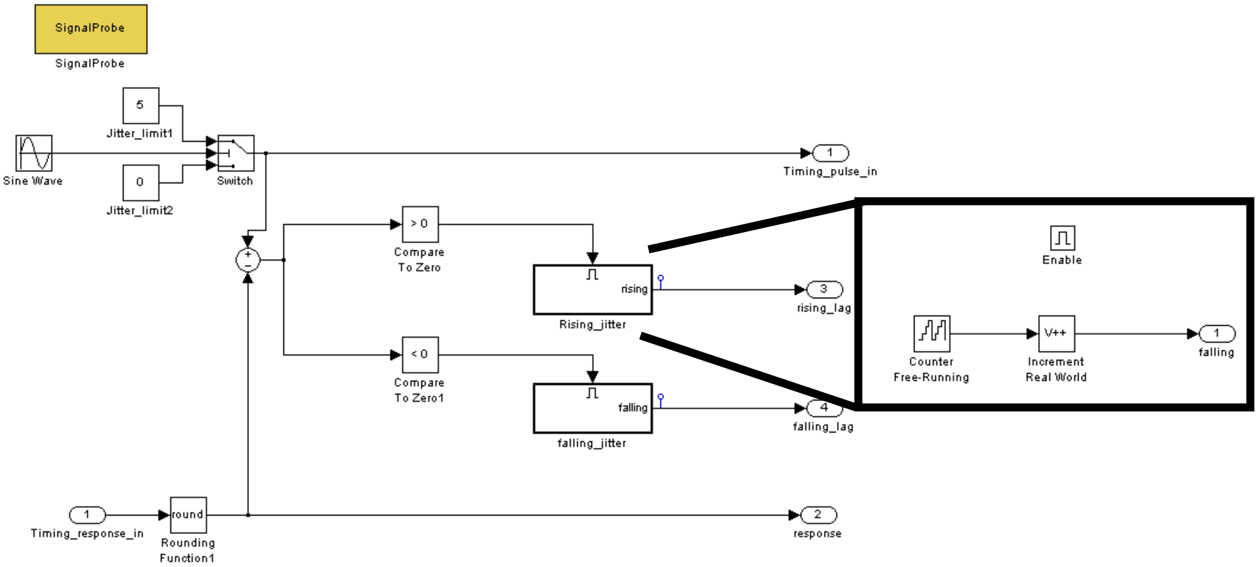

Figure 28: Timing pulse algorithm. Inset: Rising jitter triggered subsystem

A threshold crossing was chosen to trigger the analog output because a smooth square wave is computationally intensive and one of the key assumptions in this trial is that the determinism calculation adds negligible processor overhead relative to the more computationally difficult vehicle control algorithms. The assumption that the PXI is functioning deterministically was tuned and is checked in-service by using the LabVIEW ‘is late?’ function [41]. The line inductance on the HIL system is assumed to be average relative to any line inductance on the vehicle. Effort was taken to ensure that similar relays were used and that comparable pull-down resistors were employed.

3.1.2 Communication Bus Loading

The vehicle relies heavily on its controller area network (CAN) communication bus. All of the powertrain components with the exception of the DC/DC converter have CAN-enabled sub-controllers that respond to safety and operation commands. The network's ability to handle high bus loads is therefore critical to safe operation. The CAN 2 bus is the high-traffic bus that connects most major powertrain elements. Please refer to Figure 19 in Chapter 2 for a description of the communication bus architecture. High bus loads occur on the fuel cell hybrid Equinox in particular when:

1. Testing is being performed on the DC/DC converter requiring the 1ms CAN data logging message to be sent;
2. Asynchronous fault messages are being sent; and
3. Noisy communication bus signals are causing transmission errors requiring messages to be re-transmitted.

In order to quantify the ability of the controller to handle heavy traffic on the CAN 2 network, the HIL system was configured to load the bus with signals. The signals chosen for the bus loader application are ones that would normally be seen during vehicle operation and are tabulated in Table 12.

Table 12: Messages from vehicle CAN bus sent by PXI for bus loading simulation

ID	Data	Signal
0x264	1	FCVM_MinCell_Voltage
0x316	2	MCU2_PowerReduction
0x318	3	FCPM_RuntimeMinutes
0x220	4	MCU1_PowerReduction
0x235	5	SC1_TankSolenoid
0x584	6	MCU1_ActualTorque
0x488	7	MCU1_Heatsinktemp
0x594	8	MCU2_Torque
0x396	11	MCU2_CurrentEstimation
0x298	10	MCU2_Heatsinktemp
0x387	12	FCPM_Coolant_overtemp
0x402	13	FCPM_Airflow

Their data payloads were modified to allow them to be easily identified in the analysis and their transmission rate was varied to perform the loading test. Figure 29 shows the bus loader model and the associated VI used to control the PXI as it transmitted CAN messages.

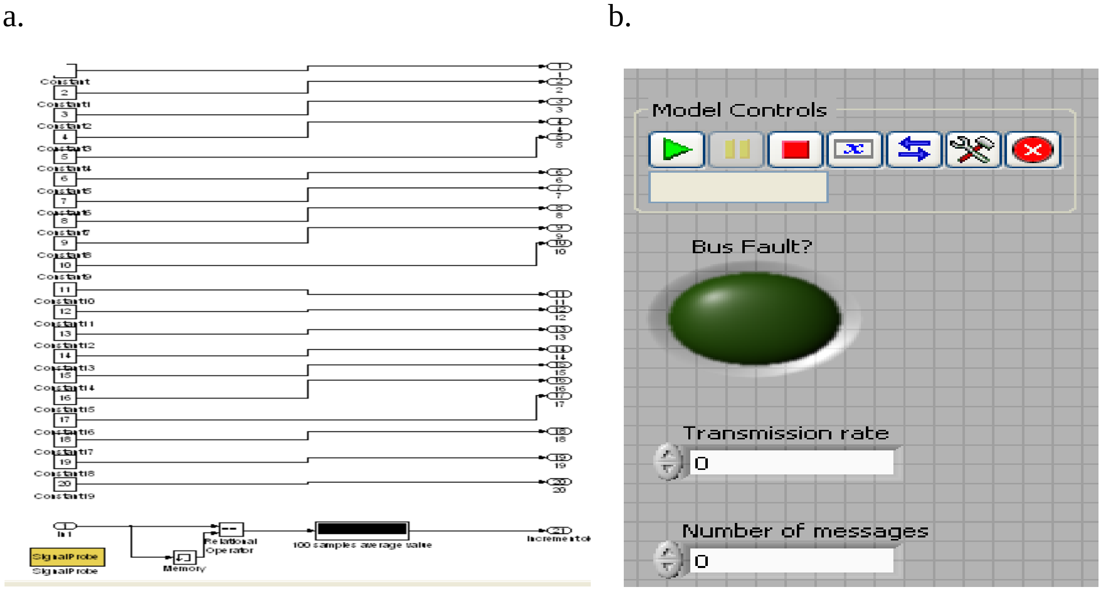

Transmission rate: 0

Number of messages: 0

Figure 29: Bus loader model (a) and associated CAN transmission VI for the PXI (b)

A bus fault was determined by observing the battery counter message that is broadcast by the controller to the battery pack. If 100 successive counts of that message are not received or received in error, a bus fault is declared.

3.2 Controller Safety Response Validation

3.2.1 Fault Message Handling

Ensuring safe vehicle operation at all times is a critical objective of the vehicle controller. In order to accomplish that goal, the controller must be validated on the Hardware-in-the-loop simulation system to ensure that it is able to manage fault messages from all of the powertrain element sub-controllers appropriately. For safety critical systems, a rigorous layer of control and diagnostic strategies that ensure that the probability of events that could lead to dangerous conditions (e.g.. startling the driver with an unintended acceleration, loss of braking function) occurring is below a reasonable value.

Countermeasures such as dual path calculations, dual processors, checksum, and serial data validity bits are implemented in these safety control layers.

A challenge faced by the team during the fault handling development was that the fuel cell power module (FCPM) component controller was consistently reporting an unexpected stream of error messages when a fault condition was present. This made appropriate control response and a subsequent guarantee of safe vehicle conditions impossible. The hardware-in-the-loop simulation allowed the assessment of control response to critical fuel cell operating conditions such as over-temperature, under-voltage and other states. Table 13 is a truth table that shows the desired response to received CAN bus fault messages.

Table 13: Fuel cell fault management truth table

Condition	Fault	Ds 1	Ds 2	Ds 3	Ds 4	Ds 5	Ds 6	Ds 7	Ds 8	Ds 00
0x187 bit 1 == 1	Coolant Overtemp	T	F	F	F	F	F	F	F	F
0x187 bit 33 == 1	Low Coolant Flow	F	T	F	F	F	F	F	F	F
0x187 bit 0 == 1	Stack Undervoltage	F	F	T	F	F	F	F	F	F
0x187 bit 7 == 1	External E-Stop	F	F	F	T	F	F	F	F	F
0x187 byte 0 == 3	Wait for OCV	F	F	F	F	T	F	F	F	F
0x187 byte 0 == 5	No Fault	F	F	F	F	F	T	F	F	F
0x187 byte 0 == 8	Fault state	F	F	F	F	F	F	T	F	F
0x187 byte 0 == 11	Open loop mode	F	F	F	F	F	F	F	T	F
Action		**Red. Pwr.**	**Limp St.**	**Restart**	**Stndby**	**Batt. St.**	**Log**	**Fault**	**Red. Pwr.**	**Pwr. Susp.**

To troubleshoot this issue and to design a response solution, a model of the fuel cell power module was composed. This extremely simple error analysis model is shown in Figure 30. A series of constants are defined in the model and are varied using the simulation interface toolkit (SIT) front panel shown in Figure 31. The SIT is a tool that was developed to automatically generate driver code to interface a compiled Simulink model with National Instruments hardware [40]. SIT writes code specifically for interfacing real-time targets to host computers.

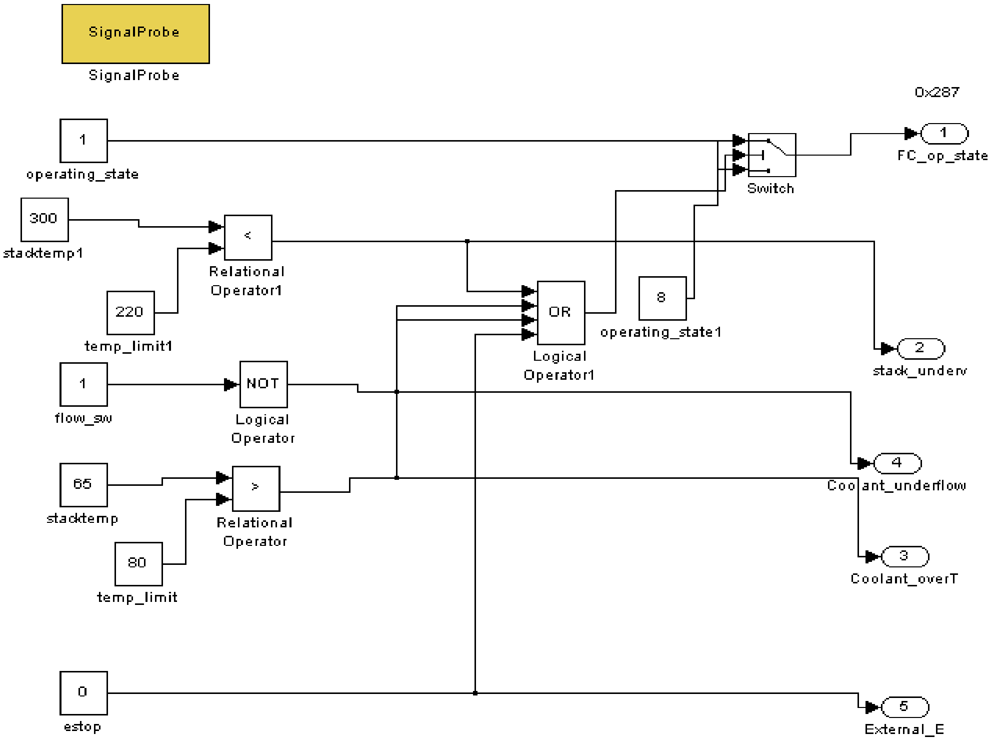

Figure 30: Fuel cell power module fault insertion model

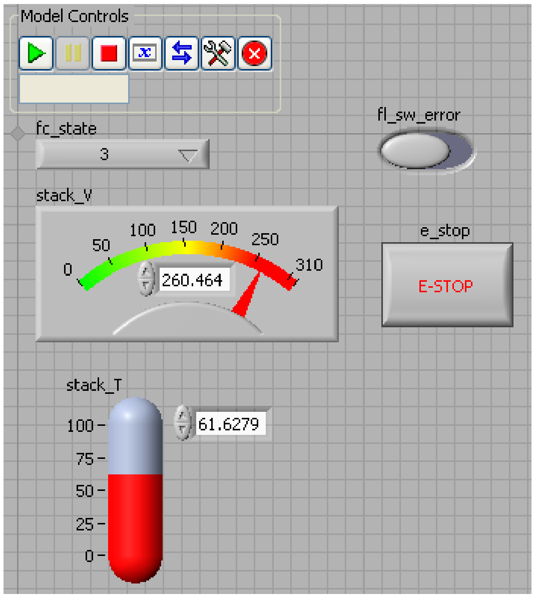

fc_state 3

stack_V 260.464

stack_T 61.6279

Figure 31: Simulation interface toolkit fault handling algorithm

The test was performed in order to develop fault memory functionality on the Mototron controller in order to capture the erratic fuel cell power module fault handling response.

3.2.2 Signal Failure Insertion

Vehicle operating environments subject wiring harnesses to extreme temperature variation, debris, water, salt, and snow and it is not uncommon for wire harnesses to fail as a result. It is crucial that, if a wiring harness fails, the elements of a vehicle control system that are affected by the broken wire do not cause unsafe vehicle operation. A good example is in throttle-by-wire operation, if one of the redundant throttle pedal position sensors fails, a wide-open-throttle condition should not result. There are three failure modes of interest:

1. Short to ground: occurs when a bare control wire contacts the chassis
2. Short high: occurs when a bare control wire contacts battery positive or live control wire
3. Floating short: occurs when a control wire is severed resulting in a unpredictable line voltage

The objective of the hardware-in-the-loop failure insertion testing is to ensure that if any of these wire harness failures occur, the controller will respond appropriately.

To perform this validation, three target control signals were selected and their control algorithms were extracted from the main control code. The selected signals were chosen because they were identified as being critical to safety in the Design Failure Modes and Effects Analysis (DFMEA) carried out by the Alternative Fuels Team. The signals and desired responses and can be found in Table 14. The ‘IGBT ok?’ signal is normally a 5V signal that is sent by the high frequency switch in the DC/DC boost converter. If the switch fails, current will be drawn in an uncontrolled manner from the fuel cell, which can cause damage to equipment and injury to passengers. The safety in the vehicle code is meant to disable the fuel cell if the 5V signal is not read as 5V, or is read above or below that value by a slight amount.

Table 14: Three safety-critical control signals selected for fault insertion

		Expected controller response		
Signal	**Intended**	**High**	**Float**	**Low**
IGBT ok?	failed IGBT	disable FCPM	may miss fault	disable FCPM
Gear position	Drive or Reverse	lock out torque	lock out torque	lock out torque
Throttle position A	Wide open throttle	lock out torque	lock out torque	lock out torque

The gear position and throttle position signals control torque direction and magnitude, respectively. Failure on either of these lines should result in a 'zero-torque' command to both front and rear motors. There is particular concern about the gear selection system because it was custom-built for the vehicle using retrofitted contacts.

The control code dealing with each of these signals was abstracted from the most current version of the competition code. The code sections were extracted verbatim and care was taken to ensure that the fidelity of the controller behaviour was maintained by copying exact syntax from the main control code to the failure insertion code shown in Figure 32.

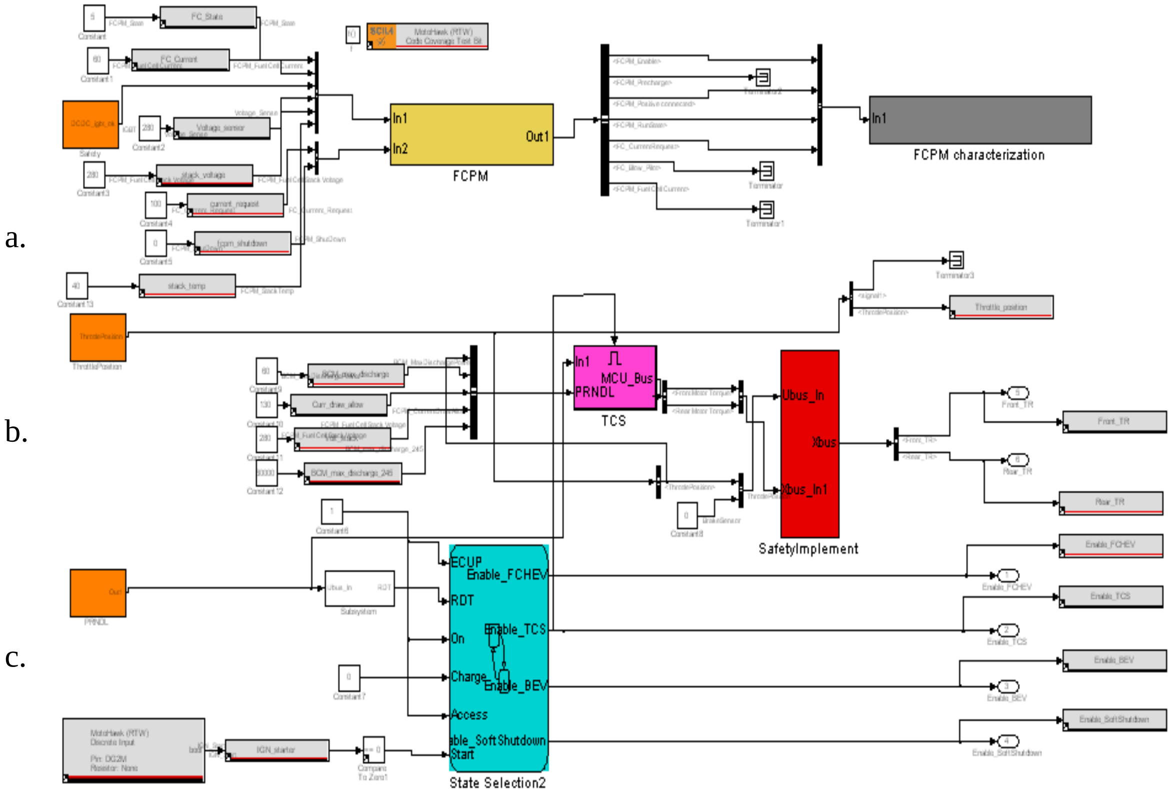

Figure 32: Failure insertion code. IGBT ok (a). Throttle position (b). PRNDL (c)

The control code was programmed to the appropriate controllers and the failure insertion code from Figure 33 was established in order to apply the desired plant signals from the vehicle. The ‘IGBT ok?’ signal was constantly set low to simulate a failed switch. The gear selector values were changed to test varied responses, as were the throttle position values.

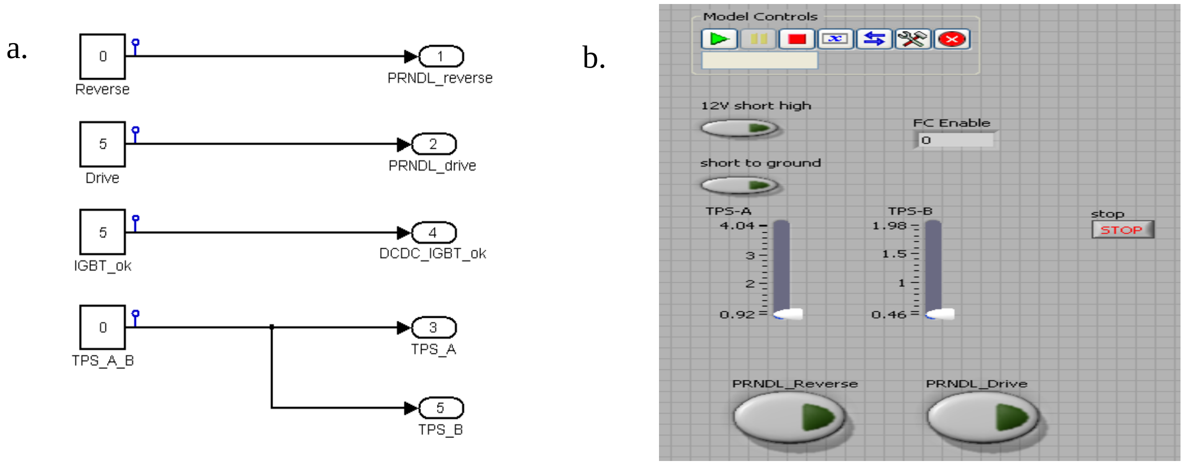

Figure 33: Failure insertion plant model. Simulink model (a) Labview control (b)

3.2.3 Voltage Droop Sensitivity

The vehicle control systems are required to respond appropriately when the 12V bus voltage drifts outside of its normal operating range. During normal operation, 12V system can droop if the NiMH battery state of charge is too low or if the instantaneous current draw is too high (during power steering, for example). The 12V can spike if the boost converters fail or receive an erroneous input signal. In either case, it is important that critical safety and operation functions performed by the controller continue uninterrupted. In order to assess the controller performance during 12V voltage spike (18V) and droop (8V) conditions, that hardware-in-the-loop simulation system was used to simulate voltage drift. Low side driver, CAN bus, and PWM signals were monitored to ensure that their outputs did not behave erratically with variations in the 12V bus voltage, and no such behaviour was detected.

3.3 Vehicle Dynamic Control System Validation

From the perspective of safe vehicle operation, the control algorithms that determine the request for torque from the electric drive motors and the gear and throttle position are critical. The algorithms must not only consider driver intent from the throttle and gear position, but also the condition of the power delivery systems (fuel cell, DC/DC converter, and battery) and the resulting effect of an increase in power. Experience has shown that torque control on full electric hybrid vehicles is not trivial. During the second year of the hybrid fuel cell vehicle development, at least two unintended accelerations were caused by torque control algorithms lacking the required level of safety. To avoid these problems in the third competition year, software-in-the-loop (SIL) verification methods were applied to traction control and regenerative braking control algorithms before they were implemented in the vehicle.

The software-in-the-loop model was extracted from the hardware-in-the-loop model. This was done to target relevant torque control signals only and to avoid confounding with other potential errors in the control code that could mask the analyzed responses. The drive train and power generation plant models are shown in Figure 34. The chassis and drive train model consists of a vehicle dynamics block, four tire blocks, and inertial elements from Simulink’s SimDriveLine™ toolbox.

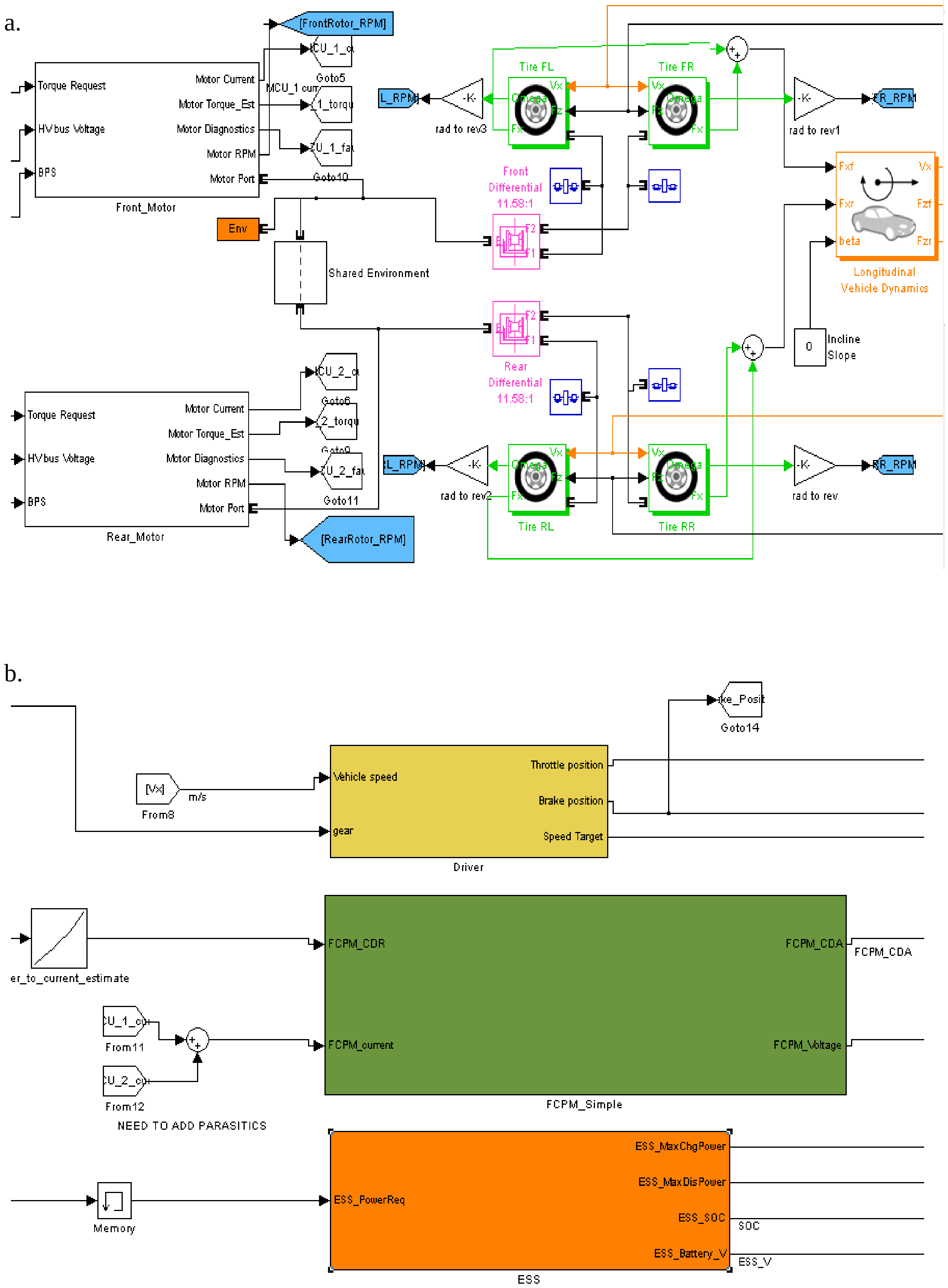

Figure 34: Dynamic vehicle model (a) Powertrain model (b)

The motor models are empirically developed and use efficiency under specific torque and speed operation depicted in Figure 35 to calculate instantaneous current and voltage values. The motor models broadcast actual fault messages according to how they are operated. The battery and fuel cell models, which will be discussed in greater detail in the following chapters, are also capable of reporting faults according to the way that the controller and powertrain are handled.

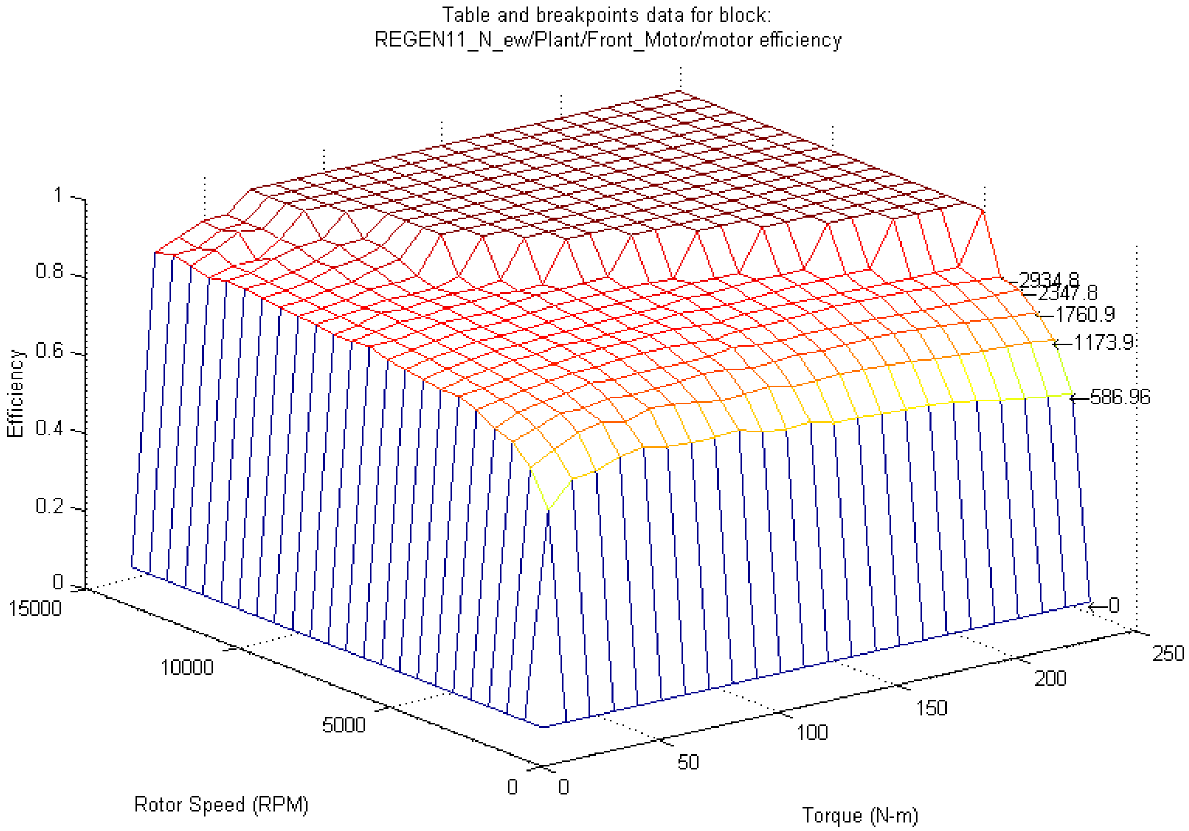

Figure 35: Efficiency table for the Ballard 312V67 MG AC induction motors

The dynamics blocks are loaded with the vehicle characteristics shown in Table 15 and have undergone sensitivity validation. No single input variable was found to have an overriding influence on the dynamic model's behaviour. These assumptions have proven to yield stable model responses to driver inputs and are based closely on the Equinox characteristics.

Table 15: Dynamic simulation model assumptions

Motors	**Unit/Description**
11.58:1	gear ratio in Ranger motor
RPM/torque curve	calculated from Ballard IPT data
Torque, current, efficiency curve	calculated from Ballard IPT data
0.05	response time (s) from manufacturer specifications
359	max motor voltage
239	min motor voltage
25	Nm- torque request offset
13500	max motor speed
435	A - max motor current (propel and regen)
Vehicle	**Unit/Description**
2178	vehicle mass (kg)
0.417	Coefficient of drag
2.686	Frontal Area (m^2)
2.3975	length from CG(assumed centered due to our 50/50 weight split) to front
2.3975	length from CG(assumed centered due to our 50/50 weight split) to rear
0.4	height of CG (assumed based on low weight distribution from fuel cells)
Half-shafts	**Unit/Description**
10.5	lbs (front)
11.2	lbs (rear)
0.04446	kg-m^2 (front)
0.08892	kg-m^2 (rear)
Tire	**Unit/Description**
0.35605	rolling radius (m)
Braking torque	**Unit/Description**
30	starting speed (mph)
0	ending speed (mph)
35	stopping distance (ft)
1.60060015	time to stop (s)
-8.33125	deceleration (m/s^2)
2095	mass (kg)
-17453.96875	force (N)
0.3	braking radius (m)
-5236.190625	N-m braking torque

The traction control and regenerative braking simulation models require specific input from the plant model and create output commands accordingly. These inputs and outputs are listed in Table 16.

Table 16: Traction control and regenerative braking inputs and outputs

Input	Unit	Output	Unit
Motor1_Speed	RPM	Front_motor_torque	N-m
Motor2_Speed	RPM	Rear_motor_torque	N-m
Motor1_Torque_est	N-m		
Motor2_Torque_est	N-m		
Throttle Position	%		
Brake Position	%		
Battery_PWR_allowed	kW		
Battery_CHRG_allowed	kW		
FCPM_Curr_allowed	A		
FCPM_Voltage	V		
Gear	enumeration		
Regen_cutoff_speed_start	RPM		
Regen_cutoff_speed_end	RPM		
Max_regen_torque	N-m		

The dynamic plant model is able to provide each of the inputs to the traction control block so that regenerative braking and traction control functionality can be validated.

3.4 12V system validation

The second section of this modeling effort applied to the method of controlling the 12V NiMH battery charging system. The 12V systems were identified as having a higher probability of failure with significant failure effects on vehicle operation in the team’s DFMEA. It was therefore imperative to design a robust and lightweight 12V system and to test its operation and control before it was implemented. Vicor DC/DC buck converters and an AA Portable Power MH-F13000 nickel metal hydride (NiMH) battery pack are at the heart of the 12V system [36]. The DC/DC converters step the high voltage bus (300V) down to 13.4 V during normal operation. They are also able to reduce the bus voltage to 12.5 volts in a ‘reduced parasitic’ mode if the current drawn from them exceeds 140A, and to 9 volts in a ‘shutdown’ mode if the current draw exceeds 170A. If the temperature exceeds 90°C, the Vicors reduce their output power and if the temperature exceeds 95°C, then they shut down. These operating modes serve to protect the Vicors from damage in over-temperature or over-current conditions, which are failure modes were observed in previous rounds of competition. The intended battery control logic is outlined in the stateflow chart in Figure 36 and includes the safety considerations that are made to protect the occupants and the vehicle.

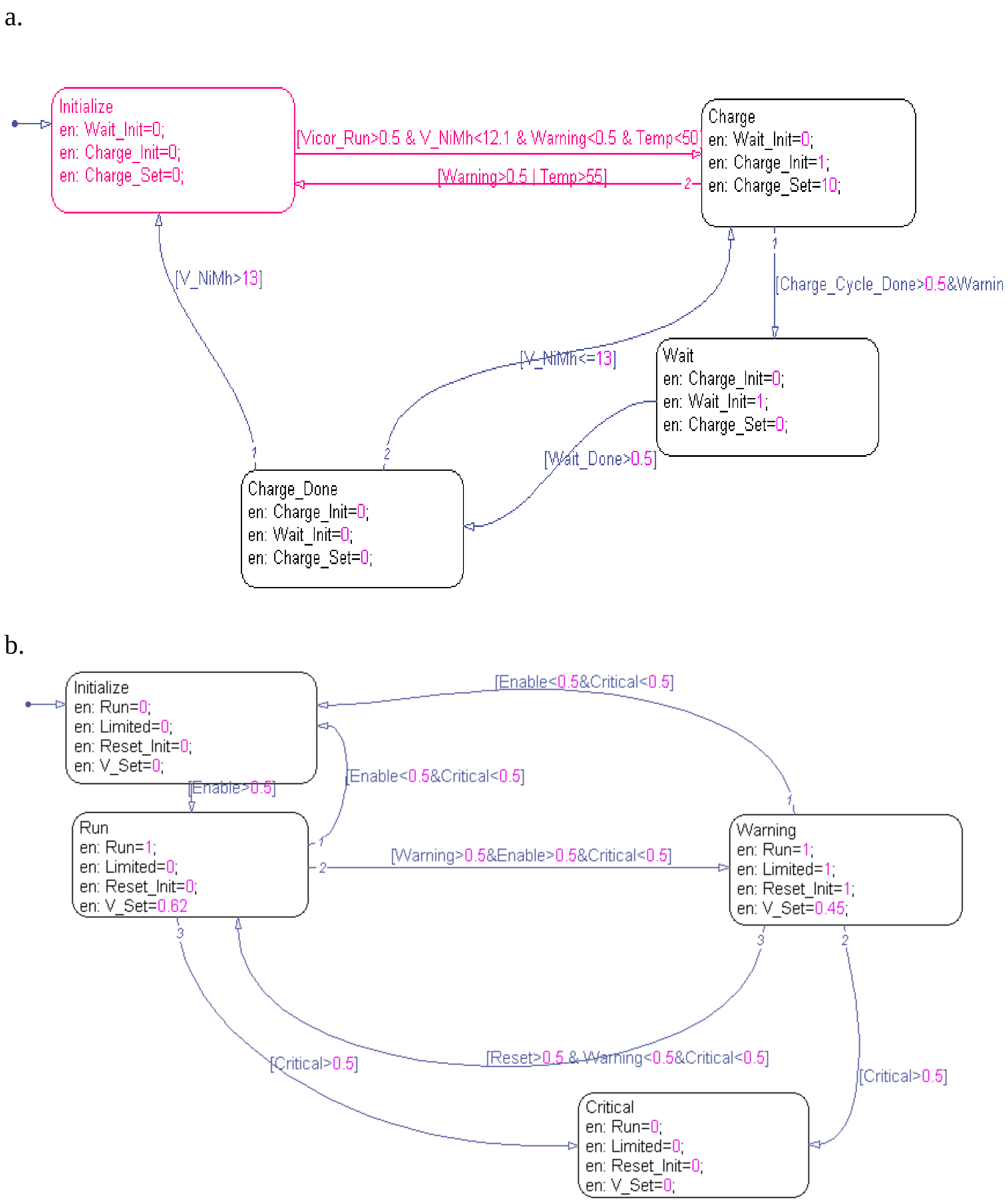

Figure 36: Battery control stateflow (a). Vicor safety stateflow (b)

The battery control inputs and outputs are outlined in Table 17.

Table 17: Battery control system input and output

Input	Unit	Output	Unit
Battery_state	N/A	Voltage setpoint	V
VicorA_temperature	C	PWM signal	%
VicorB_temperature	C		
VicorC_temperature	C		
VicorA_current	A		
VicorB_current	A		
VicorC_current	A		
12V_battery_voltage	V		
12V_battery_current	A		

To test the battery control system, a battery model was designed to simulate the behaviour of the battery pack. The pack has a nominal voltage of 12 volts and a capacity of 13 Ah. Its charge and discharge characteristics and internal resistance are known from the manufacturer's data sheet. This information is used to build the battery model shown in Figure 37.

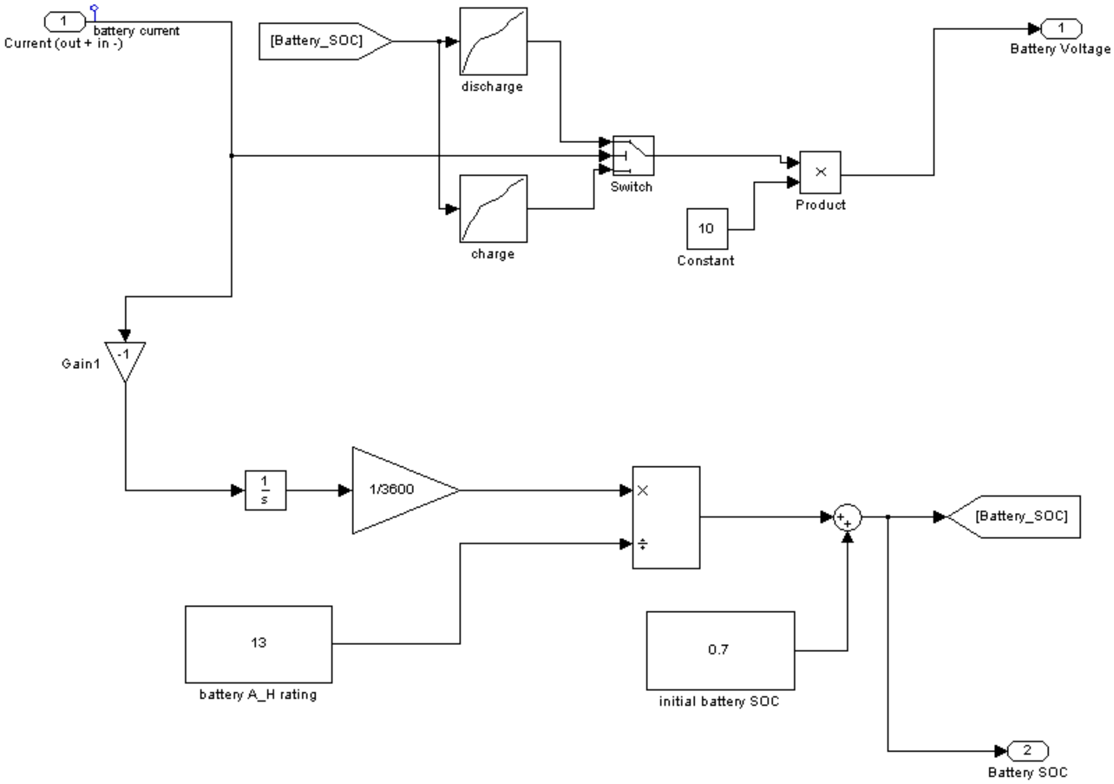

Figure 37: 12V NiMH battery Simulink model

This simple battery model is integrated into a larger HIL enabled model to be run on the PXI. The top-level model contains constants such as the 12V charge bus voltage (labeled 3) and the discharge current (labeled 4) that can be modified in real time using the simulation interface toolkit in order to test a particular control strategy. The top-level model is shown in Figure 38.

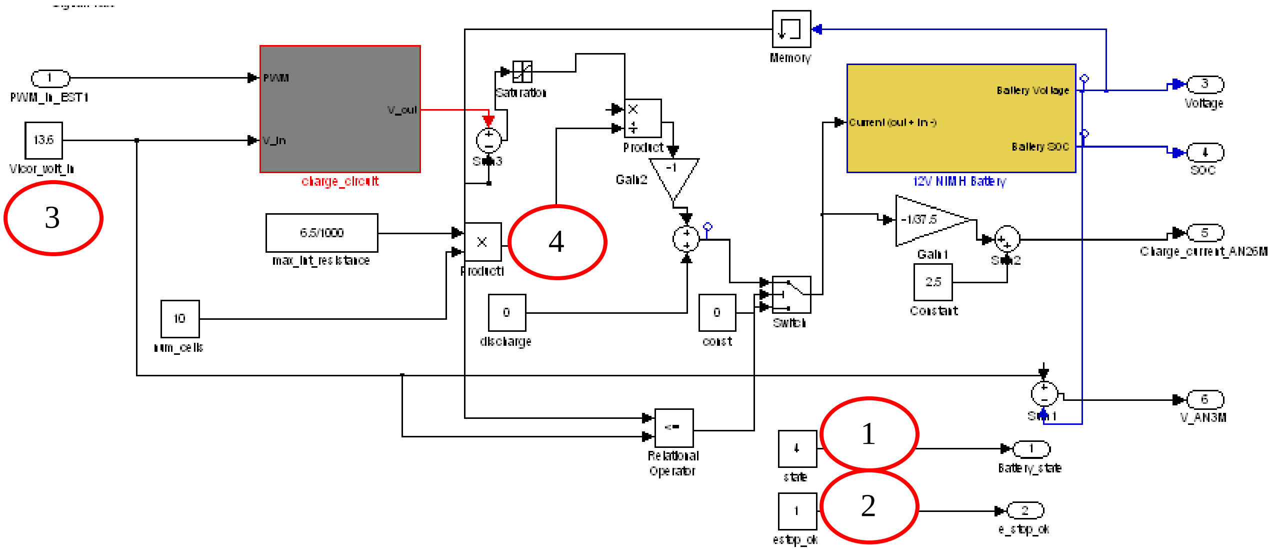

Figure 38: Top level 12V battery HIL model

Other configurable variables in this model are the battery state message (labeled 1) and E-stop ok variable (labeled 2) from the rear secondary controller. The initial SOC of the battery is assumed to be 70% and the initial drain current is 0.

3.5 Offline Development

A major advantage of the hardware-in-the-loop simulation system for the Alternative Fuels Team is the ability to develop control algorithms offline for auxiliary powertrain subsystems. A Graphical User Interface (GUI) and a Bluetooth – CAN transceiver system were established on the HIL simulation system without requiring any vehicle resources or down time. These non-powertrain essential subsystems add significant value to the vehicle's consumer acceptability, but are not important enough to warrant taking the vehicle offline for their development.

To develop the CAN to Bluetooth interface, the functional requirements were defined and can be found in Table 18. The purpose of the device is to receive critical CAN messages so that test engineers can monitor the powertrain during operation and the battery during charge mode. Of the four CAN signals that were identified as being of interest for live wireless monitoring, the battery state of charge and voltage are the most critical.

Table 18: Critical CAN messages for broadcasting via Bluetooth to wireless device

CAN Signal of Interest	Period	Unit
Battery SOC	100 ms	%
Battery V	100 ms	V
FCPM power	Asynch	kW
Vehicle speed	100 ms	kph

The model that was developed to perform this testing was then built for the PXI. The model function is to create artificial CAN signals that are broadcast to the R.M. Michaelides hardware called the CANVIEW-Bluetooth™. The technical specifications for this device can be found in Appendix A. The model is extremely simplistic. It simply outputs repeated sequences to specific Simulink out ports. These out ports are defined as CAN signals using the simulation interface toolkit (SIT) and the CAN baud rate must be hand-coded to 500 kbits/s in the SIT “io_init” virtual instrument. The simple model, the CAN definition for the battery SOC signal, and the data transmission path are shown in Figure 39.

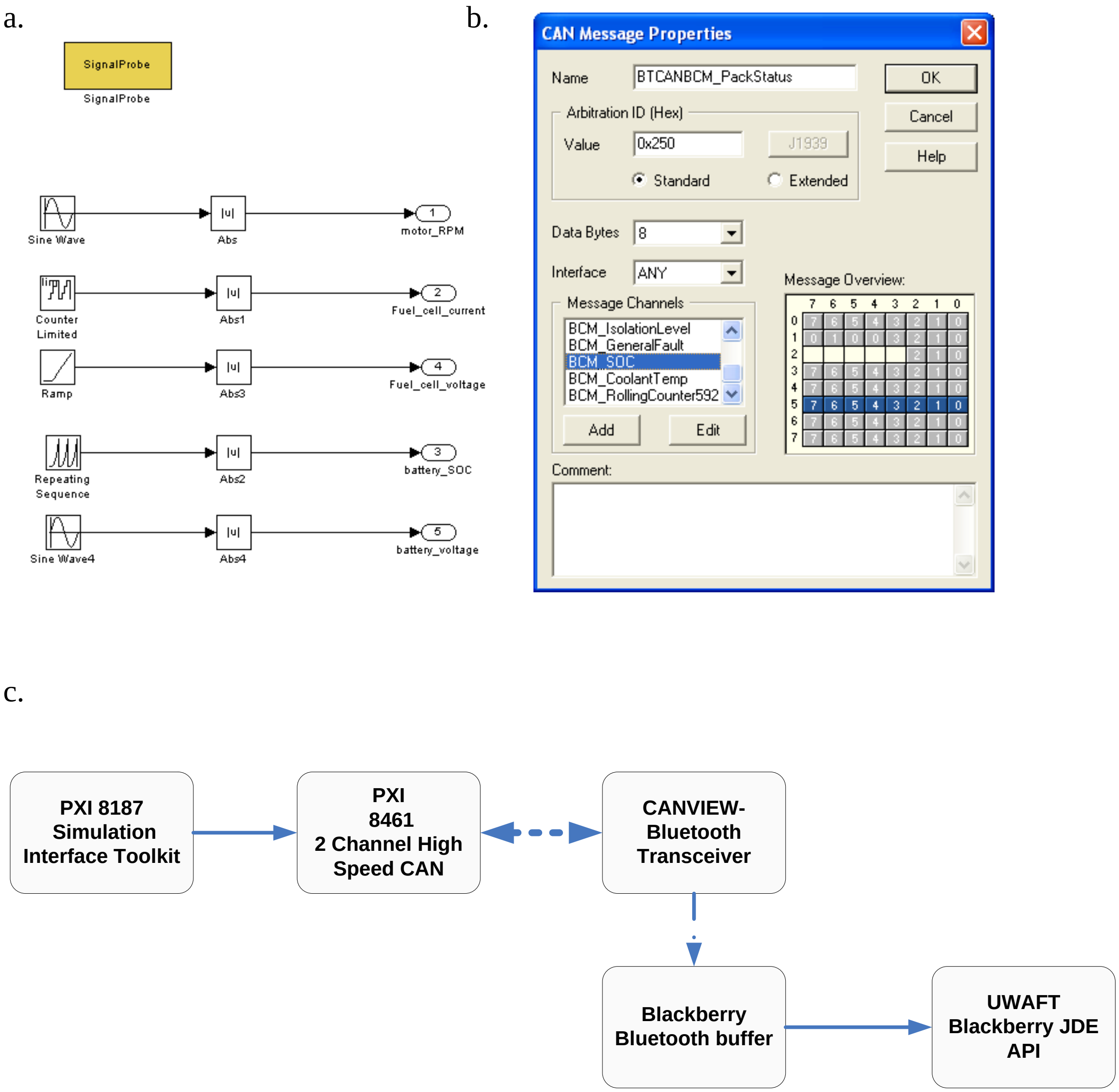

Name BTCANBCM_PackStatus

Arbitration ID (Hex)

Value 0x250

● Standard ○ Extended

Data Bytes 8

Interface ANY

Message Channels

- BCM_IsolationLevel
- BCM_GeneralFault
- BCM_SOC
- BCM_CoolantTemp
- BCM_RollingCounter592

Comment:

Figure 39: Bluetooth to CAN development on the HIL system. Simple HIL model (a) Battery CAN message definition (b) Data transmission pathway (c)

Two major challenges existed for the integration of the graphical user interface (GUI). The first was establishing a method of communication between the GUI and the vehicle, and the second was ensuring that the GUI displayed the correct value during operation. The National Instruments TPC-2006 is a touch screen device that runs Windows CE™ and is shown in Figure 40. It has four serial ports, of which one is a 2-wire RS-485 port. The Mototron ECU-565 is also capable of communicating over 2-wire RS-485. The availability of this communication port and protocol and the lack of CAN device drivers written for WinCE drove the decision to use the 485 ports to communicate with the GUI.

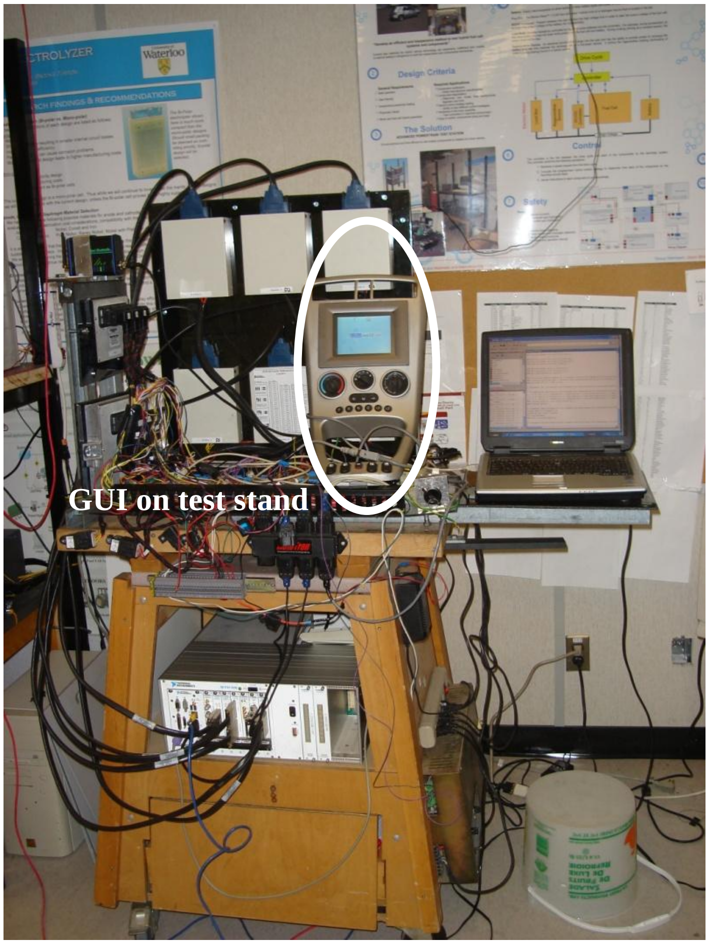

Figure 40: Graphical user interface being developed on the HIL system

The GUI test HIL model is shown in Figure 41 and would be identical to the code implemented in-vehicle. This interface simulates the gear selection through a LabVIEW front page and also allows a ground fault event to be simulated. The GUI displays required information for the driver related to traction, necessitating a high level of reliability. These messages are then sent over RS-485 using code identical to that which is loaded on the Mototron controller.

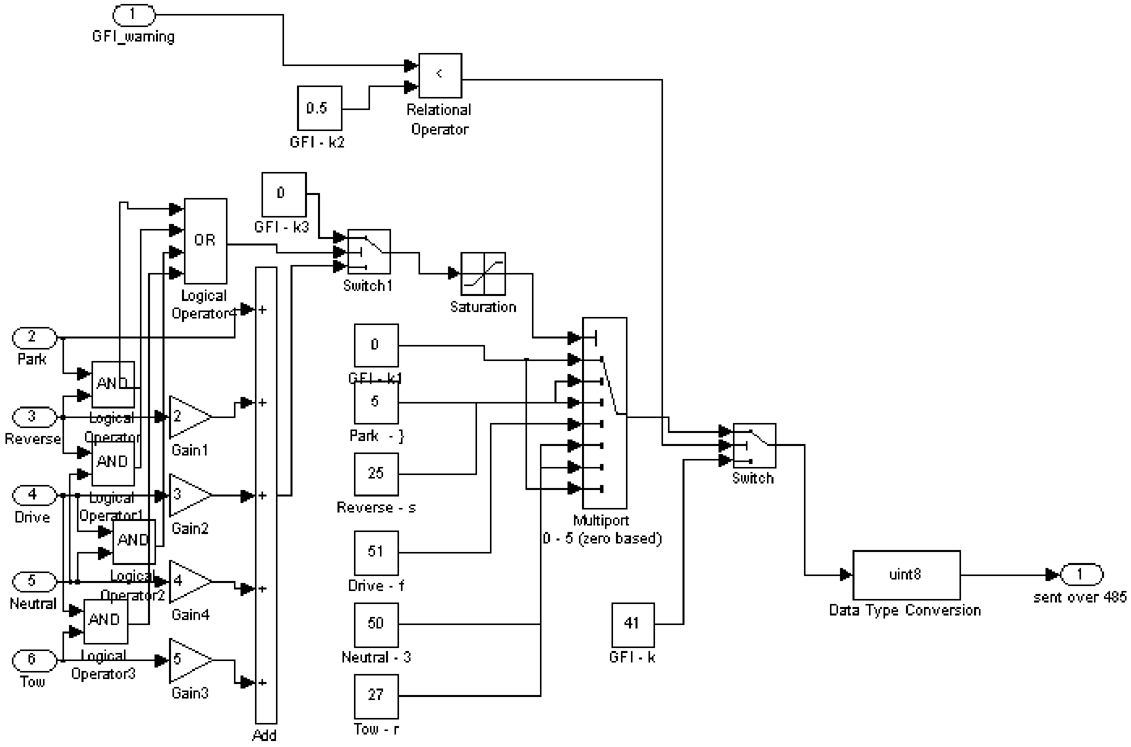

Figure 41: GUI vehicle controller interface code

In order to meet consumer acceptability requirements, the gear selection function on the GUI must respond to the mechanical movement of the parking pall without a perceived time lag. In addition, the colours must be selected to ensure that the selected gear is visible even when sunlight is streaming into the vehicle.

Chapter 4: Validation Results and Discussion

The control validation performed in this thesis solved several critical controls issues and added value to the hybrid fuel cell vehicle development during the third year of the ChallengeX competition. The development time saved, the improved safety to personnel and materials, and the improved systems understanding has justified the effort expended in extensive virtual control validation. Parallelizing the control development in order to develop and debug control strategies and to create first estimates for calibration parameters prior to vehicle availability was made possible through HIL on battery charging, Bluetooth™ interface, and graphical user interface control code. Software-in-the-loop torque control validation was used to reduce troubleshooting and calibration time once a vehicle became available for dynamic testing.
HIL simulation was instrumental in ensuring that problems that are very difficult to identify at the vehicle level such as processor RAM failures like 'bit flips' and data type errors were caught at the simulation stage before they could cause any damage in the vehicle system [42].

Throughout the control system development and validation, a comparative analysis of desired versus actual control response was performed to judge the suitability of changes. Control system performance was optimized where possible and judged on a pass/fail basis from a safety perspective. For these models, absolute model fidelity was not required and rough empirical models were appropriate. However, for some of the control tuning and calibration work, highly accurate models were required to ensure that correct gain and offset values were selected, for example. Even for these models, virtual control validation was treated as a good 'first estimate' and tuning of control parameters was often performed after code was loaded onto the controllers.

Empirical instead of mechanistic models were selected for the motor, fuel cell, battery, and most other powertrain components. The exception was the vehicle dynamics models which were taken from the SimDriveLine library. The overriding reason for this decision was the availability of all of the data required to build the accurate system models. The fuel cell vehicle operating data provided a comprehensive source of steady-state as well as some transient empirical correlations for battery, motor, and fuel cell operation. Detailed descriptions of the modeling results will be provided in this section.

4.1 Vehicle Communication Validation

4.1.1 Signal bus lag

Testing the signal bus lag was the first HIL simulation performed. This was performed first because the intent was to benchmark the lag across all additional tests to evaluate the impact of processor utilization on communication lag. The DC/DC converter is the powertrain element that is most sensitive to signal bus lag. If the controller is unable to execute its algorithms within 1 ms, then it may miss the most current input and output voltages and will not be able to effectively control the DC/DC switching frequency. All other signal bus elements have time factors in the 20-100ms range, such as thermistors, pressure transducers, and potentiometers. A lag of over 20 ms in the time required to perform a signal read/write operation may result in the controller missing critical dynamic powertrain behaviour and is unacceptable for safe vehicle control.

The I/O operation with the longest anticipated signal lag was chosen for this test. The actuation of a low side driver circuit and the measuring of a response across a pull down resistor is the event which requires significant processor overhead and has the most line inductance. The simulation model described in the previous chapter was debugged and tested using a digital oscilloscope to verify that the signal being logged was identical to the signal being sent and received. To be able to monitor performance, the signal values displayed on the host machine needed to be decimated to display one signal value for every 100 sent/received. This compensated for the lag in TCP/IP communication and served to avoid host over-write failure when no decimation was applied.

The test methodology required that the signal output pulse be stepped through a series of frequencies to see if the period has an effect on the delay between the sent and received signals. The results from the first test are shown in Figure 42.

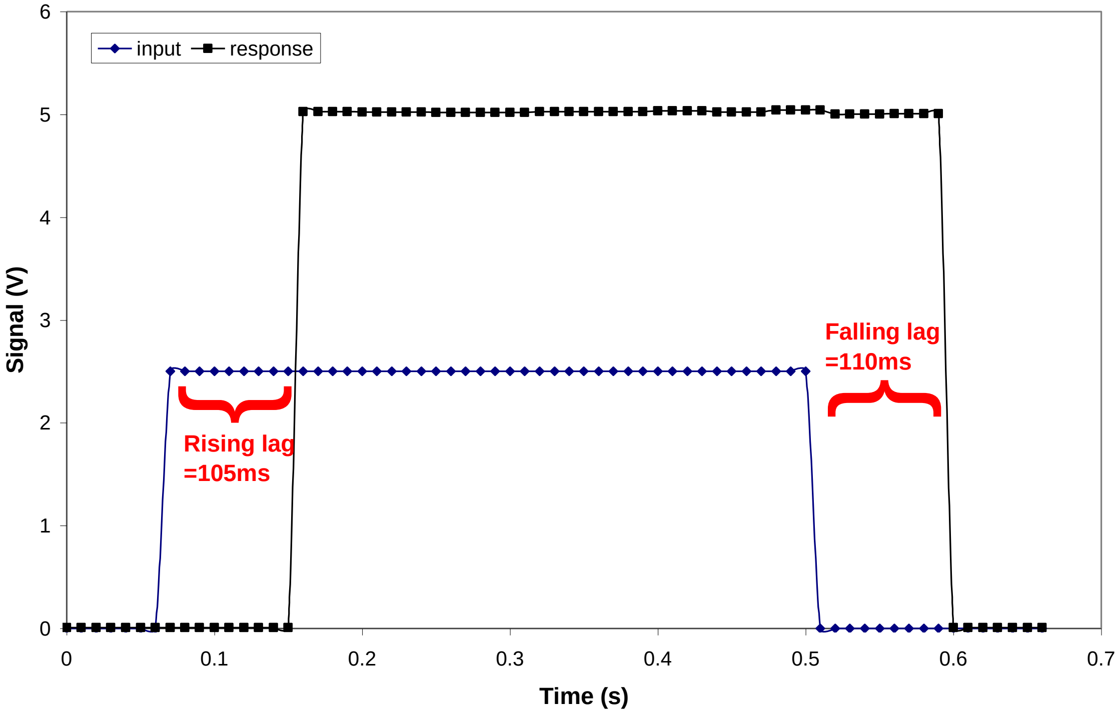

Figure 42: Lag resulting from signal bus test with PXI simulator sleep

The rising lag was measured at 50% of its resting value and was approximately 105 ms, and the falling lag was 110 ms throughout the entire test frequency cycle. This was an unexpectedly long lag on both the rising and the falling edge and warranted examination of the control code. A 100 ms delay block was found in the code, and was replaced with a 10ms delay for the second trial.

The full trace from the second lab experiment is shown in Figure 43, and serves to highlight the experimental procedure. The frequency of the pulses was varied from 10, 15, 20, 25, 30 to 40 Hz during the trail. The second I/O lag trial resulted in an average rising lag of 12 ms and an average falling lag of 16 ms which can be seen in the zoom image in Figure 44. Note that both the pulse and response are at 5V, a change from the initial trial where the pulse was set at 2.5V. The base 10 ms lag is caused by the inherent loop delay to allow the processor to sleep. The additional lag on the rising edge is a combination of the time taken to actuate the relay coil and the time required to write the data to the buffer. The additional lag on the falling edge is a combination of the line inductance and the time taken to write the data to the buffer. Experiments replacing the 1Kohm pull down resistors with 120 ohm resistors showed no perceivable improvement in falling lag, leading to the conclusion that the data acquisition board's internal pull down resistance is producing this latency.

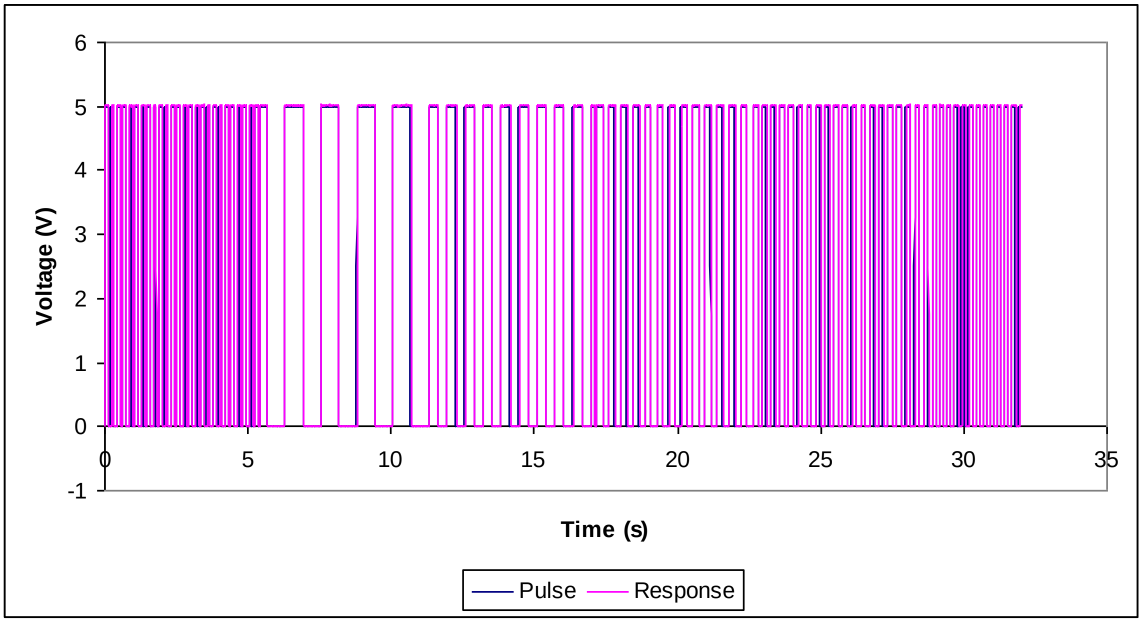

Figure 43: Varied frequency bus lag trial with PXI sleep time removed

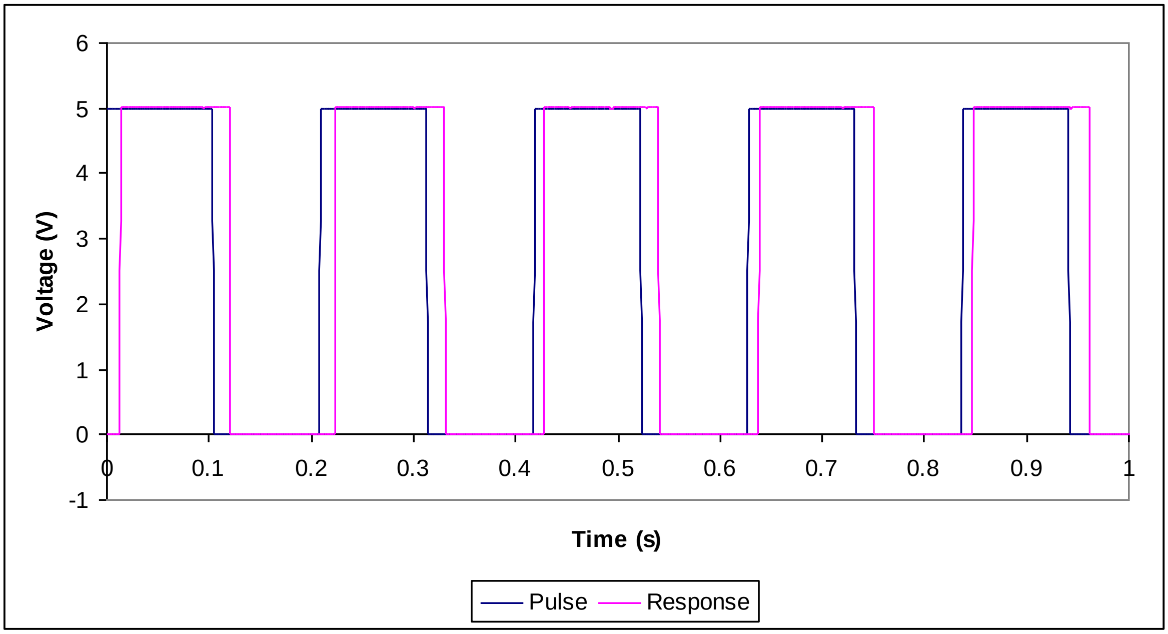

Figure 44: Close-up view of signal bus lag trial with PXI sleep removed

The instantaneous lag was recorded over time and can be seen in Figure 45. The non-steady state values which are represented as spikes in the curve can be neglected because they are a function of how the lag is determined. The steady-state lag values show no correlation between the quantity of lag present and the frequency of the pulse signal. The hardware is configured to continuously acquire samples and to send those samples to the model as soon as they are ready. The software is not always ready to accept the hardware-acquired samples. Depending on the number of samples in the buffer at a given instant, there may be different processing times associated with each switching event, giving rise to the random behaviour of Figure 45.

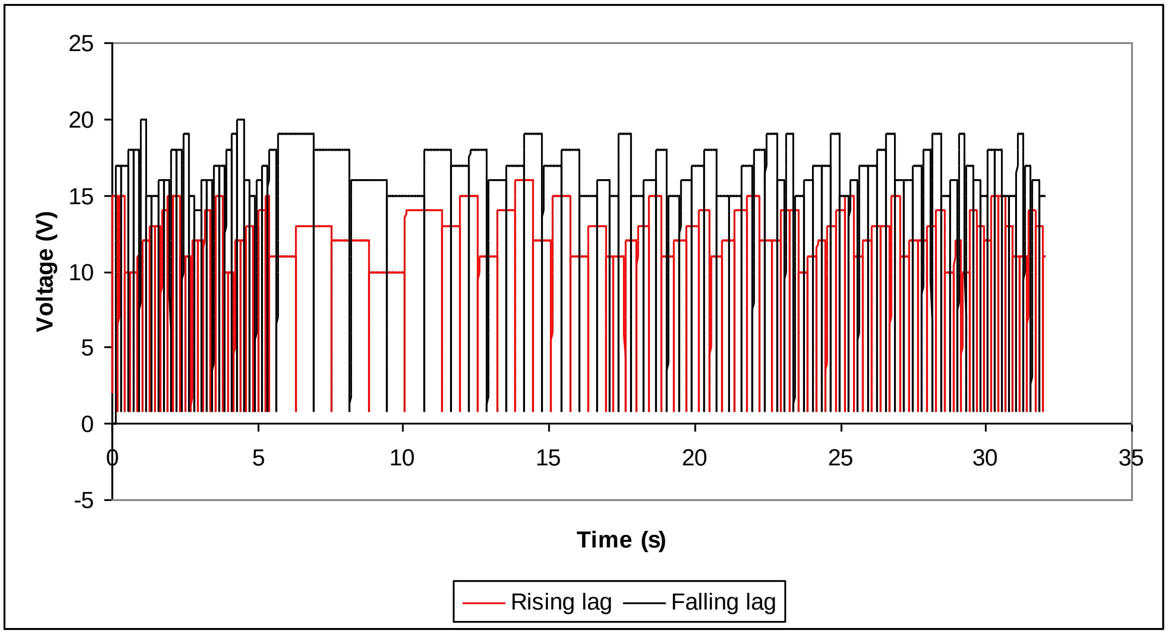

Figure 45: Cycle lag recorded over time for PXI sleep removed data lag

The results of this test show that there is less than 20 ms of lag in the longest signal event on the HIL system. It is expected that all other signal bus operations will occur in less than 20 ms, because the low side driver actuation and signal measurement across a pull down resistor require the maximum amount of system resources and physical/mechanical switching. Most of the physical systems that will be simulated on the vehicle have time factors that are significantly larger than 20ms. The only operation on the vehicle which requires a controller response speed in the order of 1 ms is the DC/DC control. To be able to accurately simulate the DC/DC control, another study must be performed on the ability of the PXI to read in the 10 kHz PWM signal from the controller accurately in order to properly output the DC/DC response.

4.1.2 CAN bus loading

Validation of the CAN bus loading was performed using the Kvaser CANking™ bus monitoring tool as seen in Figure 46. The CAN messages, payload, and transmission rate corresponds to the expected communication over both CAN busses with the code loaded on the controllers.

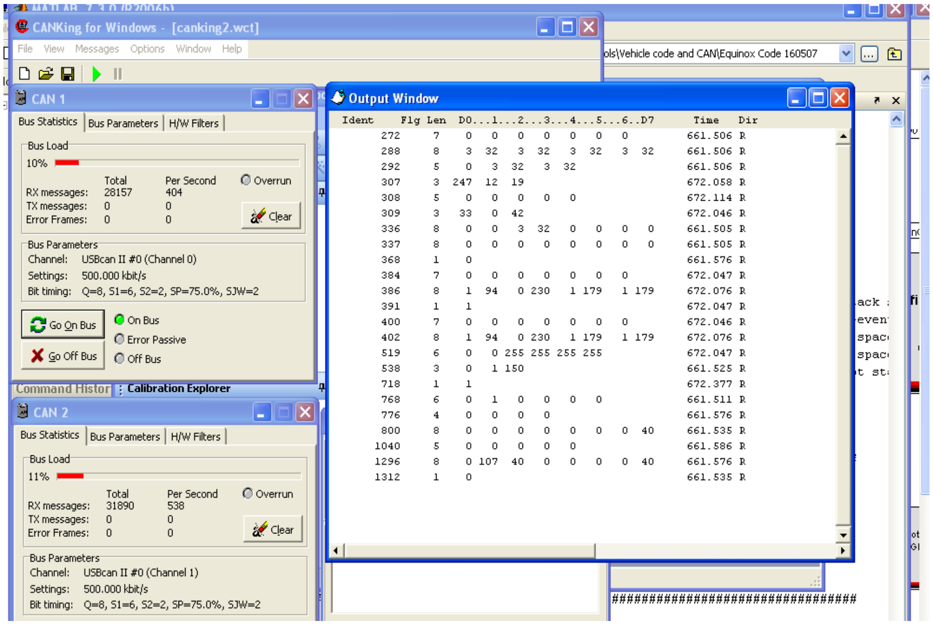

CAN 1 — Bus Load: 10%

```
                 Total     Per Second
RX messages:     28157     404
TX messages:     0         0
Error Frames:    0         0
```

○ Overrun

Bus Parameters
Channel: USBcan II #0 (Channel 0)
Settings: 500.000 kbit/s
Bit timing: Q=8, S1=6, S2=2, SP=75.0%, SJW=2

● On Bus
○ Error Passive
○ Off Bus

CAN 2 — Bus Load: 11%

```
                 Total     Per Second
RX messages:     31890     538
TX messages:     0         0
Error Frames:    0         0
```

○ Overrun

Bus Parameters
Channel: USBcan II #0 (Channel 1)
Settings: 500.000 kbit/s
Bit timing: Q=8, S1=6, S2=2, SP=75.0%, SJW=2

```
Ident     Flg Len  D0...1...2...3...4...5...6..D7      Time   Dir
      272        7   0   0   0   0   0   0   0       661.506 R
      288        8   3  32   3  32   3  32   3  32   661.506 R
      292        5   0   3  32   3  32               661.506 R
      307        3 247  12  19                       672.058 R
      308        5   0   0   0   0   0               672.114 R
      309        3  33   0  42                       672.046 R
      336        8   0   0   3  32   0   0   0   0   661.505 R
      337        8   0   0   0   0   0   0   0   0   661.505 R
      368        1   0                               661.576 R
      384        7   0   0   0   0   0   0   0       672.047 R
      386        8   1  94   0 230   1 179   1 179   672.076 R
      391        1   1                               672.047 R
      400        7   0   0   0   0   0   0   0       672.046 R
      402        8   1  94   0 230   1 179   1 179   672.076 R
      519        6   0   0 255 255 255 255           672.047 R
      538        3   0   1 150                       661.525 R
      718        1   1                               672.377 R
      768        6   0   1   0   0   0   0           661.511 R
      776        4   0   0   0   0                   661.576 R
      800        8   0   0   0   0   0   0   0  40   661.535 R
     1040        5   0   0   0   0   0               661.586 R
     1296        8   0 107  40   0   0   0   0  40   661.576 R
     1312        1   0                               661.535 R
```

Figure 46: Kvaser bus monitor showing CAN bus load with competition code

The signal bus lag was determined to be greater than 10ms on the HIL simulation system in the previous thesis section. This was deemed adequate for simulating all powertrain elements requiring analog or digital control signal interface except for the DC/DC converter. The CAN communication network is where most of the high speed closed-loop powertrain control takes place. A CAN signal must be received and transmitted within a single controller loop cycle of 10 ms without exception. The results of the CAN bus loading experiment show that meeting this CAN communication speed requirement is possible on the HIL simulation system. Even under heavier communication bus loads than are present on the vehicle, CAN communication takes place deterministically with no latency issues.

Table 19 shows the communication bus loading trials that were undertaken and the results generated. The loop rate column refers to the rate that the SIT model broadcasts the 13 target vehicle CAN messages across the HIL system bus and is directly proportional to the quantity of CAN data that the PXI sends each second. The CAN bus load with only PXI vehicle model broadcasting CAN is a function of the payload of each

CAN message, as well as the message transmission frequency. Each PXI vehicle model CAN message is carrying a maximum of 16 bits of data.

Table 19: Results from bus loading tests

Trail	loop (ms)	PXI load (%)	Total load (%)	Error?	Pass?
1	50	6	42	N	Y
2	20	14	50	N	Y
3	10	29	64	N	Y
4	5	55	83	Y	Y
5	1	263	N/A	N/A	N

Although a CAN error flag was set during the 4th trial when the bus load reached 83%, the test was still deemed a pass because the error was reset and the target controller CAN message was not received late. With the 5th trial, the CAN bus crashed immediately each time the PXI was brought online. From Figure 47, which plots bus load relative to PXI CAN transmission rate, a 100% bus utilization loop rate for the bus loader model was calculated at 2.37 ms. Additional bus loading trials were performed to test the prediction accuracy of the bus loading figure. A 3 ms loop rate transmitting the 13 messages corresponds to an exact bus loading of 90%. The PXI was unable to sustain this level of bus load for more than a few minutes, which suggests that at 90% bus load, the vehicle controller area network communication bus will be unstable. It is recommended, therefore, that the vehicle CAN bus be loaded to no more than 90% capacity. This coincides well with the control design ‘rule-of-thumb’ that an 80% loaded bus is a fully loaded bus.

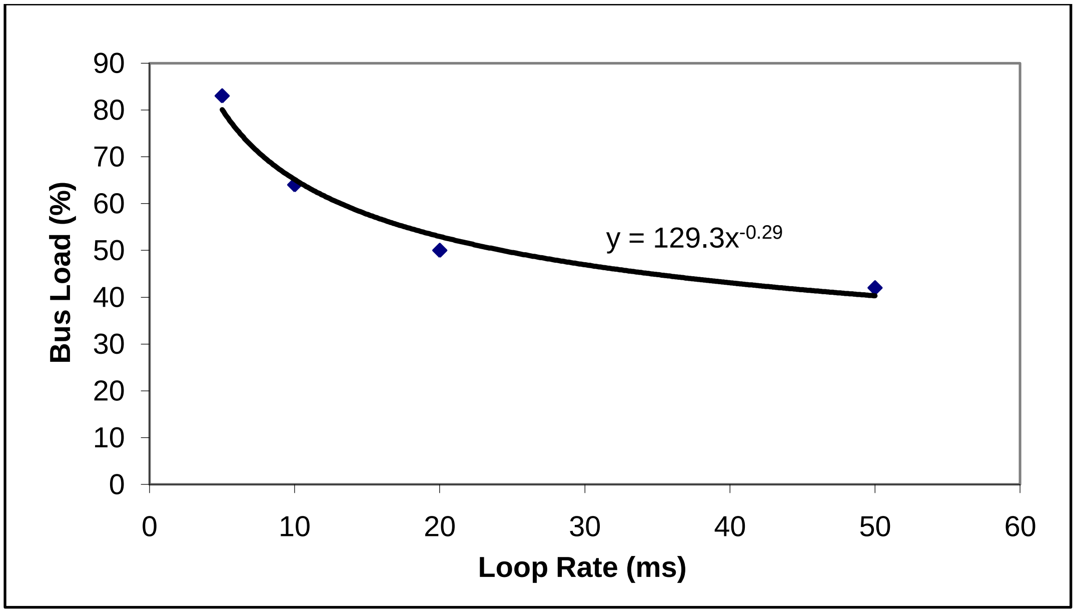

Figure 47: Bus load as a function of 13 message transmission loop rate

The maximum controller bus load that has been recorded during vehicle operation is less than 50%. At this level of CAN bus utilization, the results of the bus testing suggest that there will be no concern of CAN signal latency interfering with safe vehicle operation. It is important to note, however, that the vehicle CAN signal bus is significantly longer and is subject to higher levels of electromagnetic interference. All of these factors contribute to signal noise which increases data loss on the communication network. The vehicle CAN network is less tolerant to heavy bus loading than the HIL system, even though a wide utilization safety factor has been shown to exist.

4.2 Controller Safety Response Validation

4.2.1 Fault Message Handling

The fault message simulation model’s simplicity is its utility. The simulator was used to asynchronously transmit fault messages to the vehicle controller. The fault messages shown in Table 20 were simulated and the expected response from the controller in each of the cases was verified. If the fault message was stored appropriately in the Mototune failure memory and the access operation was successful, a ‘Pass’ was designated.

Table 20: Simulated fault messages

Fault Message Transmitted	Response	Pass?
stack_undervoltage	Temporary in occurred faults	Y
coolant_underflow	Held in active faults	Y
coolant_overtemperature	Held in occurred faults	Y
external_estop	Held in active faults	Y

This behaviour is demonstrated in the screenshots of Mototune in Figure 48. In each case, the controller correctly identified and responded to the fault. Case (a.) shows the stack undervoltage fault saved to controller memory, case (b.) shows an active stack undervoltage fault, and case (c.) shows the stack coolant overtemperature fault occurring while the undervoltage fault has been saved.

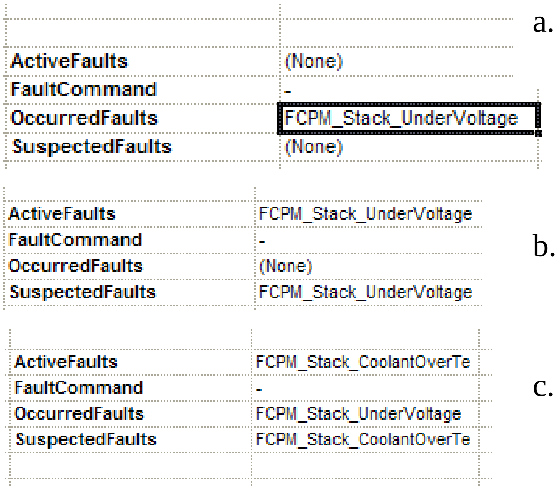

ActiveFaults	(None)
FaultCommand	-
OccurredFaults	FCPM_Stack_UnderVoltage
SuspectedFaults	(None)

ActiveFaults	FCPM_Stack_UnderVoltage
FaultCommand	-
OccurredFaults	(None)
SuspectedFaults	FCPM_Stack_UnderVoltage

ActiveFaults	FCPM_Stack_CoolantOverTe
FaultCommand	-
OccurredFaults	FCPM_Stack_UnderVoltage
SuspectedFaults	FCPM_Stack_CoolantOverTe

Figure 48: Mototune screenshots demonstrating appropriate controller response

The results of this simulation showed that the controller was not the source of the undesired behaviour. Attention was then turned to the fuel cell power module controller and it was discovered that, due to an internal programming error, the failure message was being broadcast multiple times on the mirrored CAN bus in rapid succession as soon as a single fault was logged. This error was remedied in new code which properly handled the fault messages being transmitted on both controller communication busses. At this time, however, the results of the newly loaded code which included the updated fuel cell code are not available.

4.2.2 12V Bus Droop/Spike Testing

The 12V bus droop and spike testing was carried out using the same HIL model as the CAN bus loading testing. This allowed the CAN message signals that were indicative of normal function to be monitored for abnormality and unexpected behaviour resulting from 12V bus variation. The HIL setup was validated for its proximity to the actual vehicle conditions as part of the CAN bus loading procedure. In addition, the voltage across the 'MCU1 key in' high side driver was monitored.

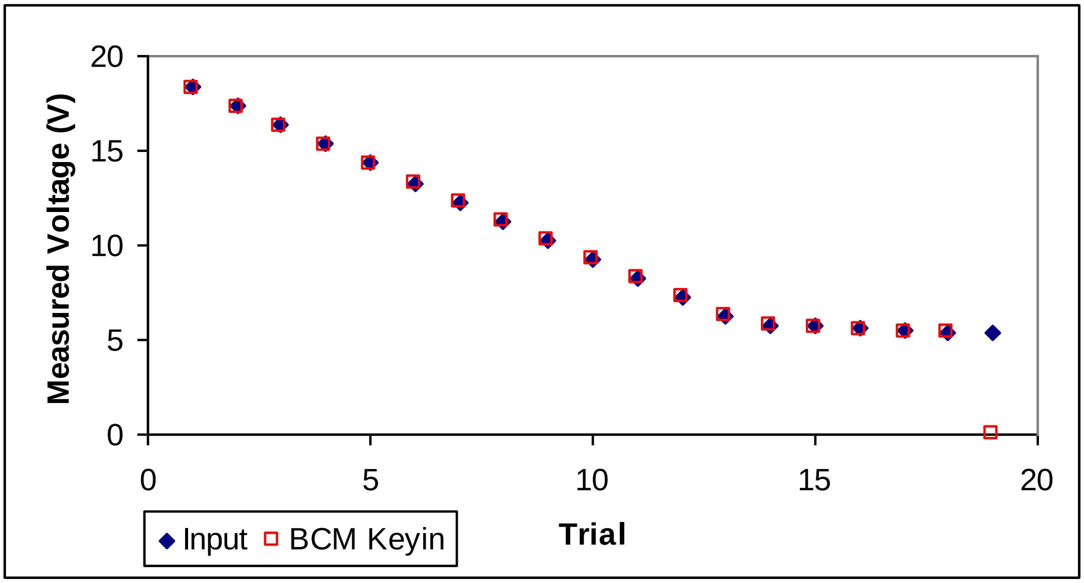

Figure 49: Control output voltage relative to input voltage

The controller high side driver output response to varied values in supply voltage was predictable and can be seen in Figure 49. Throughout the trial, the output voltage tracked the input voltage closely. Table 21 documents the controller status as the voltage is varied and agrees with Figure 49 for the voltage at which the controller ceases to function reliably. Throughout the trial, the target CAN messages and control outputs remain as expected until the voltage dipped below the minimum voltage that the controller required for operation. A control relay opened just before the rear controller shut off, after reaching its minimum coil voltage. The voltage spike to 18V resulted in no unexpected control response.

Table 21: Controller status during voltage spike/droop trial

#	V	Status	Note	#	V	Status	Note
1	13.05	ok		18	7.13	ok	
2	14.06	ok		19	7.03	ok	PXI CAN out
3	15.06	ok		20	6.93	ok	
3	16.07	ok		21	6.84	ok	
4	17.07	ok		22	6.73	ok	
5	18.07	ok		23	6.63	ok	
6	12.05	ok		24	6.53	ok	
7	11.05	ok		25	6.43	ok	
8	10.05	ok		26	6.33	ok	
9	9.05	ok		27	6.23	ok	
10	8.05	ok		28	6.13	ok	
11	7.83	ok		29	6.03	ok	
12	7.73	ok		30	5.93	ok	
13	7.63	ok	CAN error	31	5.83	warning	Control relay out
14	7.53	ok	Error clear	32	5.73	fault	Rear controller out
15	7.43	ok		33	5.63	fault	
16	7.33	ok		34	5.53	fault	
17	7.23	ok		35	5.43	fault	Front controller out

The objective of the test was to determine if variation in input voltage causes unexpected control response and to identify the minimum operation voltage for the controller. No unexpected control responses were observed until the controllers ceased operating at 5.73V (rear) and 5.43V (front). These values have an impact on the control implementation in the vehicle by setting an absolute lower limit on the amount that the 12V NiMH battery can droop. Voltage droop on the 12V line has caused the vehicle controllers to cease function in the past, but no quantification of the limits has been performed until now.

4.2.3 Failure Insertion Validation

The failure insertion model was not validated with operating data because data is unavailable for the potentially dangerous failures that were being simulated. The code used to build the model was, however, copied directly from the most current vehicle control code and is expected to behave identically to the vehicle code. While it is undesirable to use simulation results that have not been validated, in this case, the difficulty and danger in obtaining operating data justified the lack of validation.

The IGBT failure monitoring signal failure insertion trials are summarized in Table 22 . For all three fault conditions, the controller did not perform as expected. The controller was to disable the fuel cell power module in the event of any 'IGBT ok?' line irregularities. Instead, the enable line was held true as seen in Figure 50.

Table 22: 'IGBT ok?' monitoring line failure insertion results

Line condition	Induced failure	Expected response	Observed response
IGBT failure	12V line short	disable FCPM	Normal FCPM operation
IGBT failure	ground line short	disable FCPM	Normal FCPM operation
IGBT failure	floating line short	disable FCPM	Normal FCPM operation

Examining the code in light of the inability of the controller to disable the fuel cell even when a failure was not inserted in the IGBT safety line resulted in the discovery of a disabled safety switch. The terminator circled in Figure 51 prevents the IGBT fault signal from disabling the fuel cell power module.

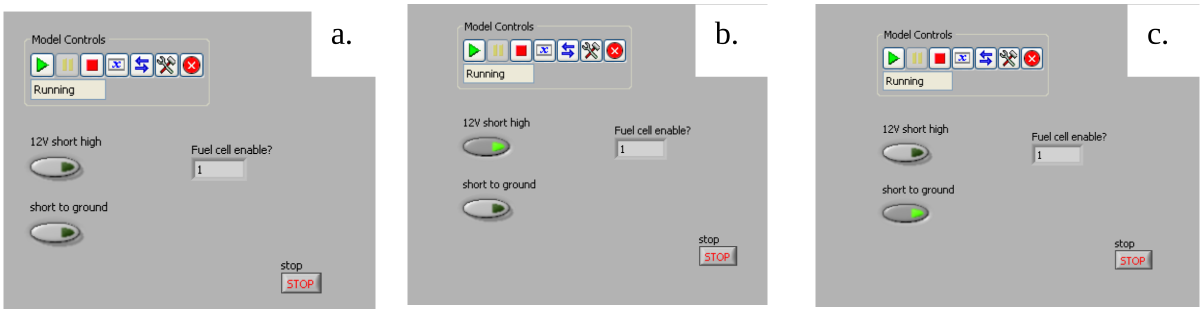

Figure 50: Undesired controller response to 'IGBT ok?' failure. No inserted line failure (a). Inserted short high (b). Inserted short to ground (c)

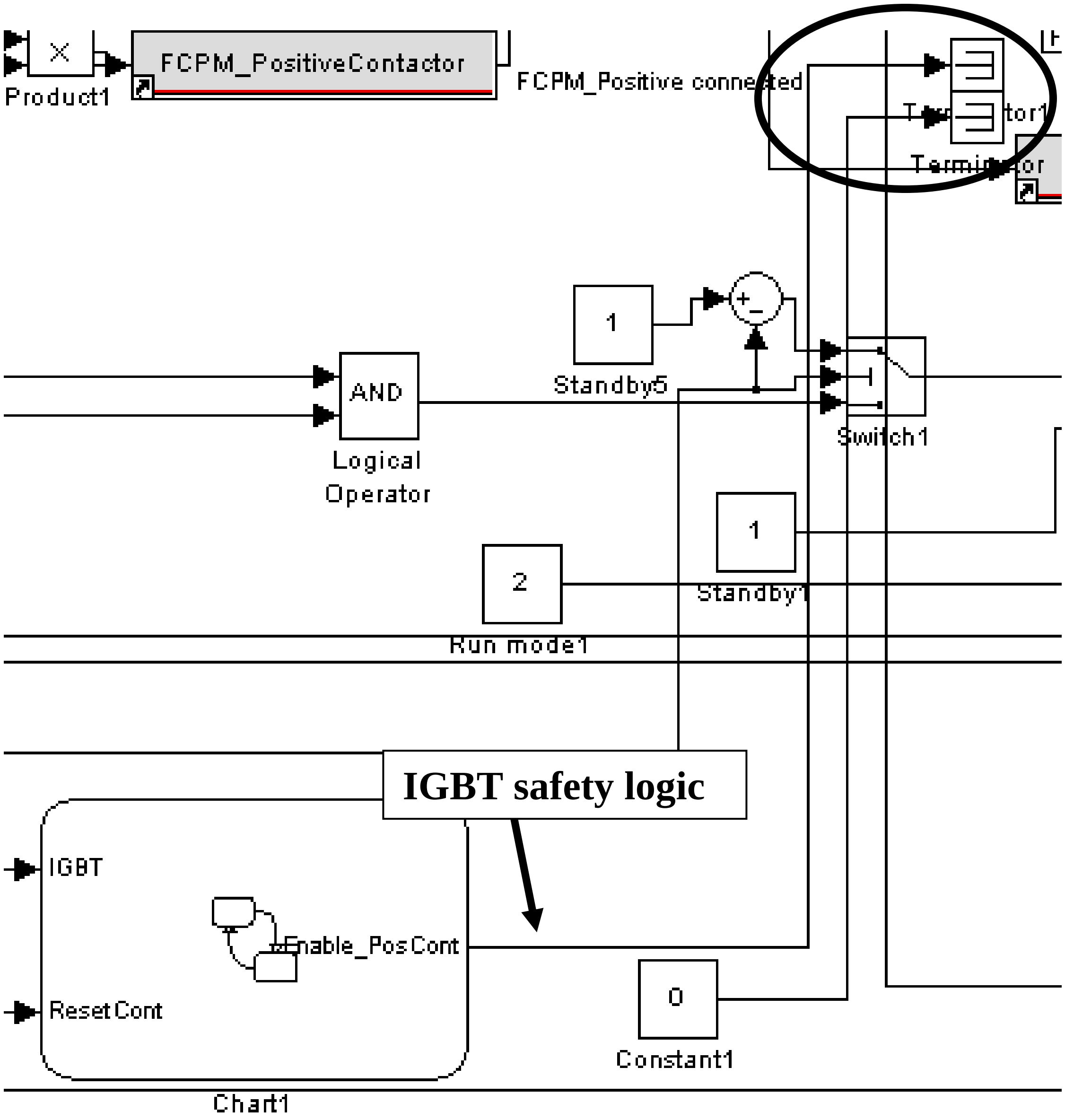

Figure 51: Terminated safety logic in competition controller code

It is recommended that this safety switch be re-enabled in future code revisions.
In order to test the ability of the controller to ensure that unintended torque is not generated due to gear selector line failure, a gear direction was chosen and the failures shown in Table 23 were induced. It was assumed that disabling the torque control strategy block (TCS) would ensure that no torque requests were sent to the motors. Close to 40% of the gear selector failure insertion trials did not exhibit the desired response and failed to disable the TCS when a failure was inserted.

Table 23: Gear selection failure insertion control response

Trial	Reverse	Drive	TCS enable?	Desired?
1	0	0	0	Y
2	1	0	1	Y
3	0	1	1	Y
4	1	1	1	N
5	high (0)	0	0	Y
6	low (0)	0	1	N
7	float(0)	0	0	Y
8	0	high (0)	0	Y
9	0	low (0)	1	N
10	0	float(0)	0	Y
11	high (0)	1	1	Y
12	low (0)	1	1	Y
13	float(0)	1	1	Y
14	1	high (0)	1	Y
15	1	low (0)	1	Y
16	1	float(0)	1	Y
17	high (1)	0	0	N
18	low (1)	0	1	Y
19	float(1)	0	0	N
20	0	high (1)	0	N
21	0	low (1)	1	Y
22	0	float(1)	0	N
23	high (1)	1	0	N
24	low (1)	1	1	Y
25	float(1)	1	0	N
26	1	high (1)	0	N
27	1	low (1)	1	Y
28	1	float(1)	0	N

Two major control logic errors were identified; one was unique to trial 4, and the rest of the trials with unexpected results are a result of another type of logic error. Figure 52 shows a subsystem in the control logic directly before the decision to allow torque to be enabled is made. The logic ensures that if either the reverse, drive, or tow gear are enabled, torque commands may pass to the motors. It is recommended that an enumeration strategy similar to the one implemented in the torque magnitude calculation shown in the second pane of Figure 52 be implemented to disable the ability to pass torque if two gears are selected. The redundancy of the safety ensures that even if two gears are selected, a ‘zero-torque’ command will be sent and that the torque control strategy will also not be active in the eventuality of this failure.

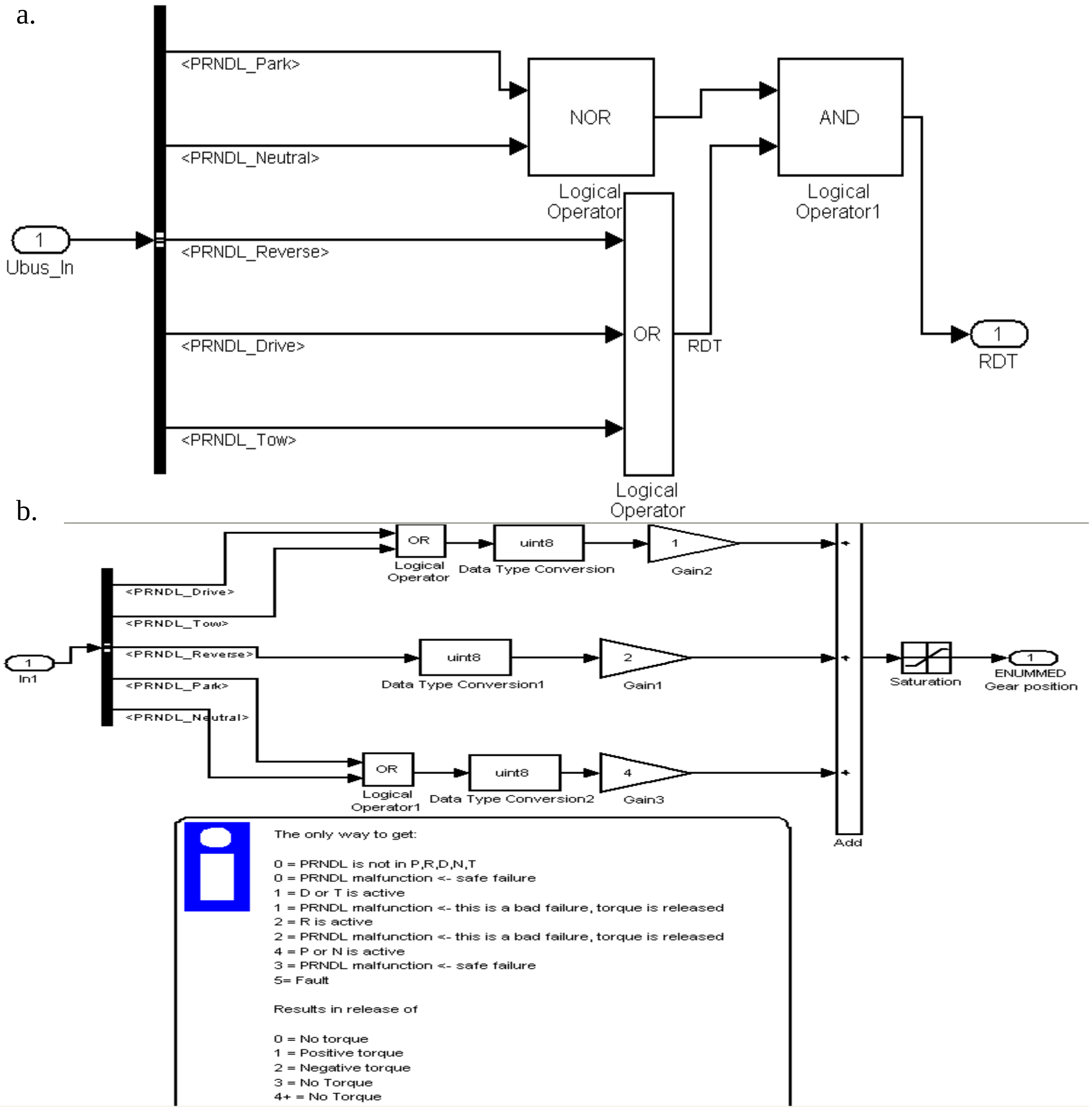

The only way to get:

0 = PRNDL is not in P,R,D,N,T
0 = PRNDL malfunction <- safe failure
1 = D or T is active
1 = PRNDL malfunction <- this is a bad failure, torque is released
2 = R is active
2 = PRNDL malfunction <- this is a bad failure, torque is released
4 = P or N is active
3 = PRNDL malfunction <- safe failure
5= Fault

Results in release of

0 = No torque
1 = Positive torque
2 = Negative torque
3 = No Torque
4+ = No Torque

Figure 52: Implemented torque pass-through arbitration (a). Recommended torque pass-through arbitration (b)

The remaining unintended torque pass-through events in this trial result from the lack of effective error checking in the gear selection algorithm. It is recommended that the possibility of short circuits should be considered in the control code, especially given the custom-built nature of the gear selector. A single NOR block that filters all of the gear selection signals and prevents the torque control system from being enabled if it reads a 'true' value would be a simple solution to the problem.

The throttle position trials yielded unexpected results, beginning with an unplanned trial during which a floating voltage signal occurred while setting up the failure insertion channels resulted in a torque request when the TCS was disabled. This result was then confirmed during the formal trials shown in Table 24.

Table 24: Throttle pedal position sensor failure insertion trails

Trial	TPS A	TPS B	Throttle pos.	gear	Front torque	Rear torque	Expected?
1	0	0	0	drive	0	0	Y
2	1	1	1	drive	152.29	152.29	Y
3	1	0	0.52	drive	76.8	76.8	N
4	0	1	0.51	drive	76.2	76.2	N
5	1	1	1.02	no gear	152.29	152.29	N
6	1	1	1.02	reverse	-152.29	-152.29	N*

*Value should be limited below maximum reverse torque and flipped instantly on switching. Actual response should be ramped on shifting after vehicle speed reaches a low threshold.

Over 65% of the throttle pedal failure insertion trials yielded unexpected performance from the controller. The desired response for a disagreement between the values read on the two redundant throttle position sensors (TPS) is to not allow torque to be applied at the wheels. When contrasted with the observed performance during Trial 3 in Figure 53, which shows the throttle signal sent to the torque calculation algorithm as the average of the two values sensor values, it is clear that this safety feature is not working correctly. Trial four confirmed that the same fault is present using the second throttle position sensor as a comparator.

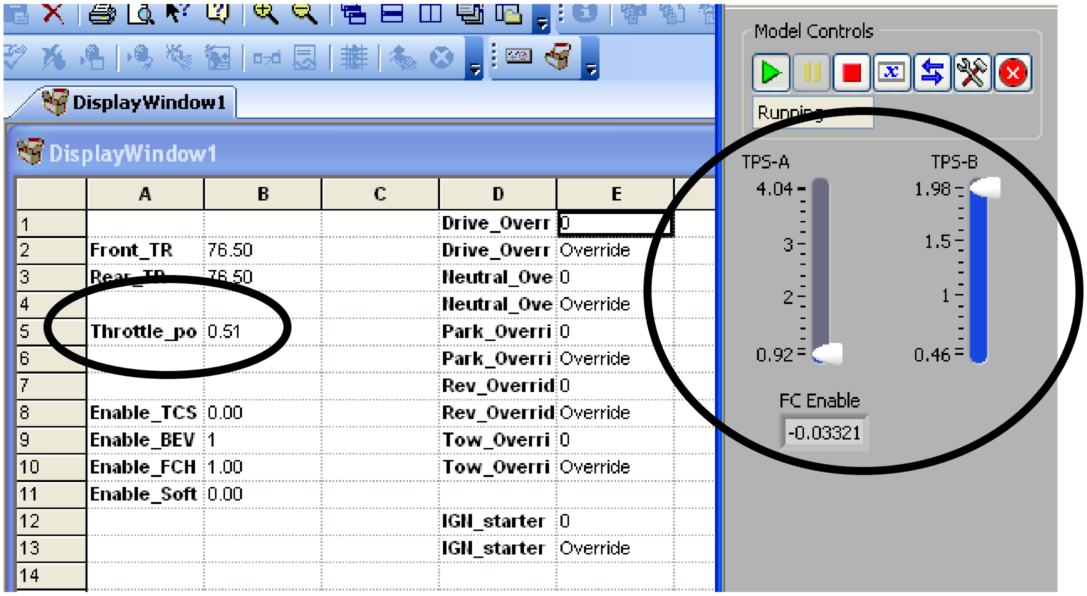

	A	B	C	D	E
1				Drive_Overr	0
2	Front_TR	76.50		Drive_Overr	Override
3	Rear_TR	76.50		Neutral_Ove	0
4				Neutral_Ove	Override
5	Throttle_po	0.51		Park_Overri	0
6				Park_Overri	Override
7				Rev_Overrid	0
8	Enable_TCS	0.00		Rev_Overrid	Override
9	Enable_BEV	1		Tow_Overri	0
10	Enable_FCH	1.00		Tow_Overri	Override
11	Enable_Soft	0.00			
12				IGN_starter	0
13				IGN_starter	Override
14					

Figure 53: Averaged instead of zeroed throttle position value when sensors disagree

In Trial 5, the gear selector was shifted out of gear (between gears) which should have placed the torque request to zero as an error state. In this case, however, without a gear to use to arbitrate the torque request, the control code continued to feed through an old torque request, regardless of the actual throttle position. This represents unsafe operating condition that needs to be addressed with fail-safe code. Trial 6 was a shift from wide open throttle moving forward to a reverse gear. The appropriate control response would be to limit the reverse torque until the vehicle speed reaches a pre-determined level which is safe for the mechanical systems. Instead, the trial witnessed an instantaneous full reverse torque request. This type of action is very likely to result in damage to the motors or to the half-shafts.

To address the out-of-gear torque request, it is recommended that the enabled subsystem containing the torque control strategy be modified. Figure 54 shows a block parameter editor with the 'state when enabling' parameter selected to be held. It is recommended that if the state when enabling is changed to 'reset', the out-of-gear issue will result in a torque request of the default values which are easily set to zero in the torque request algorithm.

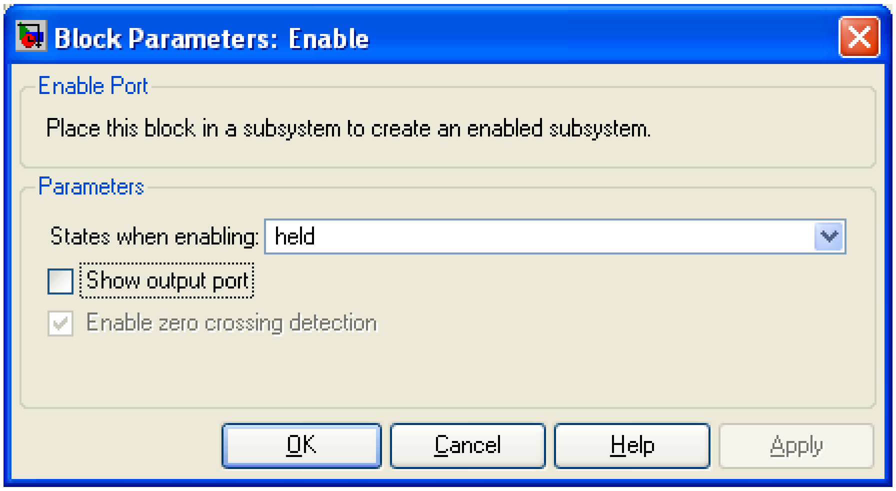

Block Parameters: Enable

Enable Port

Place this block in a subsystem to create an enabled subsystem.

Parameters

States when enabling: held

□ Show output port

☑ Enable zero crossing detection

Figure 54: Torque request enabled subsystem parameter: change 'held' to 'reset'

In order to ensure that the redundant throttle position sensors behave in a fail safe manner, it is recommended that the code circled in Figure 55 be fully implemented. The initial comparison has been made between the throttle position sensor values, but nothing is being done later in the code with the safety variable that is generated. It is recommended that this variable be used to arbitrate whether torque be passed through in the second pane of Figure 55.

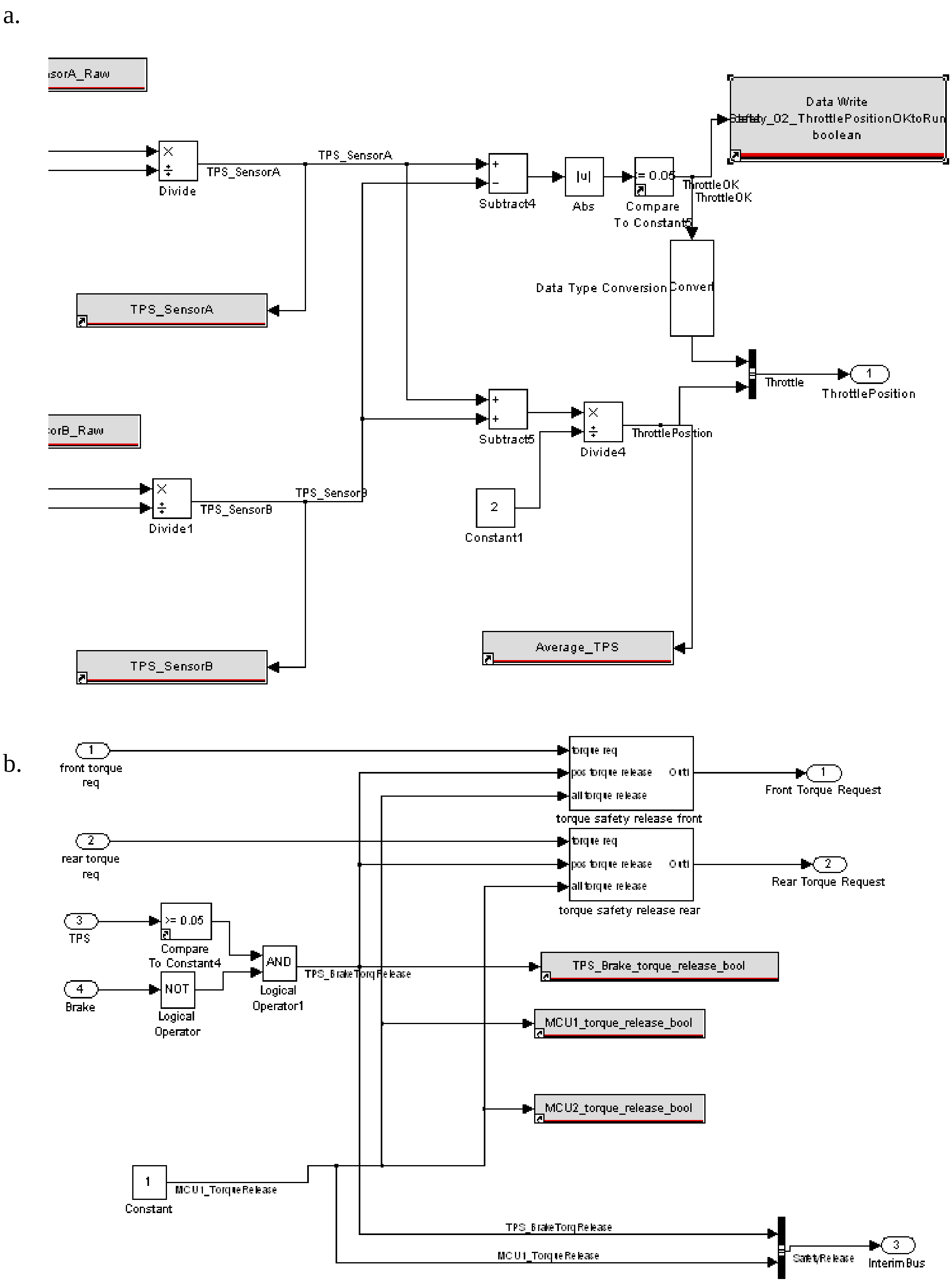

Figure 55: TPS safety variable partial implementation (a). Proposed location for TPS safety variable (b)

In the same subsystem used for implementing the TPS rationality check variable, called ‘Safety Implement’, it was noted that the MCU torque release safety checks had also been overridden by a constant.

Inserting faults in this system was not performed because of the lack of failure handling code identified in the preliminary trials. It was evident that there were no measures implemented to handle the sensor rationality checking and therefore there would be no provisions for failure insertion in these signal lines. It is recommended that control code be implemented to cause the controller to gracefully execute fail safe measures if any signal line inconsistency is noted.

4.3 Vehicle Dynamic Control System Validation

The fidelity of the SIL dynamic vehicle model was validated using a separate set of vehicle operating data than was used to build the model. A representative result of this validation is shown in Figure 56 which compares the vehicle high voltage busses to the predicted high voltage busses for acceleration from 18 to 50 kph. The comparison of predicted with actual operating data shows good agreement, leading to the conclusion that the powertrain model has a high degree of accuracy. It should be noted that the validation did uncover weaknesses in the model, particularly when considering non-critical vehicle component failure. The rear drive motor was often in a power reduction or fault state during vehicle testing. This behaviour was not considered in the control validation model for simplicity, but should be considered in future revisions to improve model fidelity.

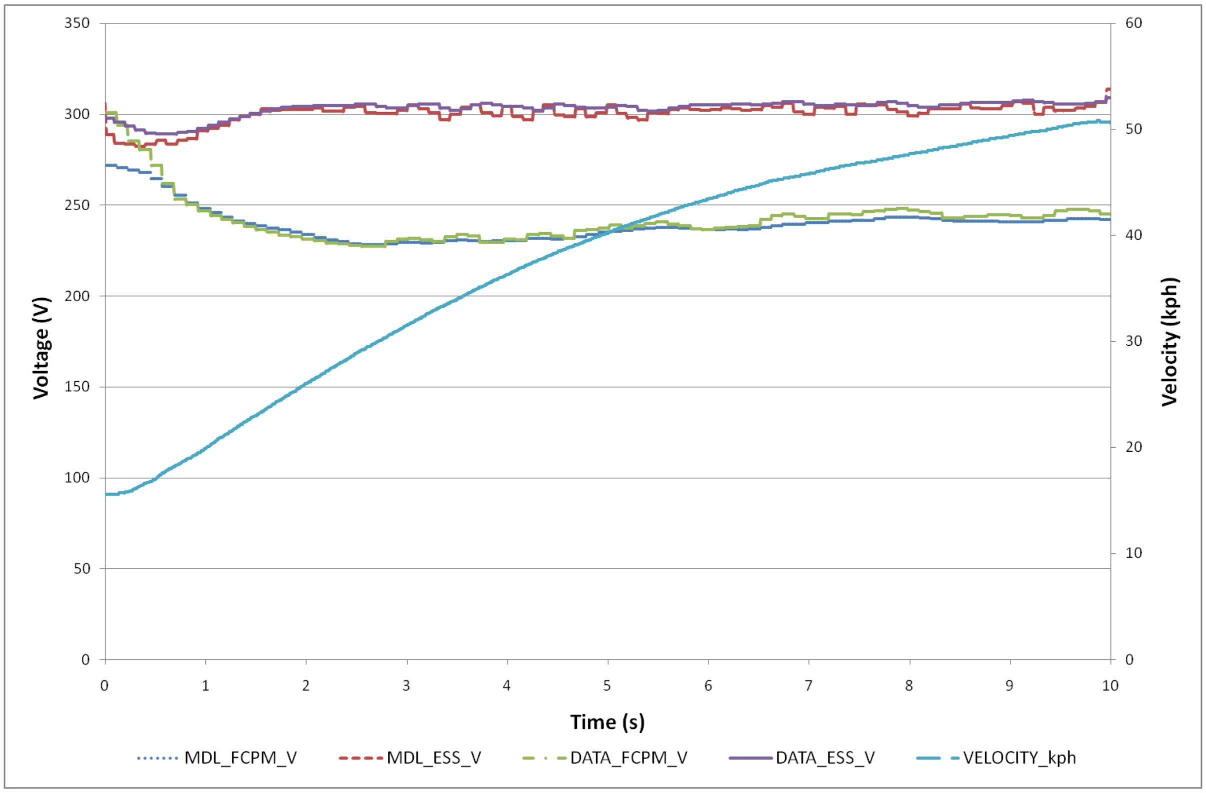

Figure 56: Validation of model predicted bus voltages vs vehicle acceleration data

Once the model fidelity was confirmed, the torque control and regenerative braking algorithm validation was an iterative software-in-the-loop (SIL) process that was performed before each new code revision was loaded to the vehicle controller. This mandatory check took place because of previous experience loading untried code to the controller and witnessing unintended acceleration events. The intended torque control algorithm can be seen in Figure 57 [43].

The first SIL effort was directed at debugging code. Once the code was debugged, the simulation was used to provide approximate braking torque slew rates for regenerative braking.

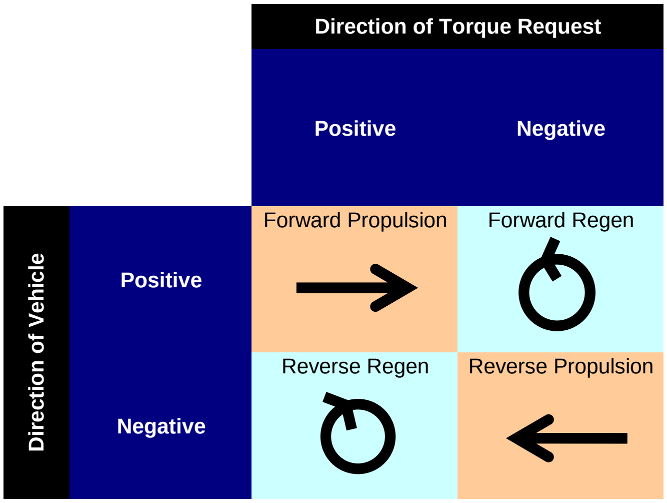

Figure 57: Intended torque control algorithm

The first version of the regenerative braking and traction control code that was loaded in the SIL simulation system resulted in unintended behaviour. Table 25 outlines the development and shows the iteration cycle that was performed to bring the code to an acceptable performance level.

Table 25: Torque control strategy troubleshooting process

Error	Fix	Vehicle Capable?
Both motor full torque applied to single motor	Remove doubling gain	N
Torque passed through in park	Add safety to enumeration block	N
No torque available for reversing	Fix double safety redundancy	N
RPM limited at 500	Remove RPM limiting saturation	Y
Full negative torque requested at initial brake	Add saturation to limit regen torque	Y
Torque ramp too steep causing jarring decel	Add slew rate limitation to ramp	Y

These code fixes were all identified and implemented without running full SIL trials with actual drive cycle inputs. They were performed using static input blocks and semi-dynamic models. Additional errors were discovered when real driver torque requests were made using full dynamic simulation. Figure 58 shows no regenerative braking being performed during deceleration, shown circled in the figure and characterized by a lack of negative torque.

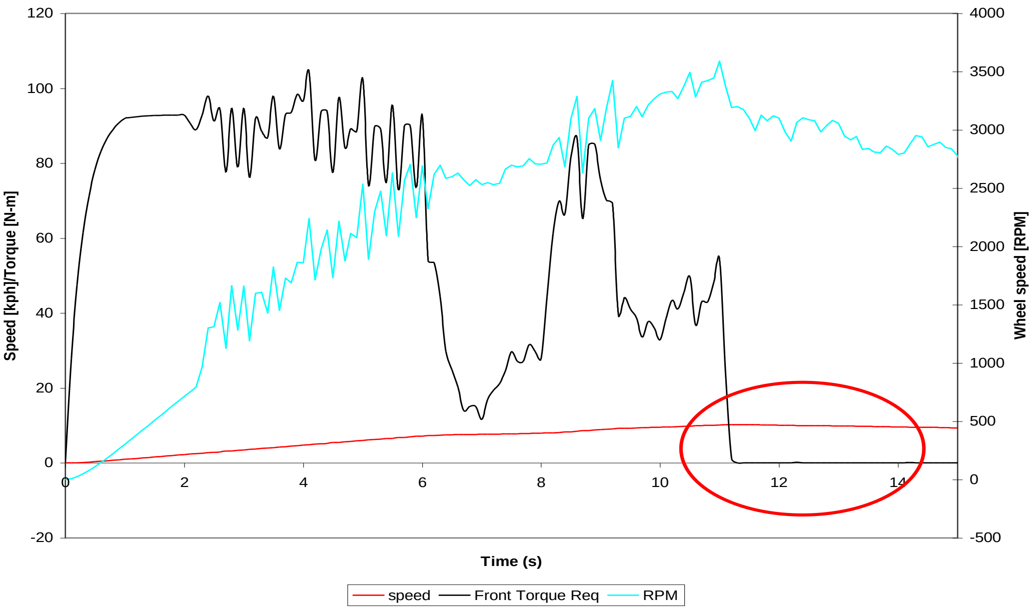

Figure 58: Regenerative braking control strategy not functioning as intended

The cause of this behaviour was eventually identified as a safety logic error. Redundant safety checks to ensure that regenerative braking would be performed during forward motion were not receiving the required input speeds to unlatch the regenerative braking function. Once this error was identified and corrected, regenerative braking behaviour shown as negative torque requests, circled in Figure 59, was obtained through the software-in-the-loop modeling.

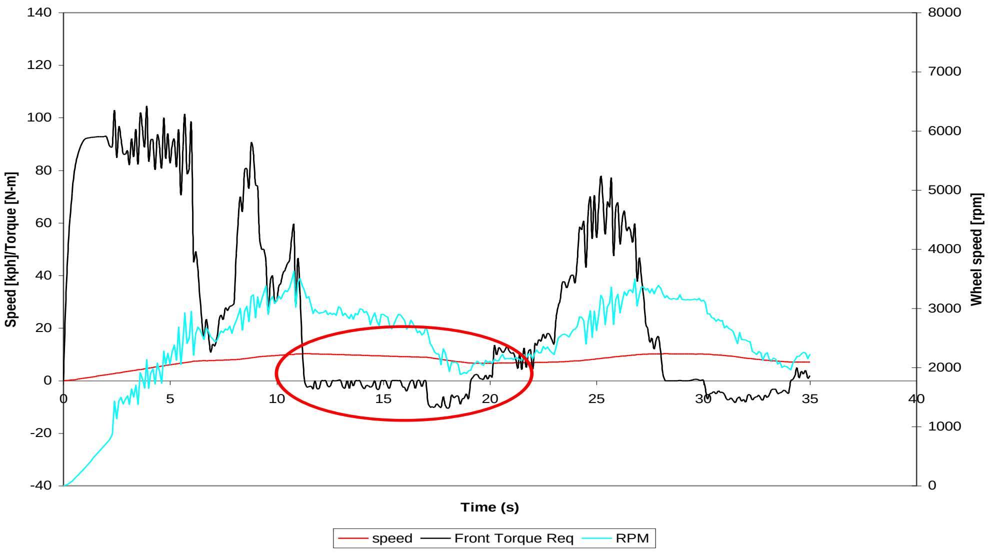

Figure 59: Regenerative braking control strategy functioning as intended

4.4 12V NiMH charge system validation

The 12V system on the vehicle was completely redesigned for the 3rd year of competition to improve its robustness and reliability after experiencing critical failures during the 2nd year of competition. The validation effort began by checking that the discharge behaviour of the battery model was consistent with the manufacturer's data for the discharge performance. Figure 60 shows the actual performance overlaid with the model predictions. It was found that the empirical data could be modeled with a third order polynomial which produced a satisfactory fit, as can be seen in Figure 60.

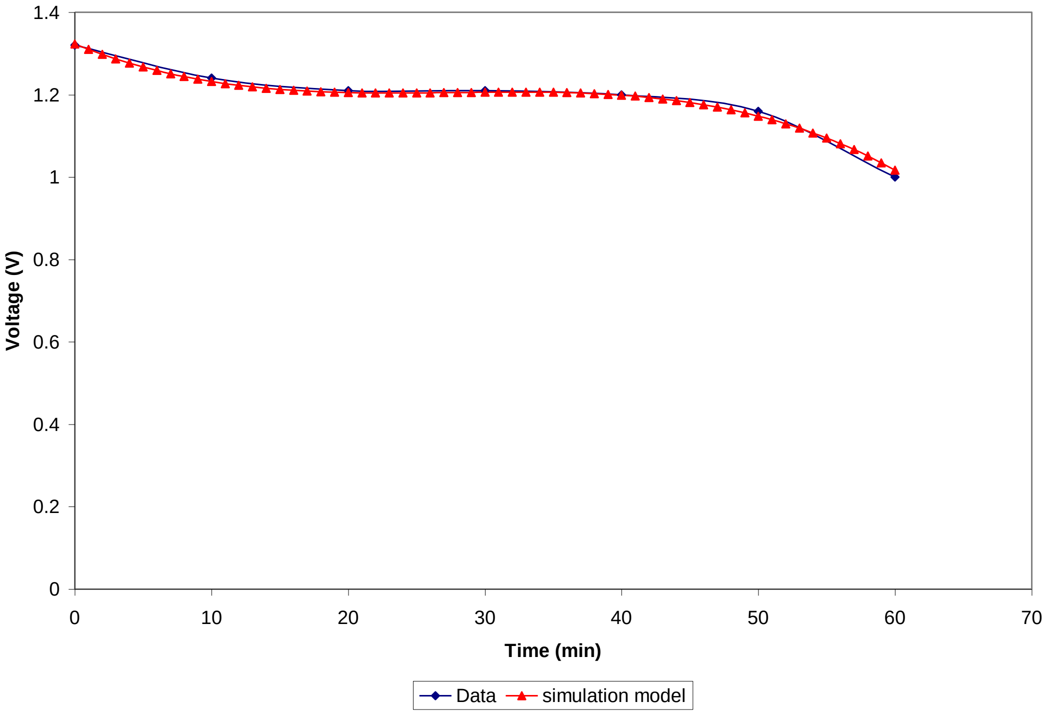

Figure 60: Empirical NiMH battery system model fit

Once satisfied that the battery model accurately represented the performance data, controls tuning was initiated, using software-in-the-loop methodology. The SIL testing was able to identify the following behaviour issues before moving to HIL:

1. Charge control enable block was not properly attached, resulting in no current pass-through; and
2. Sign reversed on integrator block caused unstable response to PWM input.

Once these issues were resolved, the code was flashed to the Mototron controllers and HIL testing uncovered further unanticipated issues. The first major issue, underlined in Table 26, was the disparity between the expected current sensor values and those that the PXI were sending it. The current sensor employed on the battery for metering charging current has a 0 current setting of 2.5V, and climbs to 3.5V for the max charging current of 37.5A. The controller was calibrated to receive the proper current sensor signal as shown in the table.

Table 26: Expected versus actual current signals

Current	Current Signal	Expected Signal
0	0	2.50
10	1	2.77
20	2	3.03
30	3	3.30
37.5	4	3.50
45.5	5	3.71

The next issue identified concerned the PI control loop used to set the charge current. The proportional error term was being artificially inflated, causing major control overshoot. This was because the PWM signal from the controller to the simulated charge circuit was not being interpreted as expected by the PXI. Line resistance was causing the expected 5.0V (RMS value for full duty cycle) to be read in as 4.11V, causing a lower current flow than expected. This in turn caused the integrator error term to ‘wind-up’ and resulted in unstable control. This is an example of where an HIL virtual system issue is not significant in the actual system. The actual charge circuit handles the PWM input differently from the way that the PXI must accept the input and to solve this problem, a threshold in the charge circuit simulation model required modification.

An interesting control challenge was noted, diagnosed and addressed in the final phase of the HIL battery control testing. The behaviour in Figure 61 was observed once all of the lower level controls issues were resolved. This oscillation was observed both during high and low charge current requests from the controller. Oscilloscope probing ruled out the possibility of signal transmission error.

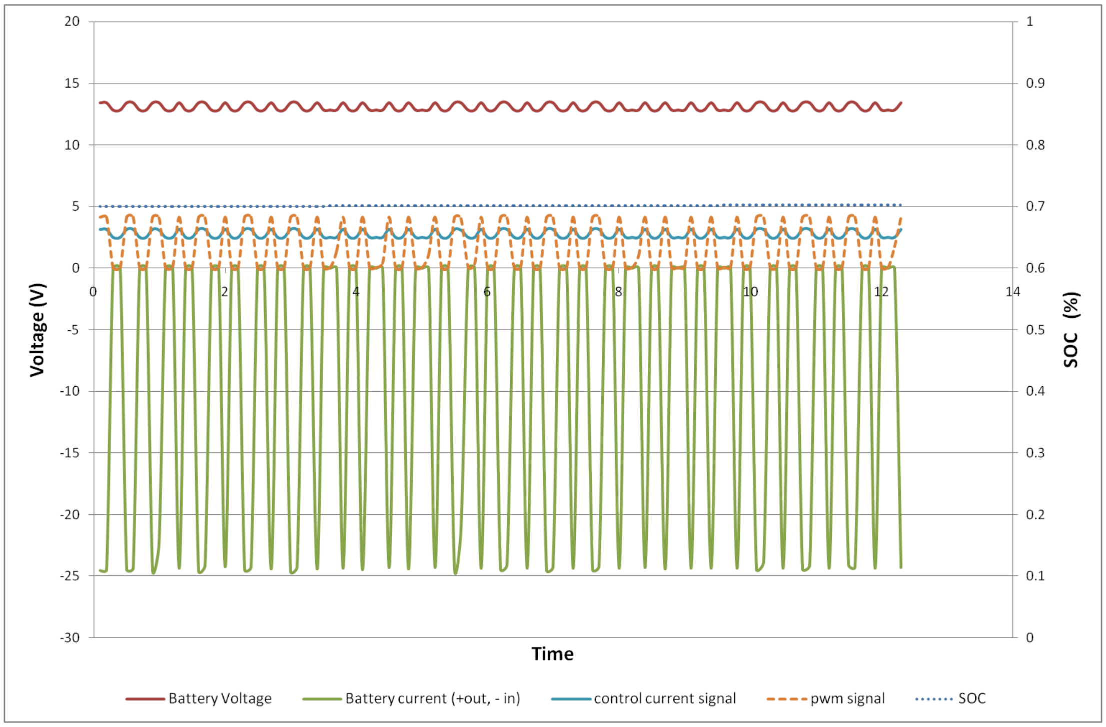

Figure 61: Faulty integration method resulting in unstable control response

It was noted that the integrator term was causing unintended operation in the PI control. The integral gain was ramped significantly when the set point and control values were actually relatively close. Hand calculations confirmed that the integral error term was being calculated erroneously. Upon analyzing the controller code, it was noted that the Simulink-native integrator block was selecting an integration time step of 1 second, although the input values were being updated every 10 ms. The 100 samples were being averaged together in the integrator block and its response was updating far too slowly, creating an unstable control response. To solve this problem and to yield the proper control response seen in Figure 62, a custom integration term calculation needed to be written.

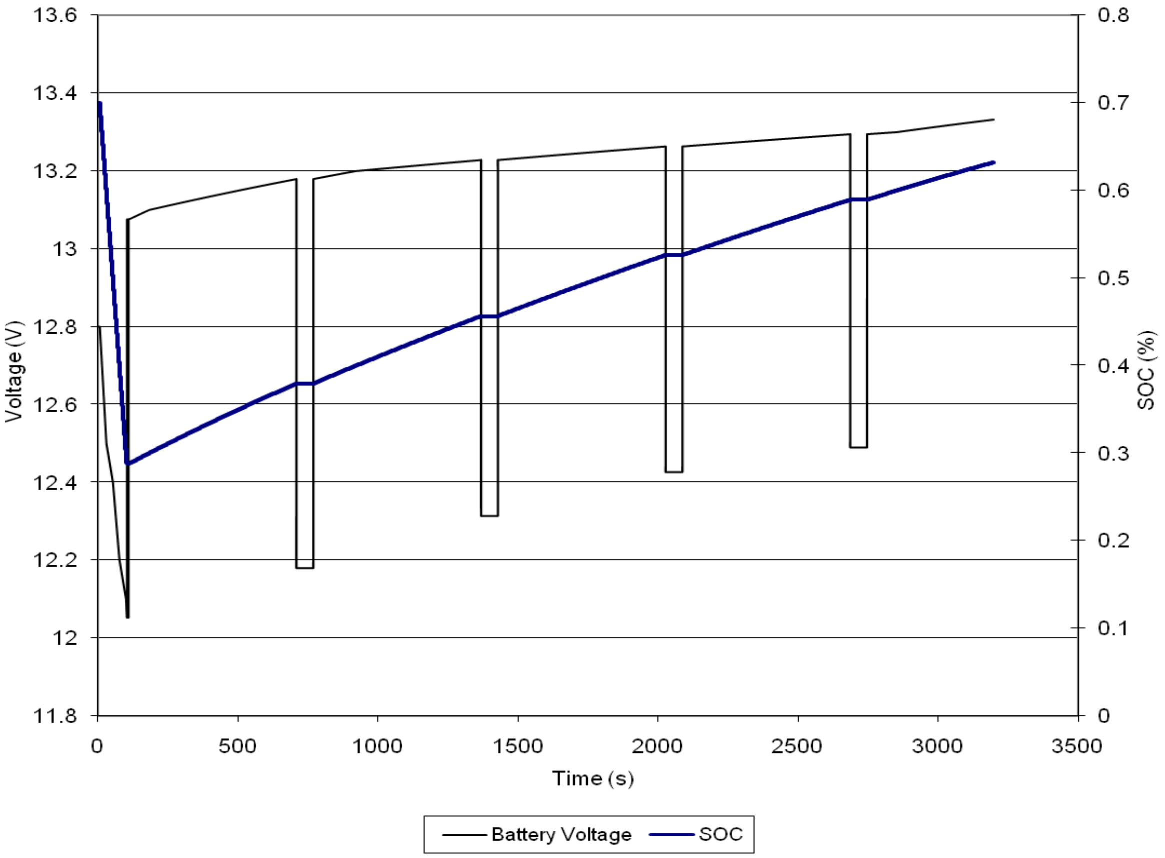

Figure 62: Expected charge circuit function. Charging the battery is interrupted periodically for 1 minute intervals to measure the battery state of charge

The NiMH charge control was validated and appropriately tuned, using the hardware-in-the-loop simulation system. The iterative approach taken not only saved vehicle down time due to 12V system troubleshooting, but also mitigated the risk of component damage by identifying and correcting unstable control logic.

4.5 Offline Development

4.5.1 Bluetooth Controller Area Network Development

To design the Bluetooth interface, Research In Motion (RIM) proprietary Java Development Environment (JDE) software was used to write an application for the Blackberry™ wireless device that was targeted for use on the vehicle during the competition. The HIL simulation system was used as a source of wireless controller area network (CAN) messages with identical timing and data payloads as would be transmitted by the vehicle CAN bus. The validation was performed in the following way:

1. ‘BT_CAN01’ model was configured in Simulation Interface Toolkit to define specific out ports as CAN message signals on CAN bus 1;
2. This model was run in real-time on the PXI. The Kvaser CAN bus monitor was used to ensure that the CAN message timing and payload was as expected on CAN 1;
3. The CANVIEW-Bluetooth hardware was connected to that data bus and properly terminated. The hardware was then configured remotely using a Bluetooth connection from the host computer;
4. The host computer was then used as a Bluetooth CAN message receiver by using the HyperTerminal application. This was done to provide an idea of exactly what data packets were being transmitted wirelessly over Bluetooth. The result of this recording is shown in Figure 63; and,
5. The recorded CAN message transmission was then used to parse the Java code to accept and read the desired CAN messages to be written onto the API screen.

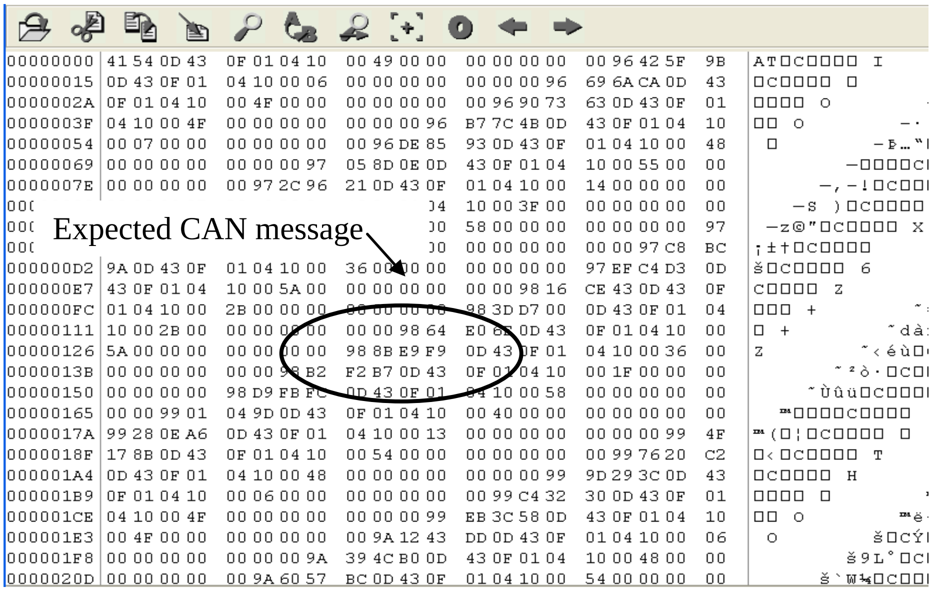

Expected CAN message

```
00000000 | 41 54 0D 43  0F 01 04 10  00 49 00 00  00 00 00 00  00 96 42 5F  9B | AT□C□□□□ I
00000015 | 0D 43 0F 01  04 10 00 06  00 00 00 00  00 00 00 96  69 6A CA 0D  43 | □C□□□□ □
0000002A | 0F 01 04 10  00 4F 00 00  00 00 00 00  00 96 90 73  63 0D 43 0F  01 | □□□□ O        ·
0000003F | 04 10 00 4F  00 00 00 00  00 00 00 96  B7 7C 4B 0D  43 0F 01 04  10 | □□ O        –·
00000054 | 00 07 00 00  00 00 00 00  00 96 DE 85  93 0D 43 0F  01 04 10 00  48 |  □        –Þ…"
00000069 | 00 00 00 00  00 00 00 97  05 8D 0E 0D  43 0F 01 04  10 00 55 00  00 |        —□□□□C
0000007E | 00 00 00 00  00 97 2C 96  21 0D 43 0F  01 04 10 00  14 00 00 00  00 |      —,–!□C□□
00(                               )4  10 00 3F 00  00 00 00 00  00 |     –S )□C□□□□
00(                               )0  58 00 00 00  00 00 00 00  97 |  —z©"□C□□□□ X
00(                               )0  00 00 00 00  00 00 97 C8  BC | ¡±†□C□□□□
000000D2 | 9A 0D 43 0F  01 04 10 00  36 00 00 00  00 00 00 00  97 EF C4 D3  0D | š□C□□□□ 6
000000E7 | 43 0F 01 04  10 00 5A 00  00 00 00 00  00 00 98 16  CE 43 0D 43  0F | C□□□□ Z
000000FC | 01 04 10 00  2B 00 00 00  00 00 00 00  98 3D D7 00  0D 43 0F 01  04 | □□□ +        ˜
00000111 | 10 00 2B 00  00 00 00 00  00 00 98 64  E0 6E 0D 43  0F 01 04 10  00 | □ +        ˜dà
00000126 | 5A 00 00 00  00 00 00 00  98 8B E9 F9  0D 43 0F 01  04 10 00 36  00 | Z        ˜‹éù□
0000013B | 00 00 00 00  00 00 98 B2  F2 B7 0D 43  0F 01 04 10  00 1F 00 00  00 |        ˜²ò·□C□
00000150 | 00 00 00 00  98 D9 FB FC  0D 43 0F 01  04 10 00 58  00 00 00 00  00 |       ˜ÙûüÜ□C□□□
00000165 | 00 00 99 01  04 9D 0D 43  0F 01 04 10  00 40 00 00  00 00 00 00  00 |   ™□□□□C□□□□
0000017A | 99 28 0E A6  0D 43 0F 01  04 10 00 13  00 00 00 00  00 00 00 99  4F | ™(□¦□C□□□□ □
0000018F | 17 8B 0D 43  0F 01 04 10  00 54 00 00  00 00 00 00  00 99 76 20  C2 | □‹□C□□□□ T
000001A4 | 0D 43 0F 01  04 10 00 48  00 00 00 00  00 00 00 99  9D 29 3C 0D  43 | □C□□□□ H
000001B9 | 0F 01 04 10  00 06 00 00  00 00 00 00  00 99 C4 32  30 0D 43 0F  01 | □□□□ □
000001CE | 04 10 00 4F  00 00 00 00  00 00 00 99  EB 3C 58 0D  43 0F 01 04  10 | □□ O        ™ë
000001E3 | 00 4F 00 00  00 00 00 00  00 9A 12 43  DD 0D 43 0F  01 04 10 00  06 |  O        š□CÝ
000001F8 | 00 00 00 00  00 00 00 9A  39 4C B0 0D  43 0F 01 04  10 00 48 00  00 |        š9L°□C
0000020D | 00 00 00 00  00 9A 60 57  BC 0D 43 0F  01 04 10 00  54 00 00 00  00 |       š`W¼□C□□
```

Figure 63: Recorded Bluetooth™ raw data with expected CAN message circled

The Java code for the Bluetooth interface can be found in Appendix F. The resulting Blackberry CAN interface is shown in Figure 64 and was a major consumer acceptability feature of the vehicle during the competition as well as being extremely useful for monitoring the battery state of charge (SOC) during a period of time that the GM CAN network was being repaired on the vehicle, but the battery still required charging. The only exact way to monitor the battery SOC was to use the RIM Blackberry™ loaded with the monitoring software.

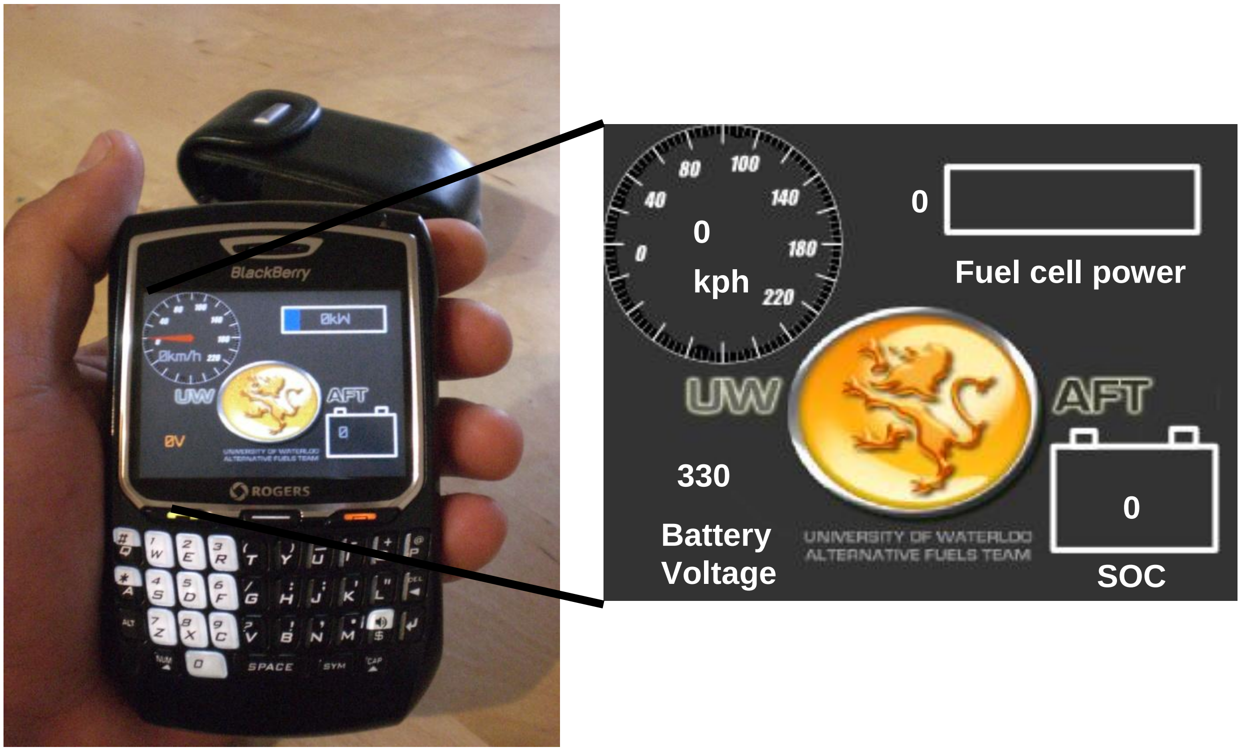

Figure 64: Bluetooth CAN message receiver on the Blackberry™ device

4.5.2 Graphical User Interface Development

To develop the graphical user interface (GUI) on the HIL simulation system, several development phases were undertaken to overcome the challenge of integrating a touch panel designed for stationary panel application into a vehicle. The main development work is outlined below:

1. The TPC-2006 has a relatively low screen resolution and colour density as shipped. National Instruments provides an online upgrade routine that upgrades the screen quality. This was implemented immediately upon power-up;
2. To have an application start upon power-up, a specific protocol for file location and WinCE configuration must be undertaken. The file must be located in the 'start' folder, or else the TPCConfig utility must be used to define startup files. The GUI virtual instrument file was configured to be loaded upon startup of the system; and,
3. To use the TPC RS-485 interface port, NI-VISA drivers must be loaded to the TPC. This would normally need to occur each time the TPC is restarted, but a *.cab file was provided by National Instruments that was used to ensure that the VISA drivers were permanently installed.

This procedure allowed the TPC to perform its basic display and communication functions. In order to interface the GUI to the hardware-in-the-loop simulation system, a 120 ohm termination resistor was integrated into the 2-wire RS-485 port connection from the controller to the GUI. The signal quality and transmission rate was then observed using an oscilloscope. An abnormal amount of noise in the communication line required a rewiring effort to replace the wound unshielded wire with a twisted shielded pair with the shielding grounded, which resulted in a marked improvement in signal quality.

Although the signal quality was improved, when the GUI communication VI was run and the controller was broadcasting a serial communication signal, the received message was unexpected and appeared to be random.   A work-around strategy was devised to decode the signal. Broadcasting specific characters on the Mototron resulted in predictable received characters on the GUI, according to Table 27.

Table 27: Predictable characters from the Mototron received by the GUI

Mototron sends	Corresponds to	LabVIEW receives
5	Park	}
25	Reverse	s
51	Drive	f
50	Neutral	3
27	Tow	r
41	GFI	k

An expected character was received, however the messages contained a significant amount of additional data that was not required, thereby requiring a parsing mechanism to be conceived. The GUI code outlining this parsing mechanism can be found in Appendix C.

The GUI display parameters selected for the year three competition vehicle were the gear selection position and the ground fault warning. The screen shot in Figure 65 shows the actual screen that is displayed to the user. The tab control on the top of the screen allows vehicle parameters to be added such as instantaneous fuel economy in future functionality expansion.

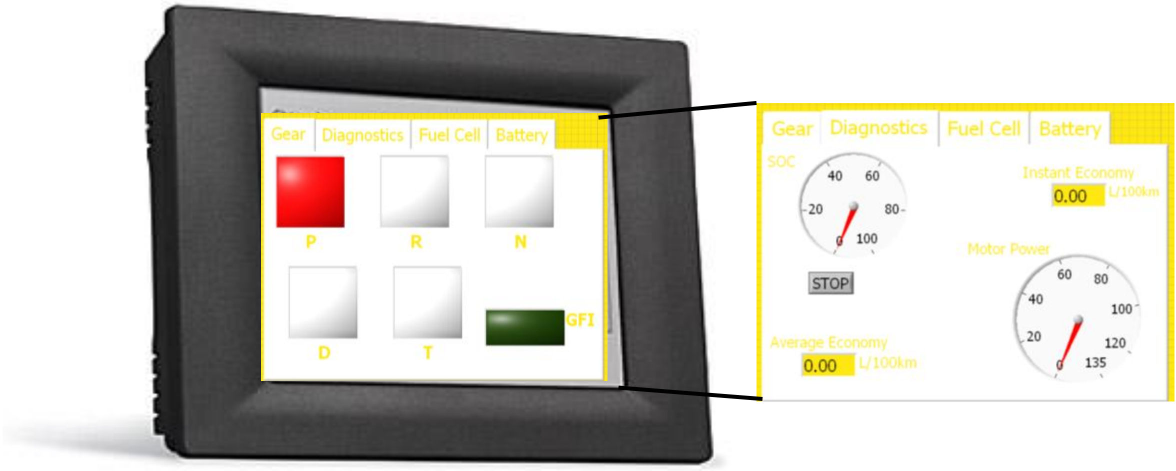

Figure 65: TPC-2006 touch screen with custom UWAFT interface [41]

Chapter 5: Conclusions and Recommendations

This thesis describes how model-based control validation and development parallelized work flow for the ChallengeX fuel cell hybrid Equinox project using a custom hardware-in-the-loop and software-in-the-loop simulation system. The ability to simulate a vehicle in real-time allows control strategy and hardware development to take place during the winter months when it is not feasible to perform on-road trials. An additional benefit is that the set-up and execution times for running virtual controls tests are much shorter than running in-vehicle tests. Virtual control development therefore allows more testing and validation to be done in a short period. Most importantly, testing control algorithms on systems that are expensive and potentially hazardous (high voltage) can be performed in a virtual environment with confidence that no damage to personnel or equipment will result.

Software-in-the-loop (SIL) testing was first performed in order to validate the vehicle models that were to be used for hardware-in-the-loop testing, as well as to evaluate the performance of regenerative braking and torque control algorithms. Once confidence in the models was established, hardware-in-the-loop (HIL) simulation was performed validate code generation, signal and communication busses, controller robustness, and fail-safe control operation. The virtual vehicle model was run on National Instruments PXI real-time control hardware using LabVIEW simulation interface toolkit. The vehicle models were exclusively built in Simulink™ and Stateflow™ and were most often empirical models created from the extensive vehicle testing data. A results summary and recommendation list is given for each of the control validations performed:

- Signal bus validation determined that the HIL simulation system can simulate all vehicle systems except for the DC/DC converter dynamics which requires a signal lag of 1ms or less. Controller CAN communication was verified to occur within 1ms, and the maximum signal lag on the rest of the system is less than 20ms. These results suggest that communication and signal lag will not pose a risk to safe vehicle control. It is recommended for future work that the DC/DC control code be tested independently so that the simulation speed can be brought under 1ms and valid results can be obtained.

- CAN bus loading trials showed that at the typical vehicle CAN bus loads of 50% utilization, the communication system will be stable. Communication failure begins to occur at 90% bus load. It is recommended that CAN bus loading always be observed when new code is implemented to ensure that bus loading never approaches the 90% threshold.

- By simulating the expected fuel cell fault messages, the controller was found to handle the faults appropriately. The source of the fault message irregularity was determined to be the fuel cell power module controller. It is recommended that new fuel cell power module control code be loaded to ensure that fault messages are appropriately handled.

- Varying the controller supply voltage found that both controllers are able to operate reliably at 18V, although their nominal input voltage should be 12V. Voltage droop testing found that the rear controller ceases to function reliably at 5.73V and the front controller ceases to function reliably at 5.43V. In order to maintain proper controller functionality and thus occupant safety, it is recommended that appropriate shut-down procedures are implemented if the 12V bus voltage drops below a threshold of 9 volts for an extended period.

- Failure insertion trials identified serious shortcomings in the control code that handles fail safe operation in the event of signal line faults. None of the targeted signal lines responded in the expected manner and the throttle position sensor control code was found to lack important rationality checking that is an even lower level critical functionality than line fault handling. Control suggestions were made to appropriately handle a wiring harness failure and to control the throttle position switch redundancy in that section.

- A CAN/Bluetooth wireless vehicle communication bus interface as well as a touch-screen graphical user interface were developed off-line using the HIL simulation system without requiring vehicle resources. It is recommended that further functionality be implemented on the HIL stand such as driver recognition and expanded telematics.

- The regenerative braking and torque control strategies were debugged and a first tuning was performed in an SIL virtual environment. Several potentially dangerous code behaviours were identified and mitigated. The fidelity of the model was determined and the success of the SIL control validation was confirmed by on-road vehicle operating data. It is recommended that before any new motor control code is implemented, a detailed virtual validation is performed to avoid occupant safety risks.

- Full hardware-in-the-loop control validation and tuning was performed on the new 12V charging system before it was implemented. Vehicle performance confirmed the success of the control tuning effort. It is recommended that the control strategy be further optimized to ensure that charging/discharging occurs as efficiently as possible.

At competition, the University of Waterloo Alternative Fuels Team entry successfully completed all of the dynamic competition events, a feat that has not been accomplished by any fuel cell vehicle entry in past advanced vehicle design competitions. The team was awarded the following prizes directly related to this thesis work:

- Best Traction Control
- Lowest Regulated Tailpipe Emissions
- Third Place, The Mathworks: Crossover to Model-Based Design
- Second Place, National Instruments Most Innovative Use of Graphical System Design
- 7th place overall out of the 17 teams competing in ChallengeX

The model-based control validation work accomplished for this thesis played a significant role in the UWAFT team’s success at competition and their successful development of a fuel cell hybrid passenger vehicle. It expanded the ability to perform accelerated controls development and identified safety concerns in the control systems before the code was implemented in the vehicle. The methodologies outlined in this thesis can be applied to future vehicle control strategy validation efforts. The concepts and results are scalable, and may be used to guide control strategy design for other types of hybrid and non-hybrid powertrains. In order to safely evaluate the effectiveness of a vehicle’s control strategy, virtual validation must be performed on its communication, fail safe features, and control algorithms.

Chapter 6: References

1. Stern, Nicholas 2007. *The Economics of Climate Change – The Stern Review* Cambridge, UK: Cambridge University Press. Also published online: http://www.hm-treasury.gov.uk/independent_reviews/stern_review_economics_climate_change/stern_review_report.cfm
2. Alley, Richard; et al. 2007. *Climate Change 2007: The Physical Science Basis* Paris: Summary for Policymakers, 10th session of working group I of the IPCC
3. Yap, David; Reid, Neville; De Brou, Gary; Bloxam, Robert. 2005. *Transboundary Air Pollution in Ontario* Toronto: Ontario Ministry of Environment Report
4. Dunn, Seth. 2002. Hydrogen futures: towards a sustainable energy system *International Journal of Hydrogen Energy* 27. 235-264
5. Fraser, Don. 2003. *Solutions for Hydrogen Storage and Distribution* Charlottetown: PEI Wind-Hydrogen Symposium. Presented June 23-24.
6. Anonymous. 2001. *Beyond the Internal Combustion* American Methanol Institute: Whitepaper. Published online http://www.methanol.org/contentIndex.cfm?section=fuelCells&topic=specialReports&title=Index
7. Carlson, Eric. 2005. *PEM Fuel Cell Cost Status* Palm Springs, USA: Fuel Cell Seminar, November 14-18
8. Granovskii, Mikhail; Dincer, Ibrahim; Rosen, Marc A. 2006. Environmental and economic aspects of hydrogen production and utilization in fuel cell vehicles *Journal of Power Sources*. 157. 411-421
9. Carpenter, Andrew R.; Hinze, Peter C. 2004. System safety analysis of hydrogen and methanol vehicle fuels *Process Safety Progress* 23. 292-299
10. Lovins, Amory B. 2005. *Twenty Hydrogen Myths* Boulder, Colorado: Rocky Mountain Institute whitepaper published online https://www.rmi.org/images/other/Energy/E03-05_20HydrogenMyths.pdf
11. Helena L. Chum, Ralph P. Overend. 2001. Biomass and renewable fuels *Fuel Processing Technology* 71. 187-195

12. Anonymous. 2005 Worldwide look at oil reserves and production. *Oil and Gas Journal* 103. 24-25

13. Anonymous 2007. *World Solar Insulation Values* Available online: http://howto.altenergystore.com/Reference-Materials/Solar-Insolation-Map-World/a43/

14. Granovskii, M. et al. 2006. Life cycle assessment of hydrogen fuel cell and gasoline vehicles. *International Journal of Hydrogen Energy* 31. 337-352

15. Anonymous. 2005. *Electric Vehicle History*. Electric Automobile Association Whitepaper available online: www.eaaev.org

16. Bandivadekar, Anup. 2007. *Impact of Vehicle Performance-Fuel Consumption Trade-off on Light-Duty Vehicle Fuel Use*. Cambridge, MA: MIT Before the Transition to a Hydrogen Economy working group meeting, June 3rd.

17. Ayers, C.M. et al. 2004. *Evaluation of 2004 Toyota Prius Hybrid Electric Drive System Interim Report*. Oakridge, TN: Engineering Science and Technology Division report. Available online: http://www.ornl.gov/~webworks/cppr/y2001/rpt/121813.pdf

18. Larminie, James; Dicks, Andrew. 2000. *Fuel Cell Systems Explained*. New York: John Wiley and Sons

19. Anonymous. 2003. *Fuel Cell Vehicle World Survey 2003-Specialty Vehicles*. US DOE Office of Energy Efficiency and Renewable Energy whitepaper. Available online: http://www1.eere.energy.gov/hydrogenandfuelcells/pdfs/specialty_vehicles.pdf

20. Walsh, Brian; Moores, Peter. 2002. *Auto Companies On Fuel Cells*. Fuel Cells 2000 Special Report. Available online: www.fuelcells.org/info/charts/vehiclestudy.pdf

21. Haak, David; 2004. *Scale-Up of Carbon/Carbon Composite Bipolar Plates*. DOE Hydrogen Program FY2004 progress report. Available online: http://www.hydrogen.energy.gov/annual_progress04.html

22. Brandon, N.P.; Brett, D.J. 2006. Engineering porous materials for fuel cell applications. *Philosophical Transactions of the Royal Society* 364. 147-159

23. Wang, Q. et al. 2004. Functionally Graded Cathode Catalyst Layers for Polymer Electrolyte Fuel Cells. *Journal of The Electrochemical Society* 151. A950-A957

24. Musil, David. 2006. *Fuel Cells –Current Status and Prospects for the Future*. Burnaby, BC: Ballard Power Systems Working Group Presentation. Available online: www.greenfleet.com.au/uploads/pdfs/DMF%20Presentation%20-%20D%20Musil.pdf

25. Anonymous. 2004. *HFP Prototype Data Sheet: Hy-Light*. European Hydrogen and Fuel Cell Technology Platform Datasheet. Available online: www.event.hfpeurope.org/exhibition/specs/Michelin_-_Specs.pdf

26. Fathy, H. et al. 2006. Review of Hardware-in-the-Loop Simulation and Its Prospects in the Automotive Area. *Modeling and Simulation for Military Applications, edited by Kevin Schum, Alex F. Sisti Proc. of SPIE*. 6228. 1-20

27. Boot, R. et al. 1999. Automated Test of ECUs in a Hardware-in-the-Loop Simulation Environment. Hawai'i, USA: *Proceedings of the 1999 EEE International Symposium on Computer Aided Control System Design*. 22-27

28. Köhl, S.; Jegminat, D. 2005. How to Do Hardware-in-the-Loop Simulation Right. Detroit, MI: *Proceedings of the 2005 SAE World Congress*. 2005-01-1657.

29. Hagiwaraa, K.; Terayamab,T.; Takedaa,Y. Yodab,K. Suzukia, S. 2002. Development of automatic transmission control system using hardware-in-the-loop simulation system. *JSAE Review* 23. 55-59

30. Lee, Jae-Cheon.; Suh, Myung-Won. Hardware-in-the Loop Simulator for ABS/TCS. Hawai'i, USA: *Proceedings of the 1999 EEE International Symposium on Computer Aided Control System Design*. 652-657

31. Cho, J.M.; et al. 2001. Design and Implementation of HILS system for ABS ECU of commercial vehicles. Pusan, Korea: IEEE transactions *0-7803-7090-2/01*

32. Leaphart, Eldon G.; Muldoon, Steve E.; Irlbeck, Jill N. 2006. Application of Robust Engineering Methods to Improve ECU Software Testing. *Proceedings of 2006 SAE World Congress, Detroit, Michigan, April 3-6*

33. Jehlick, Forrest. 2007. *ChallengeX Competition Rules*. Argonne National Laboratory, Advanced Vehicle Technology Competition Document

34. Mendes, Chris. 2006. *Fuel Cell Mounting Waiver*. University of Waterloo Alternative Fuels Team ChallengeX Competition Document.

35. Stevens, Matt.; et al. 2006. *University of Waterloo ChallengeX Spring Technical Report*. University of Waterloo Alternative Fuels Team ChallengeX Competition Document.
36. Lawerence, Christopher. 2007. *Improving Fuel Economy Via Management of Electrical Loads in Fuel Cell Electric Vehicles*. Waterloo, Ontario: Masters Thesis, University of Waterloo
37. Kopic, Peter. 2006. *Fuel System Installation and Operation Manual*. Enviromech Industries Fuel System Service Manual
38. Kopic, Peter. 2006. *Engineering Analysis Summary: Cylinder Mounting Structure, GM Equinox*. Enviromech Industries Fuel System Service Manual.
39. Anonymous. 2005. *HyPM 65: Fuel Cell Power Module*. Mississauga, Ontario: Hydrogenics Fuel Cell Operating Manual
40. Anonymous. 2006. *LabVIEW Real-Time Architecture and Good Programming Practices.* National Instruments LabVIEW Developers Zone. Available online: http://zone.ni.com/devzone/cda/tut/p/id/2833
41. Anonymous. 2006. *Benchmarking a Typical Control Application using LabVIEW Real-Time & NI-DAQmx*. National Instruments LabVIEW Developers Zone. Available online: http://zone.ni.com/devzone/cda/tut/p/id/5424
42. Ender, Tom. 2007. Email correspondence on April 16th, 2007.
43. Stevens, Matthew; Wahlstrom, Michael. 2007. *Control Strategy Presentation*. Milford, MI: ChallengeX Competition Presentation Session. June 6th, 2007.
44. Mali, Taylor, J. *Youth Outreach Presentation*. Internal UWAFT outreach presentation.
45. Conrad, Mirko. 2005. Automatic Evaluation of ECU Software Tests. *Proceedings of 2005 SAE World Congress, Detroit, Michigan, April 11-14. 2005-01-1659*
46. Lang, Oliver; Kindl, Helmut. 2005. Development of Fuel Cell System Air Management Utilizing HIL Tools. *Proceedings of 2002 SAE World Congress, Detroit, Michigan, March 4-7. 2002-01-0409*
47. Cardanha, Tim. 2005. Validating Powertrain Controller Systems With the VPACS-HIL Powertrain Simulator. *Proceedings of 2005 SAE World Congress, Detroit, Michigan, April 11-14. 2005-01-1663*

48. Pasquier, Maxime; Monnet, Gilles. 2006. *Diesel Hybridization and Emissions: A Report to DOE from the ANL Vehicle Systems and Fuels Team*. Government report: For the U.S. Department of Energy Office of Advanced Automotive Technologies.
49. Akers, Andrew. 2006. *Electronic Service Request*. National Instruments technical support representative discussion.
50. Huizing, Ryan. 2006. *Engineering Analysis of Fuel Cell Air Delivery*. Coursework performed for the Alternative Fuels Team.
51. Adams, Robert. 2005. *Hydrogen Test Cell Safety Upgrade Report*. Marathon Technical Services Commissioned Report. University of Waterloo Alternative Fuels Team.

Appendices

Appendix A: Hardware Data Sheets

MOSFET on HIL simulator: Supplier provided data sheet

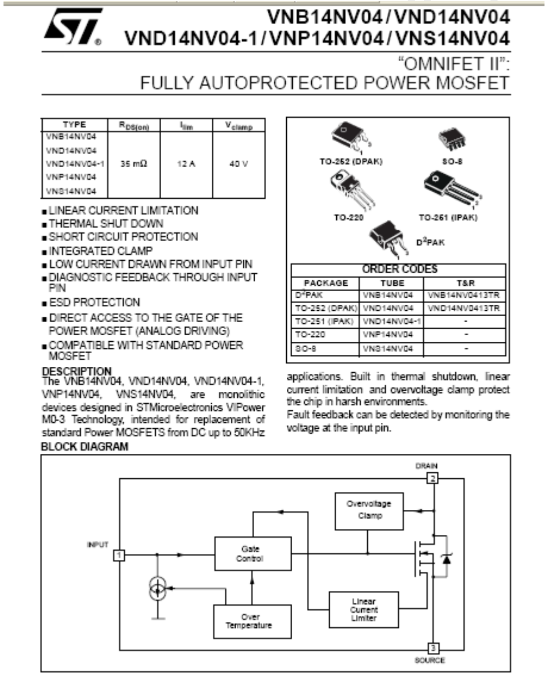

VNB14NV04 / VND14NV04
VND14NV04-1 / VNP14NV04 / VNS14NV04

"OMNIFET II":
FULLY AUTOPROTECTED POWER MOSFET

TYPE	$R_{DS(on)}$	I_{lim}	V_{clamp}
VNB14NV04 VND14NV04 VND14NV04-1 VNP14NV04 VNS14NV04	35 mΩ	12 A	40 V

- LINEAR CURRENT LIMITATION
- THERMAL SHUT DOWN
- SHORT CIRCUIT PROTECTION
- INTEGRATED CLAMP
- LOW CURRENT DRAWN FROM INPUT PIN
- DIAGNOSTIC FEEDBACK THROUGH INPUT PIN
- ESD PROTECTION
- DIRECT ACCESS TO THE GATE OF THE POWER MOSFET (ANALOG DRIVING)
- COMPATIBLE WITH STANDARD POWER MOSFET

ORDER CODES		
PACKAGE	TUBE	T&R
D^2PAK	VNB14NV04	VNB14NV0413TR
TO-252 (DPAK)	VND14NV04	VND14NV0413TR
TO-251 (IPAK)	VND14NV04-1	-
TO-220	VNP14NV04	-
SO-8	VNS14NV04	-

DESCRIPTION

The VNB14NV04, VND14NV04, VND14NV04-1, VNP14NV04, VNS14NV04, are monolithic devices designed in STMicroelectronics VIPower M0-3 Technology, intended for replacement of standard Power MOSFETS from DC up to 50KHz applications. Built in thermal shutdown, linear current limitation and overvoltage clamp protect the chip in harsh environments.

Fault feedback can be detected by monitoring the voltage at the input pin.

BLOCK DIAGRAM

NI-PXI 8187 real time controller: www.ni.com

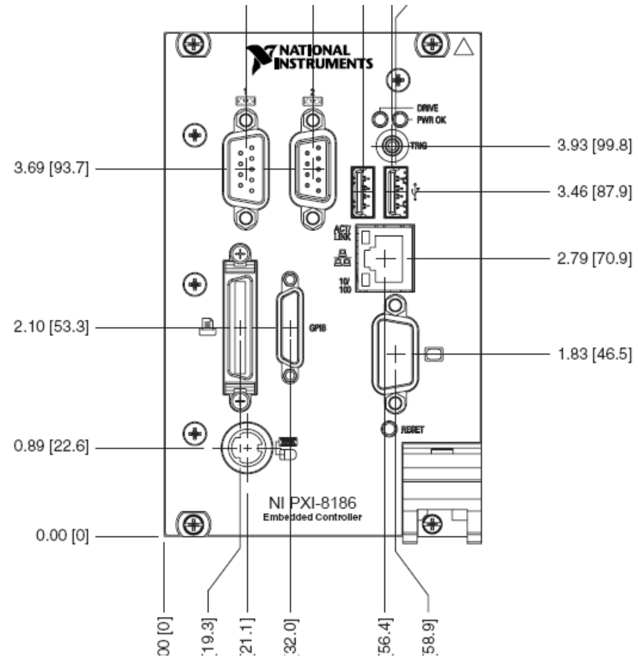

PXI 6229 Low cost M-series DAQ: www.ni.com

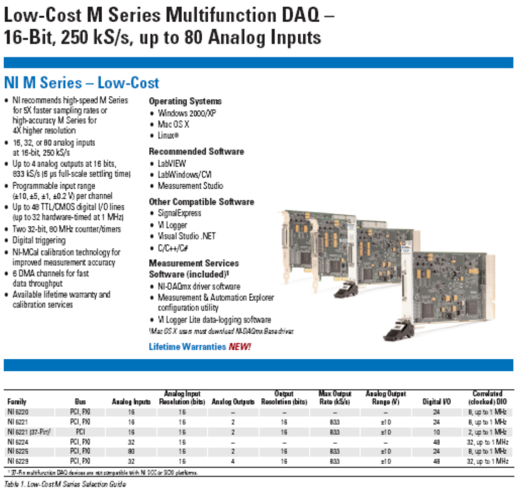

Low-Cost M Series Multifunction DAQ – 16-Bit, 250 kS/s, up to 80 Analog Inputs

NI M Series – Low-Cost

- NI recommends high-speed M Series for 5X faster sampling rates or high-accuracy M Series for 4X higher resolution
- 16, 32, or 80 analog inputs at 16-bit, 250 kS/s
- Up to 4 analog outputs at 16 bits, 833 kS/s (6 µs full-scale settling time)
- Programmable input range (±10, ±5, ±1, ±0.2 V) per channel
- Up to 48 TTL/CMOS digital I/O lines (up to 32 hardware-timed at 1 MHz)
- Two 32-bit, 80 MHz counter/timers
- Digital triggering
- NI-MCal calibration technology for improved measurement accuracy
- 6 DMA channels for fast data throughput
- Available lifetime warranty and calibration services

Operating Systems
- Windows 2000/XP
- Mac OS X
- Linux®

Recommended Software
- LabVIEW
- LabWindows/CVI
- Measurement Studio

Other Compatible Software
- SignalExpress
- VI Logger
- Visual Studio .NET
- C/C++/C#

Measurement Services Software (included)[1]
- NI-DAQmx driver software
- Measurement & Automation Explorer configuration utility
- VI Logger Lite data-logging software

[1] Mac OS X users must download NI-DAQmx Base driver.

Lifetime Warranties *NEW!*

Family	Bus	Analog Inputs	Analog Input Resolution (bits)	Analog Outputs	Output Resolution (bits)	Max Output Rate (kS/s)	Analog Output Range (V)	Digital I/O	Correlated (clocked) DIO
NI 6220	PCI, PXI	16	16	–	–	–	–	24	8, up to 1 MHz
NI 6221	PCI, PXI	16	16	2	16	833	±10	24	8, up to 1 MHz
NI 6221 (37-Pin)[1]	PCI	16	16	2	16	833	±10	10	2, up to 1 MHz
NI 6224	PCI, PXI	32	16	–	–	–	–	48	32, up to 1 MHz
NI 6225	PCI, PXI	80	16	2	16	833	±10	24	8, up to 1 MHz
NI 6229	PCI, PXI	32	16	4	16	833	±10	48	32, up to 1 MHz

[1] 37-Pin multifunction DAQ devices are not compatible with NI SCC or SCXI platforms.

Table 1. Low-Cost M Series Selection Guide

PXI 6259 High speed M-series DAQ

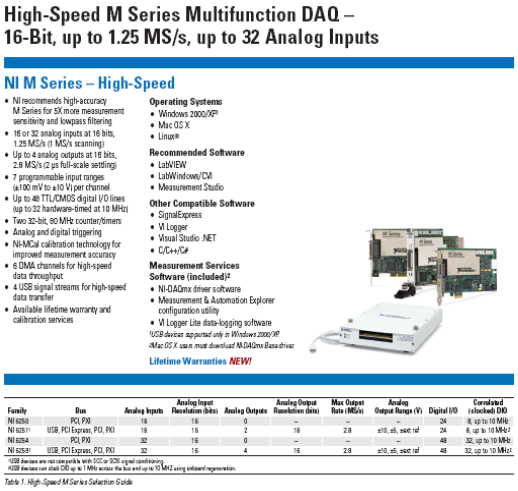

High-Speed M Series Multifunction DAQ – 16-Bit, up to 1.25 MS/s, up to 32 Analog Inputs

NI M Series – High-Speed

- NI recommends high-accuracy M Series for 5X more measurement sensitivity and lowpass filtering
- 16 or 32 analog inputs at 16 bits, 1.25 MS/s (1 MS/s scanning)
- Up to 4 analog outputs at 16 bits, 2.8 MS/s (2 µs full-scale settling)
- 7 programmable input ranges (±100 mV to ±10 V) per channel
- Up to 48 TTL/CMOS digital I/O lines (up to 32 hardware-timed at 10 MHz)
- Two 32-bit, 80 MHz counter/timers
- Analog and digital triggering
- NI-MCal calibration technology for improved measurement accuracy
- 6 DMA channels for high-speed data throughput
- 4 USB signal streams for high-speed data transfer
- Available lifetime warranty and calibration services

Operating Systems
- Windows 2000/XP[1]
- Mac OS X
- Linux®

Recommended Software
- LabVIEW
- LabWindows/CVI
- Measurement Studio

Other Compatible Software
- SignalExpress
- VI Logger
- Visual Studio .NET
- C/C++/C#

Measurement Services Software (included)[2]
- NI-DAQmx driver software
- Measurement & Automation Explorer configuration utility
- VI Logger Lite data-logging software

[1] USB devices supported only in Windows 2000/XP.
[2] Mac OS X users must download NI-DAQmx Base driver.

Lifetime Warranties *NEW!*

Family	Bus	Analog Inputs	Analog Input Resolution (bits)	Analog Outputs	Analog Output Resolution (bits)	Max Output Rate (MS/s)	Analog Output Range (V)	Digital I/O	Correlated (clocked) DIO
NI 6250	PCI, PXI	16	16	0	–	–	–	24	8, up to 10 MHz
NI 6251[1]	USB, PCI Express, PCI, PXI	16	16	2	16	2.8	±10, ±5, ±ext ref	24	8, up to 10 MHz[2]
NI 6254	PCI, PXI	32	16	0	–	–	–	48	32, up to 10 MHz
NI 6259[1]	USB, PCI Express, PCI, PXI	32	16	4	16	2.8	±10, ±5, ±ext ref	48	32, up to 10 MHz[2]

[1] USB devices are not compatible with SCC or SCXI signal conditioning.
[2] USB devices can clock DIO up to 1 MHz across the bus and up to 10 MHZ using onboard regeneration.

Table 1. High-Speed M Series Selection Guide

NI PXI 6289 High accuracy M-series DAQ: www.ni.com

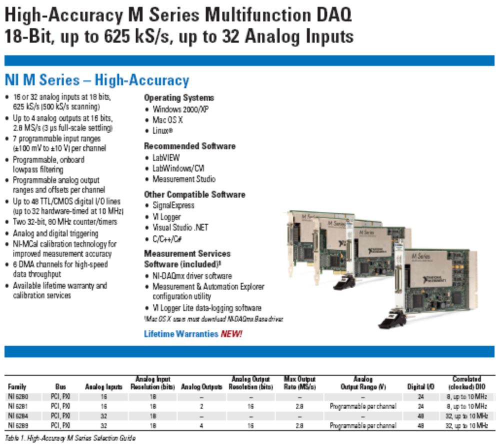

High-Accuracy M Series Multifunction DAQ 18-Bit, up to 625 kS/s, up to 32 Analog Inputs

NI M Series – High-Accuracy

- 16 or 32 analog inputs at 18 bits, 625 kS/s (500 kS/s scanning)
- Up to 4 analog outputs at 16 bits, 2.8 MS/s (3 µs full-scale settling)
- 7 programmable input ranges (±100 mV to ±10 V) per channel
- Programmable, onboard lowpass filtering
- Programmable analog output ranges and offsets per channel
- Up to 48 TTL/CMOS digital I/O lines (up to 32 hardware-timed at 10 MHz)
- Two 32-bit, 80 MHz counter/timers
- Analog and digital triggering
- NI-MCal calibration technology for improved measurement accuracy
- 6 DMA channels for high-speed data throughput
- Available lifetime warranty and calibration services

Operating Systems
- Windows 2000/XP
- Mac OS X
- Linux®

Recommended Software
- LabVIEW
- LabWindows/CVI
- Measurement Studio

Other Compatible Software
- SignalExpress
- VI Logger
- Visual Studio .NET
- C/C++/C#

Measurement Services Software (included)[1]
- NI-DAQmx driver software
- Measurement & Automation Explorer configuration utility
- VI Logger Lite data-logging software

[1] Mac OS X users must download NI-DAQmx Base driver.

Lifetime Warranties *NEW!*

Family	Bus	Analog Inputs	Analog Input Resolution (bits)	Analog Outputs	Analog Output Resolution (bits)	Max Output Rate (MS/s)	Analog Output Range (V)	Digital I/O	Correlated (clocked) DIO
NI 6280	PCI, PXI	16	18	–	–	–	–	24	8, up to 10 MHz
NI 6281	PCI, PXI	16	18	2	16	2.8	Programmable per channel	24	8, up to 10 MHz
NI 6284	PCI, PXI	32	18	–	–	–	–	48	32, up to 10 MHz
NI 6289	PCI, PXI	32	18	4	16	2.8	Programmable per channel	48	32, up to 10 MHz

Table 1. High-Accuracy M Series Selection Guide

Appendix B: HIL Simulator wiring and Controller CAN

File name: HIL_IOandCAN_140407. 2 pages long, 3 pages wide.

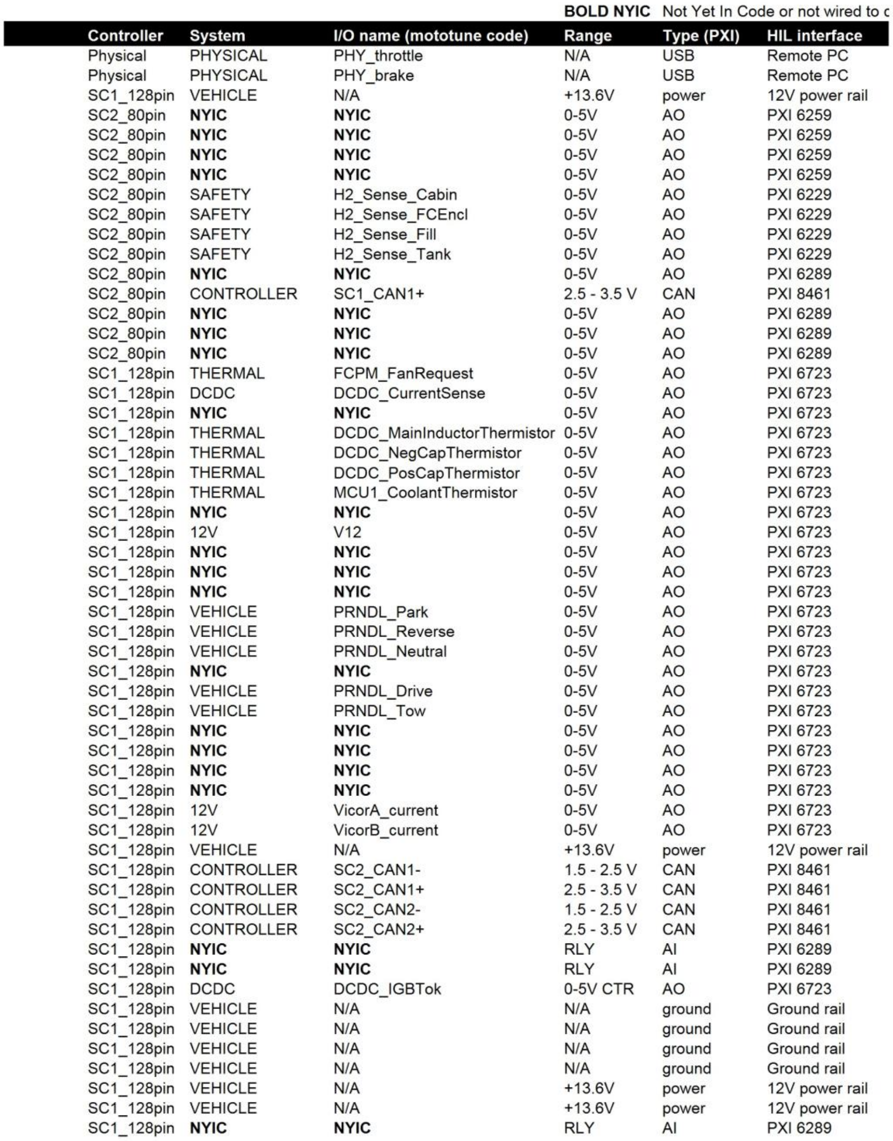

BOLD NYIC Not Yet In Code or not wired to c

Controller	System	I/O name (mototune code)	Range	Type (PXI)	HIL interface
Physical	PHYSICAL	PHY_throttle	N/A	USB	Remote PC
Physical	PHYSICAL	PHY_brake	N/A	USB	Remote PC
SC1_128pin	VEHICLE	N/A	+13.6V	power	12V power rail
SC2_80pin	**NYIC**	**NYIC**	0-5V	AO	PXI 6259
SC2_80pin	**NYIC**	**NYIC**	0-5V	AO	PXI 6259
SC2_80pin	**NYIC**	**NYIC**	0-5V	AO	PXI 6259
SC2_80pin	**NYIC**	**NYIC**	0-5V	AO	PXI 6259
SC2_80pin	SAFETY	H2_Sense_Cabin	0-5V	AO	PXI 6229
SC2_80pin	SAFETY	H2_Sense_FCEncl	0-5V	AO	PXI 6229
SC2_80pin	SAFETY	H2_Sense_Fill	0-5V	AO	PXI 6229
SC2_80pin	SAFETY	H2_Sense_Tank	0-5V	AO	PXI 6229
SC2_80pin	**NYIC**	**NYIC**	0-5V	AO	PXI 6289
SC2_80pin	CONTROLLER	SC1_CAN1+	2.5 - 3.5 V	CAN	PXI 8461
SC2_80pin	**NYIC**	**NYIC**	0-5V	AO	PXI 6289
SC2_80pin	**NYIC**	**NYIC**	0-5V	AO	PXI 6289
SC2_80pin	**NYIC**	**NYIC**	0-5V	AO	PXI 6289
SC1_128pin	THERMAL	FCPM_FanRequest	0-5V	AO	PXI 6723
SC1_128pin	DCDC	DCDC_CurrentSense	0-5V	AO	PXI 6723
SC1_128pin	**NYIC**	**NYIC**	0-5V	AO	PXI 6723
SC1_128pin	THERMAL	DCDC_MainInductorThermistor	0-5V	AO	PXI 6723
SC1_128pin	THERMAL	DCDC_NegCapThermistor	0-5V	AO	PXI 6723
SC1_128pin	THERMAL	DCDC_PosCapThermistor	0-5V	AO	PXI 6723
SC1_128pin	THERMAL	MCU1_CoolantThermistor	0-5V	AO	PXI 6723
SC1_128pin	**NYIC**	**NYIC**	0-5V	AO	PXI 6723
SC1_128pin	12V	V12	0-5V	AO	PXI 6723
SC1_128pin	**NYIC**	**NYIC**	0-5V	AO	PXI 6723
SC1_128pin	**NYIC**	**NYIC**	0-5V	AO	PXI 6723
SC1_128pin	**NYIC**	**NYIC**	0-5V	AO	PXI 6723
SC1_128pin	VEHICLE	PRNDL_Park	0-5V	AO	PXI 6723
SC1_128pin	VEHICLE	PRNDL_Reverse	0-5V	AO	PXI 6723
SC1_128pin	VEHICLE	PRNDL_Neutral	0-5V	AO	PXI 6723
SC1_128pin	**NYIC**	**NYIC**	0-5V	AO	PXI 6723
SC1_128pin	VEHICLE	PRNDL_Drive	0-5V	AO	PXI 6723
SC1_128pin	VEHICLE	PRNDL_Tow	0-5V	AO	PXI 6723
SC1_128pin	**NYIC**	**NYIC**	0-5V	AO	PXI 6723
SC1_128pin	**NYIC**	**NYIC**	0-5V	AO	PXI 6723
SC1_128pin	**NYIC**	**NYIC**	0-5V	AO	PXI 6723
SC1_128pin	**NYIC**	**NYIC**	0-5V	AO	PXI 6723
SC1_128pin	12V	VicorA_current	0-5V	AO	PXI 6723
SC1_128pin	12V	VicorB_current	0-5V	AO	PXI 6723
SC1_128pin	VEHICLE	N/A	+13.6V	power	12V power rail
SC1_128pin	CONTROLLER	SC2_CAN1-	1.5 - 2.5 V	CAN	PXI 8461
SC1_128pin	CONTROLLER	SC2_CAN1+	2.5 - 3.5 V	CAN	PXI 8461
SC1_128pin	CONTROLLER	SC2_CAN2-	1.5 - 2.5 V	CAN	PXI 8461
SC1_128pin	CONTROLLER	SC2_CAN2+	2.5 - 3.5 V	CAN	PXI 8461
SC1_128pin	**NYIC**	**NYIC**	RLY	AI	PXI 6289
SC1_128pin	**NYIC**	**NYIC**	RLY	AI	PXI 6289
SC1_128pin	DCDC	DCDC_IGBTok	0-5V CTR	AO	PXI 6723
SC1_128pin	VEHICLE	N/A	N/A	ground	Ground rail
SC1_128pin	VEHICLE	N/A	N/A	ground	Ground rail
SC1_128pin	VEHICLE	N/A	N/A	ground	Ground rail
SC1_128pin	VEHICLE	N/A	N/A	ground	Ground rail
SC1_128pin	VEHICLE	N/A	+13.6V	power	12V power rail
SC1_128pin	VEHICLE	N/A	+13.6V	power	12V power rail
SC1_128pin	**NYIC**	**NYIC**	RLY	AI	PXI 6289

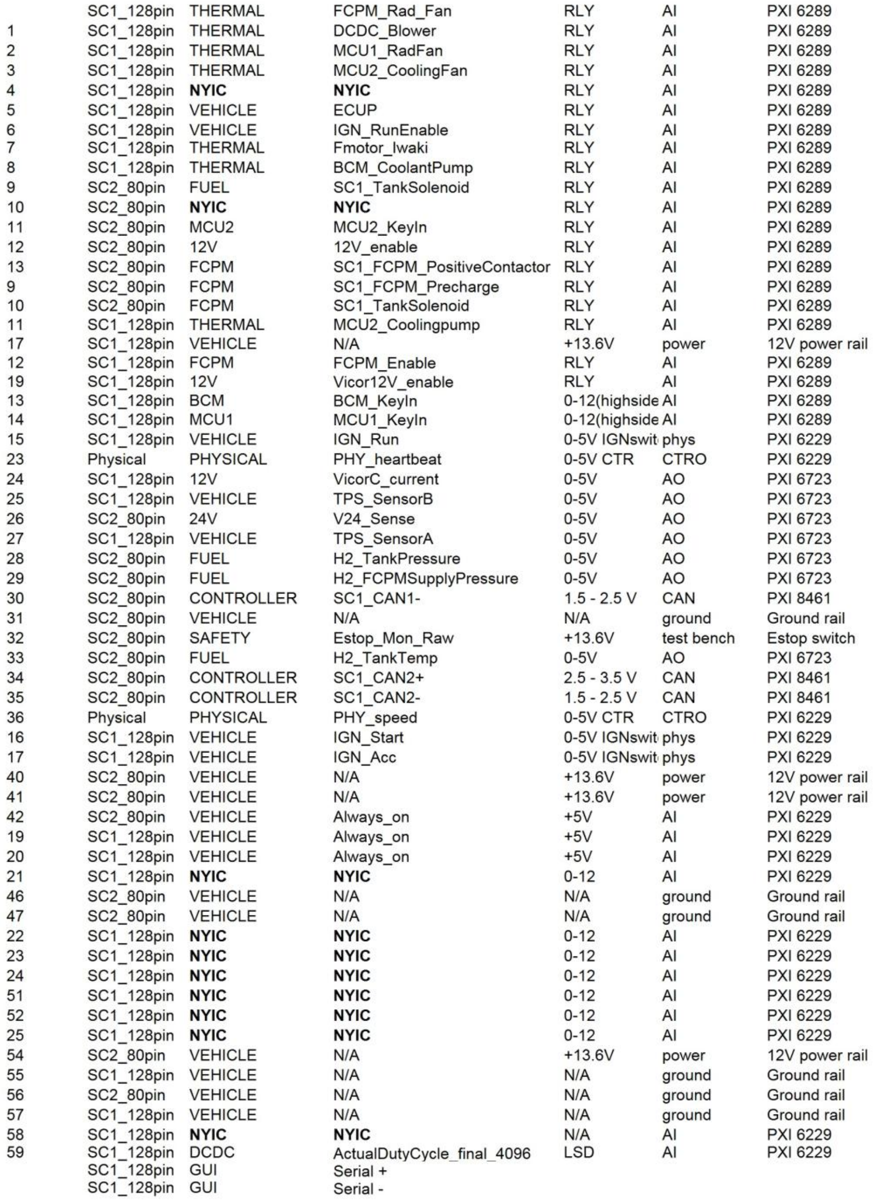

	SC1_128pin	THERMAL	FCPM_Rad_Fan	RLY	AI	PXI 6289
1	SC1_128pin	THERMAL	DCDC_Blower	RLY	AI	PXI 6289
2	SC1_128pin	THERMAL	MCU1_RadFan	RLY	AI	PXI 6289
3	SC1_128pin	THERMAL	MCU2_CoolingFan	RLY	AI	PXI 6289
4	SC1_128pin	**NYIC**	**NYIC**	RLY	AI	PXI 6289
5	SC1_128pin	VEHICLE	ECUP	RLY	AI	PXI 6289
6	SC1_128pin	VEHICLE	IGN_RunEnable	RLY	AI	PXI 6289
7	SC1_128pin	THERMAL	Fmotor_Iwaki	RLY	AI	PXI 6289
8	SC1_128pin	THERMAL	BCM_CoolantPump	RLY	AI	PXI 6289
9	SC2_80pin	FUEL	SC1_TankSolenoid	RLY	AI	PXI 6289
10	SC2_80pin	**NYIC**	**NYIC**	RLY	AI	PXI 6289
11	SC2_80pin	MCU2	MCU2_KeyIn	RLY	AI	PXI 6289
12	SC2_80pin	12V	12V_enable	RLY	AI	PXI 6289
13	SC2_80pin	FCPM	SC1_FCPM_PositiveContactor	RLY	AI	PXI 6289
9	SC2_80pin	FCPM	SC1_FCPM_Precharge	RLY	AI	PXI 6289
10	SC2_80pin	FCPM	SC1_TankSolenoid	RLY	AI	PXI 6289
11	SC1_128pin	THERMAL	MCU2_Coolingpump	RLY	AI	PXI 6289
17	SC1_128pin	VEHICLE	N/A	+13.6V	power	12V power rail
12	SC1_128pin	FCPM	FCPM_Enable	RLY	AI	PXI 6289
19	SC1_128pin	12V	Vicor12V_enable	RLY	AI	PXI 6289
13	SC1_128pin	BCM	BCM_KeyIn	0-12(highside	AI	PXI 6289
14	SC1_128pin	MCU1	MCU1_KeyIn	0-12(highside	AI	PXI 6289
15	SC1_128pin	VEHICLE	IGN_Run	0-5V IGNswit	phys	PXI 6229
23	Physical	PHYSICAL	PHY_heartbeat	0-5V CTR	CTRO	PXI 6229
24	SC1_128pin	12V	VicorC_current	0-5V	AO	PXI 6723
25	SC1_128pin	VEHICLE	TPS_SensorB	0-5V	AO	PXI 6723
26	SC2_80pin	24V	V24_Sense	0-5V	AO	PXI 6723
27	SC1_128pin	VEHICLE	TPS_SensorA	0-5V	AO	PXI 6723
28	SC2_80pin	FUEL	H2_TankPressure	0-5V	AO	PXI 6723
29	SC2_80pin	FUEL	H2_FCPMSupplyPressure	0-5V	AO	PXI 6723
30	SC2_80pin	CONTROLLER	SC1_CAN1-	1.5 - 2.5 V	CAN	PXI 8461
31	SC2_80pin	VEHICLE	N/A	N/A	ground	Ground rail
32	SC2_80pin	SAFETY	Estop_Mon_Raw	+13.6V	test bench	Estop switch
33	SC2_80pin	FUEL	H2_TankTemp	0-5V	AO	PXI 6723
34	SC2_80pin	CONTROLLER	SC1_CAN2+	2.5 - 3.5 V	CAN	PXI 8461
35	SC2_80pin	CONTROLLER	SC1_CAN2-	1.5 - 2.5 V	CAN	PXI 8461
36	Physical	PHYSICAL	PHY_speed	0-5V CTR	CTRO	PXI 6229
16	SC1_128pin	VEHICLE	IGN_Start	0-5V IGNswit	phys	PXI 6229
17	SC1_128pin	VEHICLE	IGN_Acc	0-5V IGNswit	phys	PXI 6229
40	SC2_80pin	VEHICLE	N/A	+13.6V	power	12V power rail
41	SC2_80pin	VEHICLE	N/A	+13.6V	power	12V power rail
42	SC2_80pin	VEHICLE	Always_on	+5V	AI	PXI 6229
19	SC1_128pin	VEHICLE	Always_on	+5V	AI	PXI 6229
20	SC1_128pin	VEHICLE	Always_on	+5V	AI	PXI 6229
21	SC1_128pin	**NYIC**	**NYIC**	0-12	AI	PXI 6229
46	SC2_80pin	VEHICLE	N/A	N/A	ground	Ground rail
47	SC2_80pin	VEHICLE	N/A	N/A	ground	Ground rail
22	SC1_128pin	**NYIC**	**NYIC**	0-12	AI	PXI 6229
23	SC1_128pin	**NYIC**	**NYIC**	0-12	AI	PXI 6229
24	SC1_128pin	**NYIC**	**NYIC**	0-12	AI	PXI 6229
51	SC1_128pin	**NYIC**	**NYIC**	0-12	AI	PXI 6229
52	SC1_128pin	**NYIC**	**NYIC**	0-12	AI	PXI 6229
25	SC1_128pin	**NYIC**	**NYIC**	0-12	AI	PXI 6229
54	SC2_80pin	VEHICLE	N/A	+13.6V	power	12V power rail
55	SC1_128pin	VEHICLE	N/A	N/A	ground	Ground rail
56	SC2_80pin	VEHICLE	N/A	N/A	ground	Ground rail
57	SC1_128pin	VEHICLE	N/A	N/A	ground	Ground rail
58	SC1_128pin	**NYIC**	**NYIC**	N/A	AI	PXI 6229
59	SC1_128pin	DCDC	ActualDutyCycle_final_4096	LSD	AI	PXI 6229
	SC1_128pin	GUI	Serial +			
	SC1_128pin	GUI	Serial -			

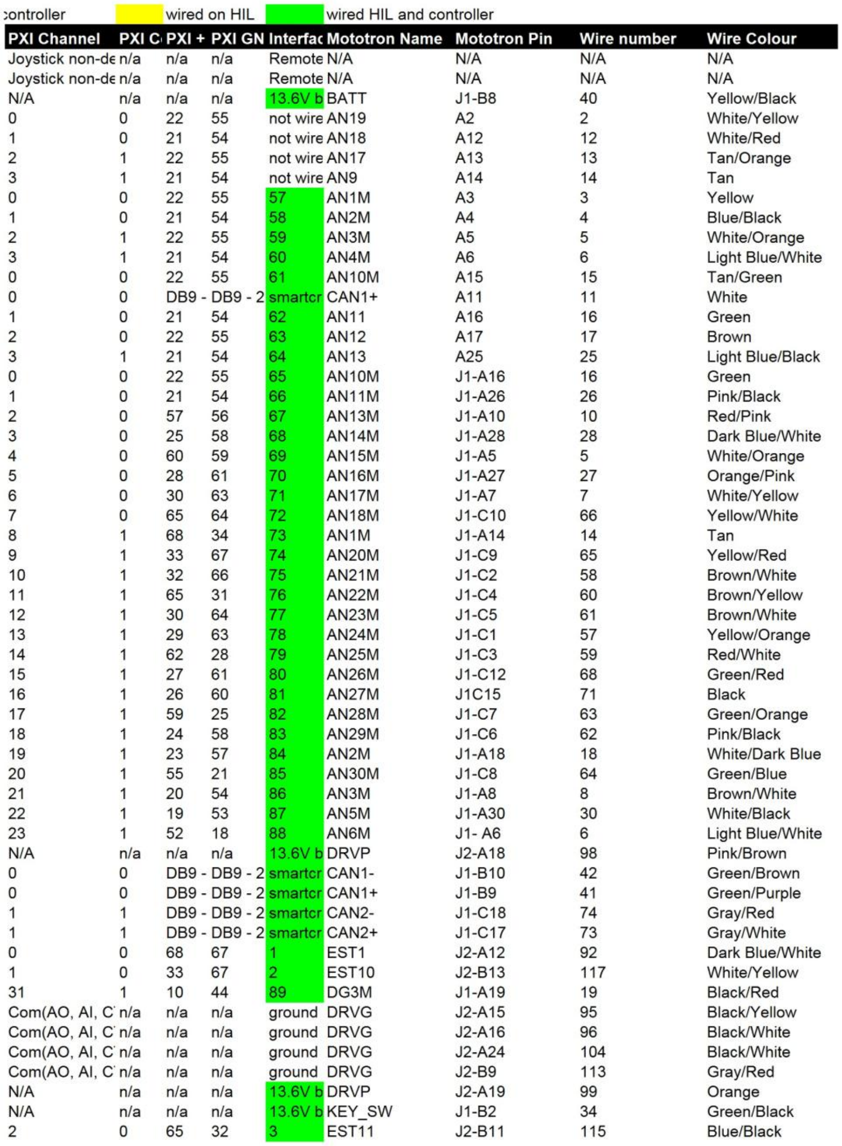

ontroller 🟨 wired on HIL 🟩 wired HIL and controller

PXI Channel	PXI C	PXI +	PXI GN	Interfac	Mototron Name	Mototron Pin	Wire number	Wire Colour
Joystick non-de	n/a	n/a	n/a	Remote	N/A	N/A	N/A	N/A
Joystick non-de	n/a	n/a	n/a	Remote	N/A	N/A	N/A	N/A
N/A	n/a	n/a	n/a	13.6V b	BATT	J1-B8	40	Yellow/Black
0	0	22	55	not wire	AN19	A2	2	White/Yellow
1	0	21	54	not wire	AN18	A12	12	White/Red
2	1	22	55	not wire	AN17	A13	13	Tan/Orange
3	1	21	54	not wire	AN9	A14	14	Tan
0	0	22	55	57	AN1M	A3	3	Yellow
1	0	21	54	58	AN2M	A4	4	Blue/Black
2	1	22	55	59	AN3M	A5	5	White/Orange
3	1	21	54	60	AN4M	A6	6	Light Blue/White
0	0	22	55	61	AN10M	A15	15	Tan/Green
0	0	DB9 - DB9 - 2		smartcr	CAN1+	A11	11	White
1	0	21	54	62	AN11	A16	16	Green
2	0	22	55	63	AN12	A17	17	Brown
3	1	21	54	64	AN13	A25	25	Light Blue/Black
0	0	22	55	65	AN10M	J1-A16	16	Green
1	0	21	54	66	AN11M	J1-A26	26	Pink/Black
2	0	57	56	67	AN13M	J1-A10	10	Red/Pink
3	0	25	58	68	AN14M	J1-A28	28	Dark Blue/White
4	0	60	59	69	AN15M	J1-A5	5	White/Orange
5	0	28	61	70	AN16M	J1-A27	27	Orange/Pink
6	0	30	63	71	AN17M	J1-A7	7	White/Yellow
7	0	65	64	72	AN18M	J1-C10	66	Yellow/White
8	1	68	34	73	AN1M	J1-A14	14	Tan
9	1	33	67	74	AN20M	J1-C9	65	Yellow/Red
10	1	32	66	75	AN21M	J1-C2	58	Brown/White
11	1	65	31	76	AN22M	J1-C4	60	Brown/Yellow
12	1	30	64	77	AN23M	J1-C5	61	Brown/White
13	1	29	63	78	AN24M	J1-C1	57	Yellow/Orange
14	1	62	28	79	AN25M	J1-C3	59	Red/White
15	1	27	61	80	AN26M	J1-C12	68	Green/Red
16	1	26	60	81	AN27M	J1C15	71	Black
17	1	59	25	82	AN28M	J1-C7	63	Green/Orange
18	1	24	58	83	AN29M	J1-C6	62	Pink/Black
19	1	23	57	84	AN2M	J1-A18	18	White/Dark Blue
20	1	55	21	85	AN30M	J1-C8	64	Green/Blue
21	1	20	54	86	AN3M	J1-A8	8	Brown/White
22	1	19	53	87	AN5M	J1-A30	30	White/Black
23	1	52	18	88	AN6M	J1- A6	6	Light Blue/White
N/A	n/a	n/a	n/a	13.6V b	DRVP	J2-A18	98	Pink/Brown
0	0	DB9 - DB9 - 2		smartcr	CAN1-	J1-B10	42	Green/Brown
0	0	DB9 - DB9 - 2		smartcr	CAN1+	J1-B9	41	Green/Purple
1	1	DB9 - DB9 - 2		smartcr	CAN2-	J1-C18	74	Gray/Red
1	1	DB9 - DB9 - 2		smartcr	CAN2+	J1-C17	73	Gray/White
0	0	68	67	1	EST1	J2-A12	92	Dark Blue/White
1	0	33	67	2	EST10	J2-B13	117	White/Yellow
31	1	10	44	89	DG3M	J1-A19	19	Black/Red
Com(AO, AI, C	n/a	n/a	n/a	ground	DRVG	J2-A15	95	Black/Yellow
Com(AO, AI, C	n/a	n/a	n/a	ground	DRVG	J2-A16	96	Black/White
Com(AO, AI, C	n/a	n/a	n/a	ground	DRVG	J2-A24	104	Black/White
Com(AO, AI, C	n/a	n/a	n/a	ground	DRVG	J2-B9	113	Gray/Red
N/A	n/a	n/a	n/a	13.6V b	DRVP	J2-A19	99	Orange
N/A	n/a	n/a	n/a	13.6V b	KEY_SW	J1-B2	34	Green/Black
2	0	65	32	3	EST11	J2-B11	115	Blue/Black

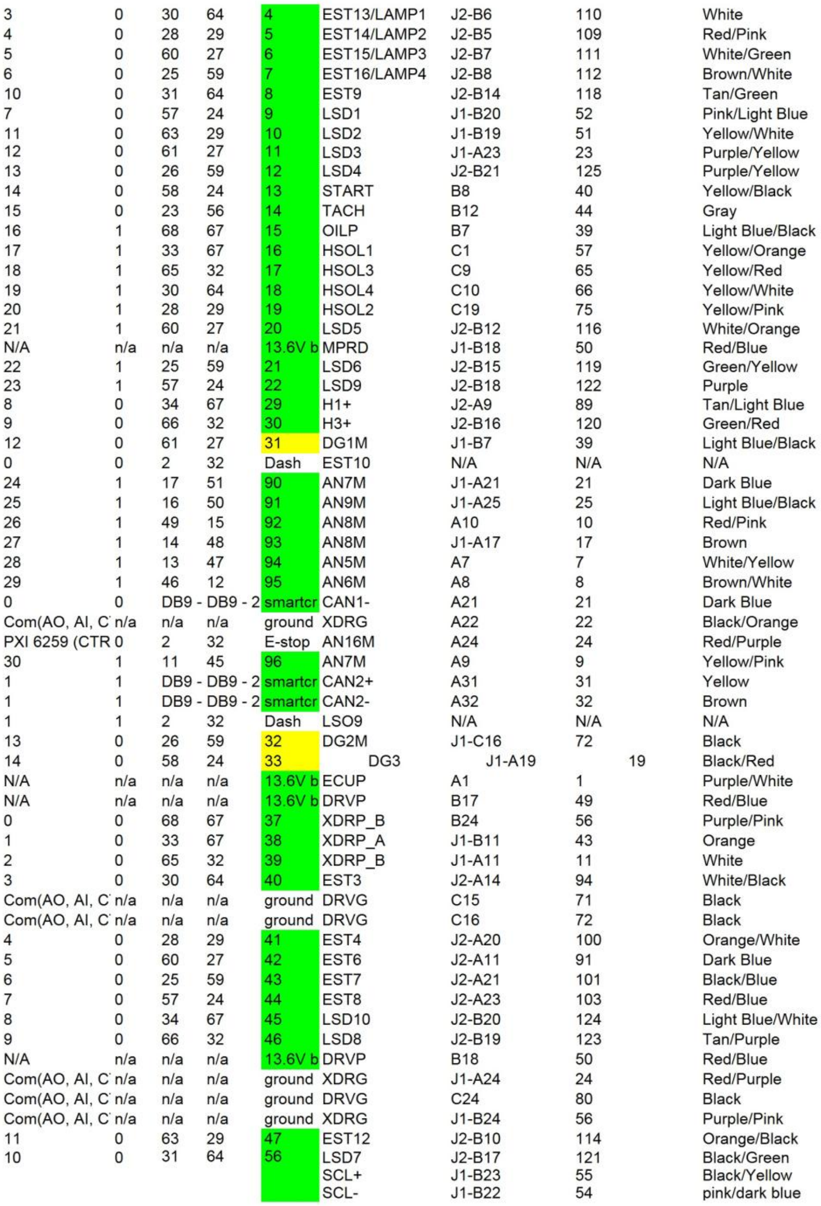

3	0	30	64	4	EST13/LAMP1	J2-B6	110	White
4	0	28	29	5	EST14/LAMP2	J2-B5	109	Red/Pink
5	0	60	27	6	EST15/LAMP3	J2-B7	111	White/Green
6	0	25	59	7	EST16/LAMP4	J2-B8	112	Brown/White
10	0	31	64	8	EST9	J2-B14	118	Tan/Green
7	0	57	24	9	LSD1	J1-B20	52	Pink/Light Blue
11	0	63	29	10	LSD2	J1-B19	51	Yellow/White
12	0	61	27	11	LSD3	J1-A23	23	Purple/Yellow
13	0	26	59	12	LSD4	J2-B21	125	Purple/Yellow
14	0	58	24	13	START	B8	40	Yellow/Black
15	0	23	56	14	TACH	B12	44	Gray
16	1	68	67	15	OILP	B7	39	Light Blue/Black
17	1	33	67	16	HSOL1	C1	57	Yellow/Orange
18	1	65	32	17	HSOL3	C9	65	Yellow/Red
19	1	30	64	18	HSOL4	C10	66	Yellow/White
20	1	28	29	19	HSOL2	C19	75	Yellow/Pink
21	1	60	27	20	LSD5	J2-B12	116	White/Orange
N/A	n/a	n/a	n/a	13.6V b	MPRD	J1-B18	50	Red/Blue
22	1	25	59	21	LSD6	J2-B15	119	Green/Yellow
23	1	57	24	22	LSD9	J2-B18	122	Purple
8	0	34	67	29	H1+	J2-A9	89	Tan/Light Blue
9	0	66	32	30	H3+	J2-B16	120	Green/Red
12	0	61	27	31	DG1M	J1-B7	39	Light Blue/Black
0	0	2	32	Dash	EST10	N/A	N/A	N/A
24	1	17	51	90	AN7M	J1-A21	21	Dark Blue
25	1	16	50	91	AN9M	J1-A25	25	Light Blue/Black
26	1	49	15	92	AN8M	A10	10	Red/Pink
27	1	14	48	93	AN8M	J1-A17	17	Brown
28	1	13	47	94	AN5M	A7	7	White/Yellow
29	1	46	12	95	AN6M	A8	8	Brown/White
0	0	DB9 -	DB9 - 2	smartcr	CAN1-	A21	21	Dark Blue
Com(AO, AI, C	n/a	n/a	n/a	ground	XDRG	A22	22	Black/Orange
PXI 6259 (CTR	0	2	32	E-stop	AN16M	A24	24	Red/Purple
30	1	11	45	96	AN7M	A9	9	Yellow/Pink
1	1	DB9 -	DB9 - 2	smartcr	CAN2+	A31	31	Yellow
1	1	DB9 -	DB9 - 2	smartcr	CAN2-	A32	32	Brown
1	1	2	32	Dash	LSO9	N/A	N/A	N/A
13	0	26	59	32	DG2M	J1-C16	72	Black
14	0	58	24	33	DG3	J1-A19	19	Black/Red
N/A	n/a	n/a	n/a	13.6V b	ECUP	A1	1	Purple/White
N/A	n/a	n/a	n/a	13.6V b	DRVP	B17	49	Red/Blue
0	0	68	67	37	XDRP_B	B24	56	Purple/Pink
1	0	33	67	38	XDRP_A	J1-B11	43	Orange
2	0	65	32	39	XDRP_B	J1-A11	11	White
3	0	30	64	40	EST3	J2-A14	94	White/Black
Com(AO, AI, C	n/a	n/a	n/a	ground	DRVG	C15	71	Black
Com(AO, AI, C	n/a	n/a	n/a	ground	DRVG	C16	72	Black
4	0	28	29	41	EST4	J2-A20	100	Orange/White
5	0	60	27	42	EST6	J2-A11	91	Dark Blue
6	0	25	59	43	EST7	J2-A21	101	Black/Blue
7	0	57	24	44	EST8	J2-A23	103	Red/Blue
8	0	34	67	45	LSD10	J2-B20	124	Light Blue/White
9	0	66	32	46	LSD8	J2-B19	123	Tan/Purple
N/A	n/a	n/a	n/a	13.6V b	DRVP	B18	50	Red/Blue
Com(AO, AI, C	n/a	n/a	n/a	ground	XDRG	J1-A24	24	Red/Purple
Com(AO, AI, C	n/a	n/a	n/a	ground	DRVG	C24	80	Black
Com(AO, AI, C	n/a	n/a	n/a	ground	XDRG	J1-B24	56	Purple/Pink
11	0	63	29	47	EST12	J2-B10	114	Orange/Black
10	0	31	64	56	LSD7	J2-B17	121	Black/Green
					SCL+	J1-B23	55	Black/Yellow
					SCL-	J1-B22	54	pink/dark blue

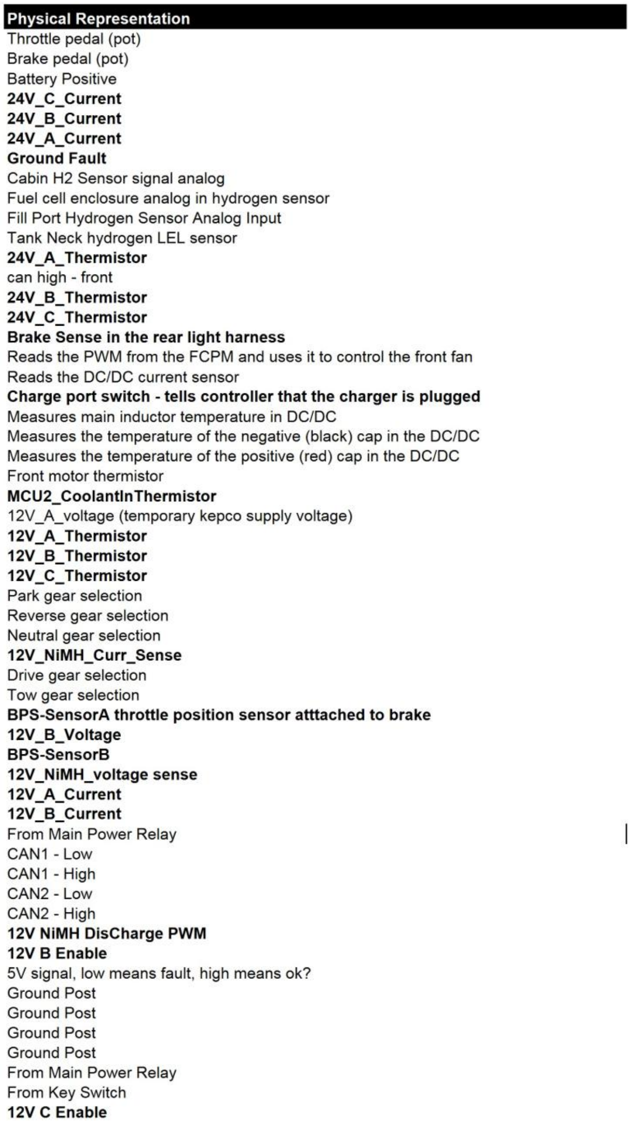

Physical Representation
Throttle pedal (pot)
Brake pedal (pot)
Battery Positive
24V_C_Current
24V_B_Current
24V_A_Current
Ground Fault
Cabin H2 Sensor signal analog
Fuel cell enclosure analog in hydrogen sensor
Fill Port Hydrogen Sensor Analog Input
Tank Neck hydrogen LEL sensor
24V_A_Thermistor
can high - front
24V_B_Thermistor
24V_C_Thermistor
Brake Sense in the rear light harness
Reads the PWM from the FCPM and uses it to control the front fan
Reads the DC/DC current sensor
Charge port switch - tells controller that the charger is plugged
Measures main inductor temperature in DC/DC
Measures the temperature of the negative (black) cap in the DC/DC
Measures the temperature of the positive (red) cap in the DC/DC
Front motor thermistor
MCU2_CoolantInThermistor
12V_A_voltage (temporary kepco supply voltage)
12V_A_Thermistor
12V_B_Thermistor
12V_C_Thermistor
Park gear selection
Reverse gear selection
Neutral gear selection
12V_NiMH_Curr_Sense
Drive gear selection
Tow gear selection
BPS-SensorA throttle position sensor atttached to brake
12V_B_Voltage
BPS-SensorB
12V_NiMH_voltage sense
12V_A_Current
12V_B_Current
From Main Power Relay
CAN1 - Low
CAN1 - High
CAN2 - Low
CAN2 - High
12V NiMH DisCharge PWM
12V B Enable
5V signal, low means fault, high means ok?
Ground Post
Ground Post
Ground Post
Ground Post
From Main Power Relay
From Key Switch
12V C Enable

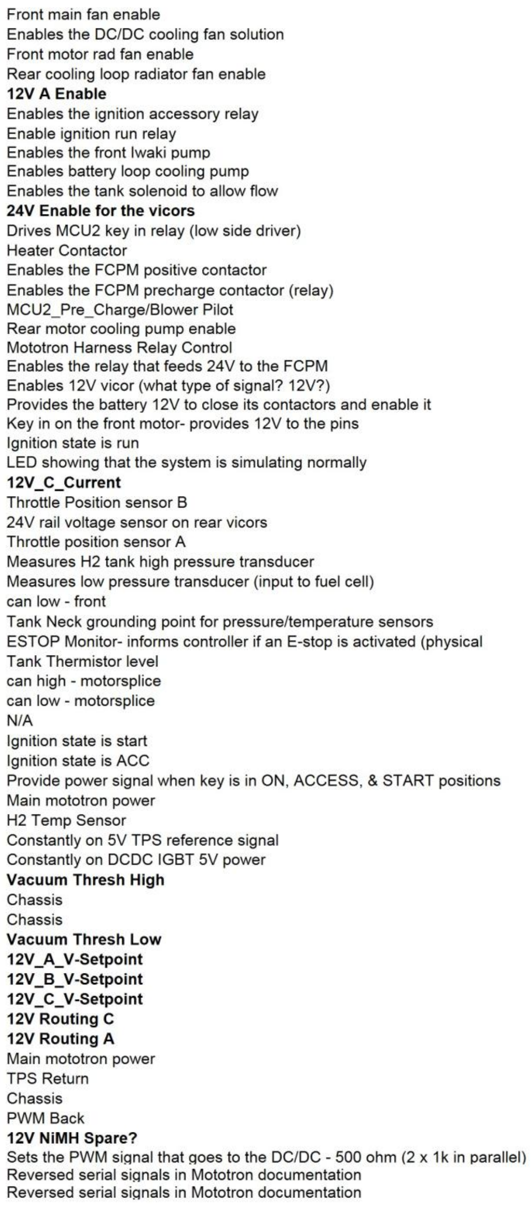

Front main fan enable

Enables the DC/DC cooling fan solution

Front motor rad fan enable

Rear cooling loop radiator fan enable

12V A Enable

Enables the ignition accessory relay

Enable ignition run relay

Enables the front Iwaki pump

Enables battery loop cooling pump

Enables the tank solenoid to allow flow

24V Enable for the vicors

Drives MCU2 key in relay (low side driver)

Heater Contactor

Enables the FCPM positive contactor

Enables the FCPM precharge contactor (relay)

MCU2_Pre_Charge/Blower Pilot

Rear motor cooling pump enable

Mototron Harness Relay Control

Enables the relay that feeds 24V to the FCPM

Enables 12V vicor (what type of signal? 12V?)

Provides the battery 12V to close its contactors and enable it

Key in on the front motor- provides 12V to the pins

Ignition state is run

LED showing that the system is simulating normally

12V_C_Current

Throttle Position sensor B

24V rail voltage sensor on rear vicors

Throttle position sensor A

Measures H2 tank high pressure transducer

Measures low pressure transducer (input to fuel cell)

can low - front

Tank Neck grounding point for pressure/temperature sensors

ESTOP Monitor- informs controller if an E-stop is activated (physical

Tank Thermistor level

can high - motorsplice

can low - motorsplice

N/A

Ignition state is start

Ignition state is ACC

Provide power signal when key is in ON, ACCESS, & START positions

Main mototron power

H2 Temp Sensor

Constantly on 5V TPS reference signal

Constantly on DCDC IGBT 5V power

Vacuum Thresh High

Chassis

Chassis

Vacuum Thresh Low

12V_A_V-Setpoint

12V_B_V-Setpoint

12V_C_V-Setpoint

12V Routing C

12V Routing A

Main mototron power

TPS Return

Chassis

PWM Back

12V NiMH Spare?

Sets the PWM signal that goes to the DC/DC - 500 ohm (2 x 1k in parallel)

Reversed serial signals in Mototron documentation

Reversed serial signals in Mototron documentation

Appendix C: Simulation Interface Toolkit Code

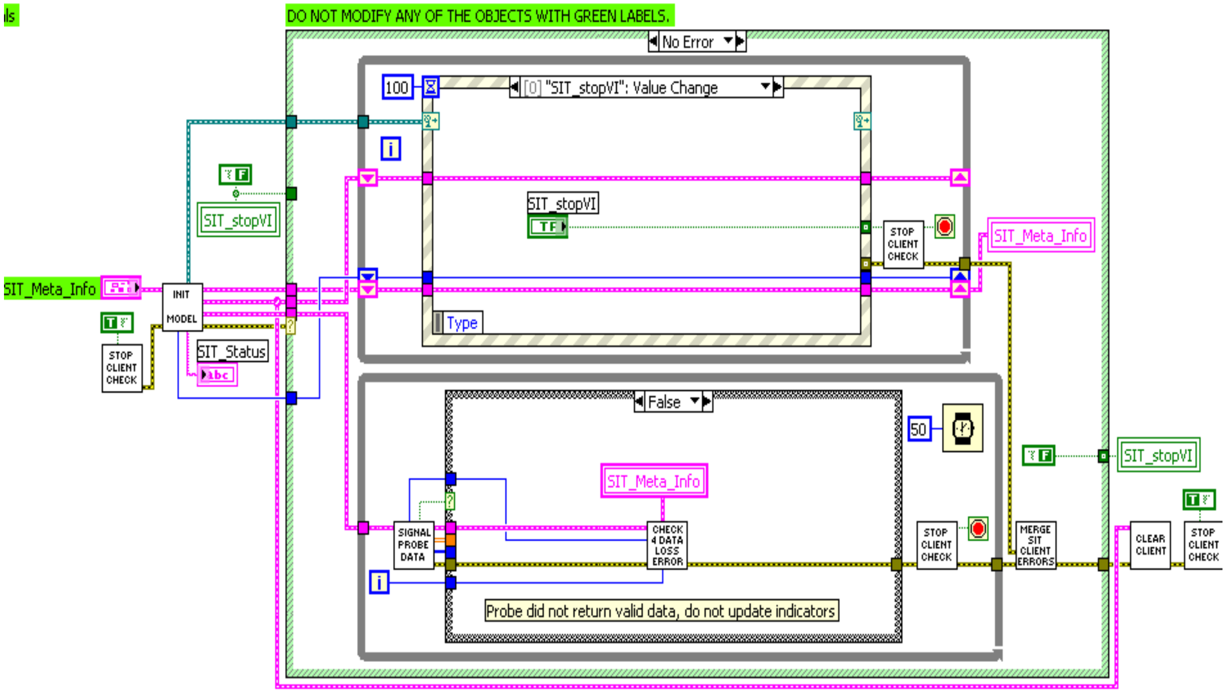

Figure C1: Host VI

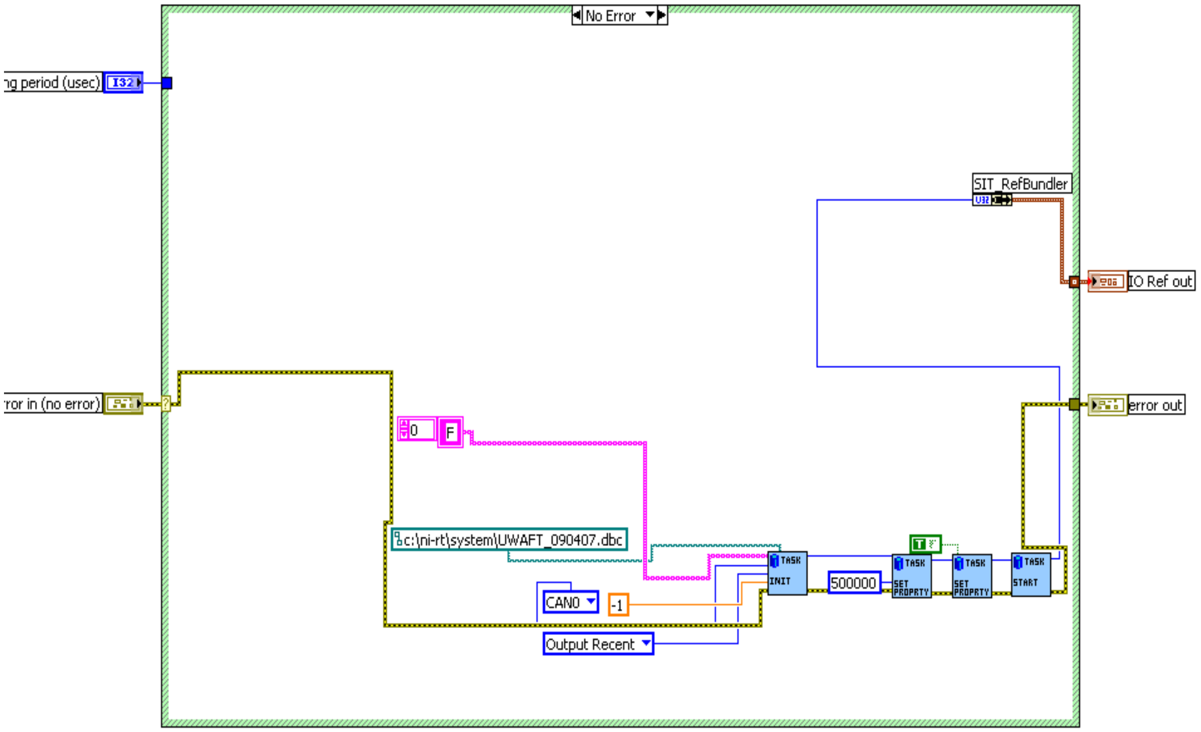

Figure C2: SIT CAN initialize VI – note setting baud rate to 500 kbps.

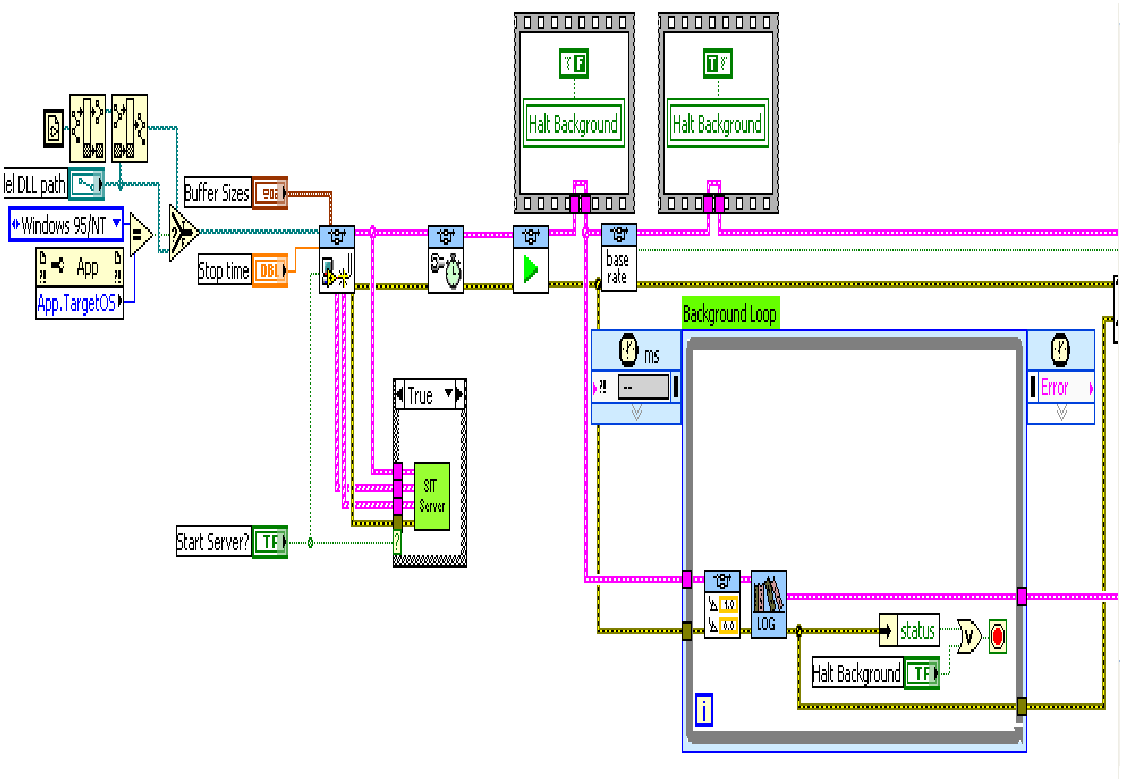

Figure C3: SIT CAN driver VI – note base rate subVI where all IO actions take place

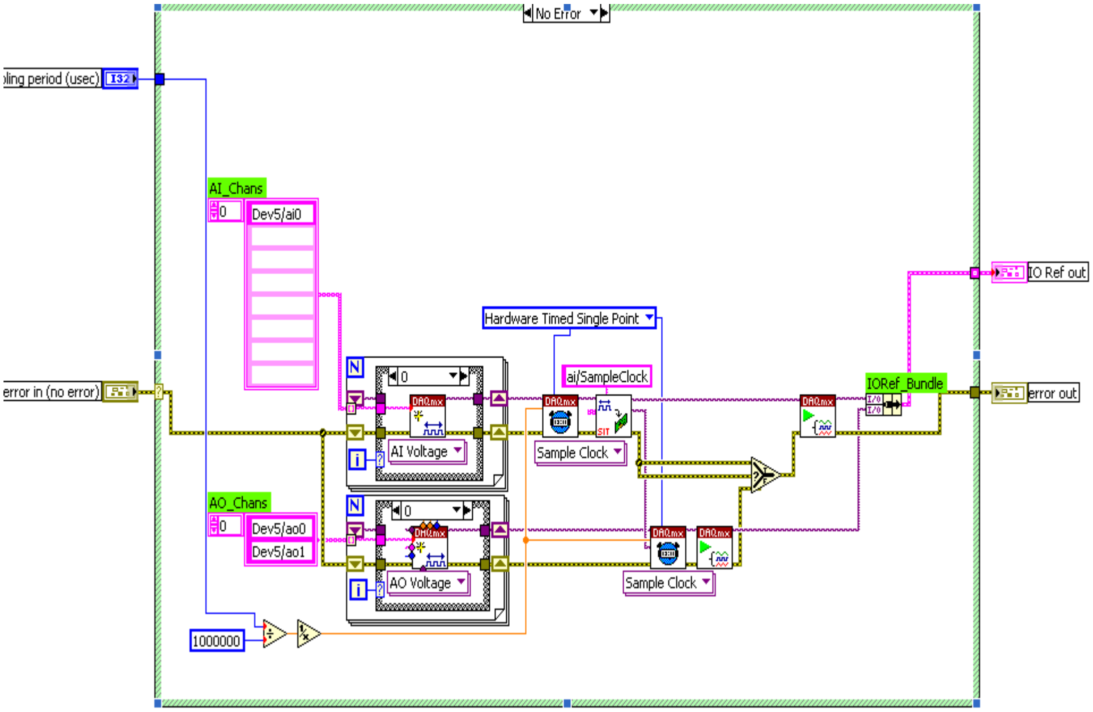

Figure C4: SIT DAQ initialize channel VI – note that even for only performing AO operation AI is defined

Appendix D: Real Time Workshop Code

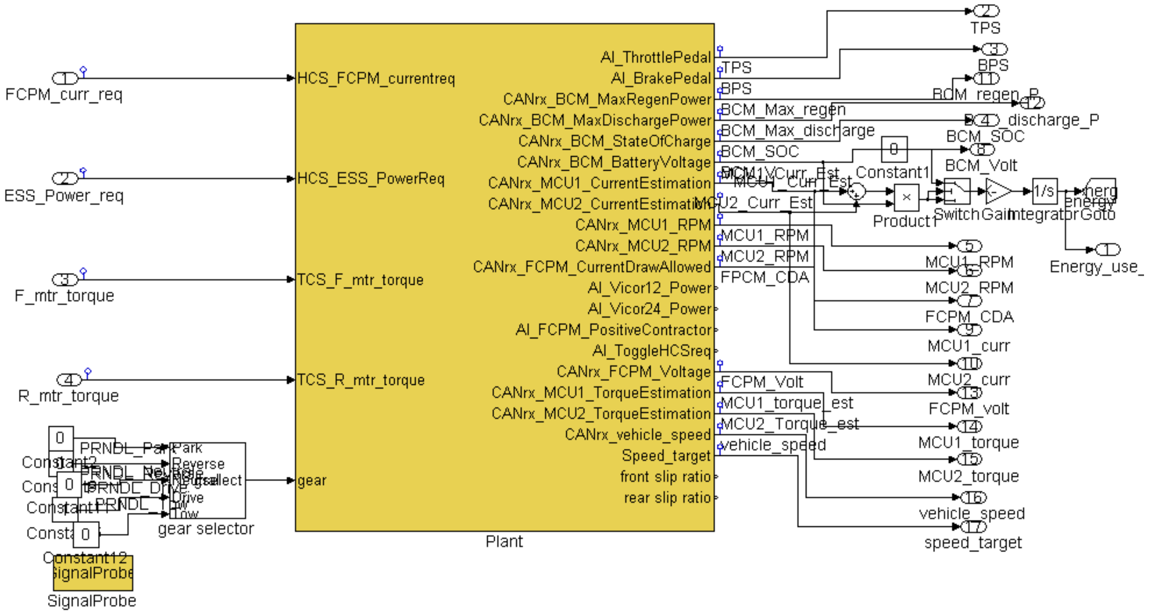

Figure D1: PXI HCS test code – note the signal probe for the NI .dll compiler

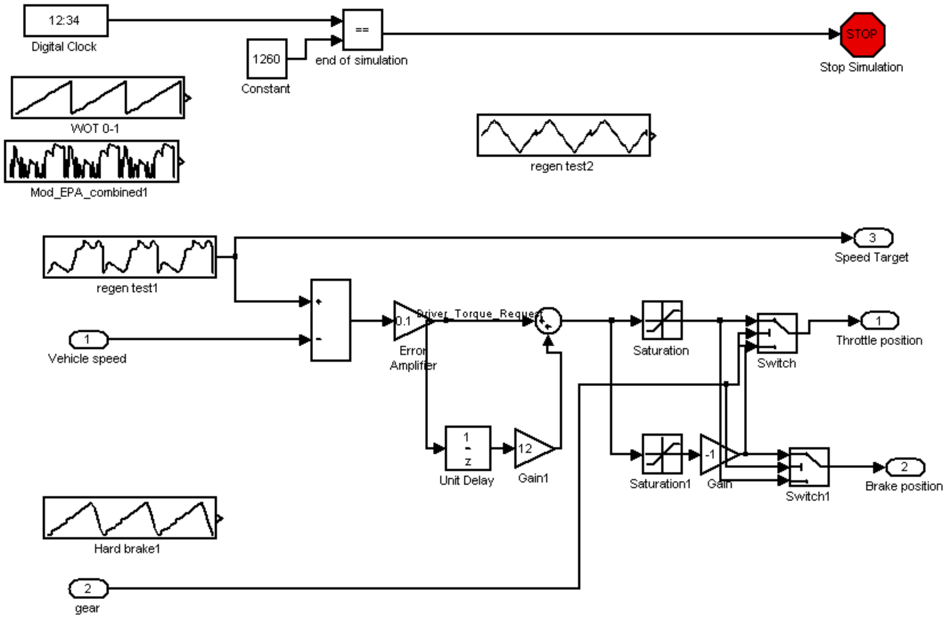

Figure D2: Drive cycle input- speed in m/s into a repeating sequence block. Stop simulation when one sequence has been completed

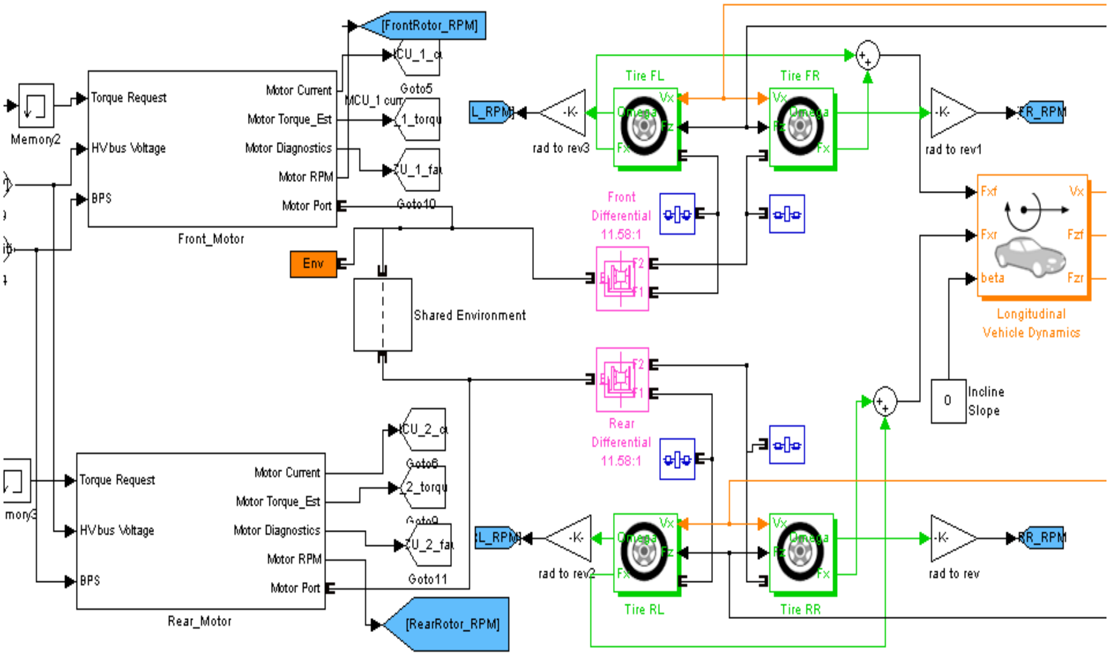

Figure D3: Dynamic plant model – note simdriveline based dynamic performance

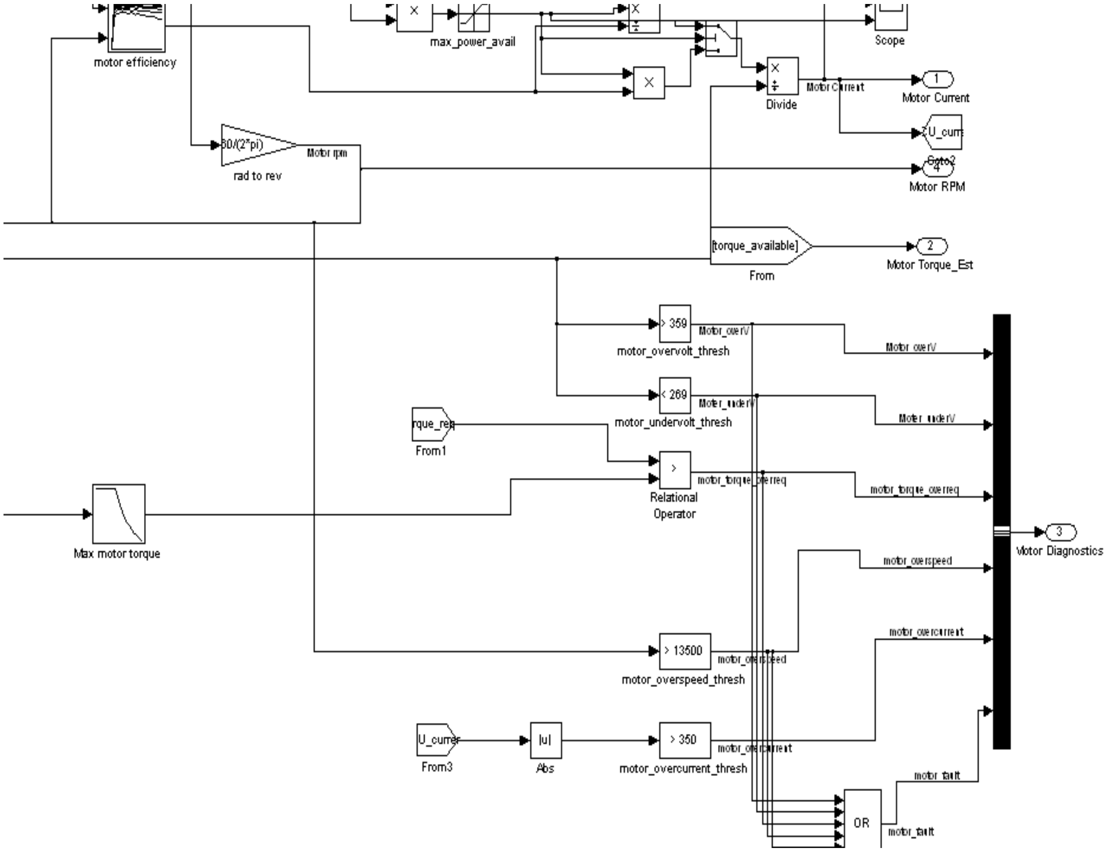

Figure D4: Motor plant model – note motor diagnostics and efficiency/torque inputs

Appendix E: Java code for Blackberry Interface

Filip Spacek 2007. Original Java code written in JDE.

```
package com.rim.samples.device.bluetoothsample;

import net.rim.device.api.bluetooth.*;
import net.rim.device.api.system.*;
import net.rim.device.api.util.*;
import net.rim.device.api.ui.container.*;
import net.rim.device.api.ui.*;
import net.rim.device.api.ui.component.*;
import java.io.*;
import java.util.*;

public class CANBluetoothGUI extends UiApplication //implements TrackwheelListener
{
    private BluetoothSerialPortInfo[] m_portInfo;
    private MainScreen m_portScreen;
    private MenuItem m_closeItem;
    private CANConnection m_can;
    private LabelField m_debug;

    public static void main(String[] args)
    {
        CANBluetoothGUI app = new CANBluetoothGUI();
        app.enterEventDispatcher();
    }

    private CANBluetoothGUI()
    {
        String menuTitle;
        m_portScreen = new MainScreen();
        m_portScreen.setTitle(new LabelField("CAN Bluetooth, yes we can."));

        if (BluetoothSerialPort.isSupported()) {
            m_portInfo = BluetoothSerialPort.getSerialPortInfo();
            for (int i = 0; i < m_portInfo.length; ++i) {
                m_portScreen.add(new ButtonField(m_portInfo[i].getDeviceName()) {
                    public boolean trackwheelClick(int status, int time) {
                        openConnection(getLabel());
                        return true;
                    }
                });
            }
        }
        else {
            final String[] names = { "FOO", "BAR" };
            for (int i = 0; i < 2; ++i) {
                m_portScreen.add(new ButtonField(names[i]) {
                    public boolean trackwheelClick(int status, int time) {
                        //System.out.println("clicked");
                        openConnection("bogus");
                        return true;
                    }
                });
            }
        }

        m_closeItem = new MenuItem("Close", 200000, 10) {
            public void run() {
                System.exit(0);
            }
        };

        pushScreen(m_portScreen);
    }

    protected void makeMenu(Menu menu, int instance)
    {
        menu.add(m_closeItem.toString(), m_closeItem, Menu.UNDEFINED);
    }

    protected void openConnection(String uri) {
        BluetoothSerialPortInfo port = null;
        for (int i = 0; i < m_portInfo.length; ++i) {
            if (m_portInfo[i].getDeviceName().equals(uri)) {
                port = m_portInfo[i];
                break;
            }
        }

        m_can = new CANConnection(port);
    }

    static class AwesomoGauge extends Field implements DrawStyle {
        private static final int WIDTH = 320;//120;
        private static final int HEIGHT = 30;//80;
        private String m_label;
        public int m_value;
        public int m_id;

        public AwesomoGauge(String label, int id) {
            m_label = label;
            m_id = id;
        }
        public int getPreferredWidth() {
            return WIDTH;
        }
        public int getPreferredHeight() {
            return HEIGHT;
        }

        protected void layout(int width, int height) {
            width = Math.min( width, getPreferredWidth() );
            height = Math.min( height, getPreferredHeight() );
            setExtent( width, height );
        }
        protected void paint(Graphics graphics) {
            //graphics.drawArc(0, 0, getWidth(), getHeight(), 0, 360);
            //graphics.drawRect(0, 0, getWidth(), getHeight());
            graphics.drawText(m_label + " " + Integer.toString(m_id) + " " +
                              Integer.toString(m_value), 10, 10);
        }
    }

    class CANConnection implements BluetoothSerialPortListener
    {
        private BluetoothSerialPort m_port;
        private String m_deviceName;

        private MainScreen m_gaugesScreen;
        private FlowFieldManager m_gaugesManager;
        private Vector m_gauges;

        public CANConnection(BluetoothSerialPortInfo info)
        {
            try {
                m_port = new BluetoothSerialPort(info, BluetoothSerialPort.BAUD_115200,
BluetoothSerialPort.DATA_FORMAT_PARITY_NONE | BluetoothSerialPort.DATA_FORMAT_STOP_BITS_1 |
BluetoothSerialPort.DATA_FORMAT_DATA_BITS_8, BluetoothSerialPort.FLOW_CONTROL_NONE, 1024, 1024, this);
                m_deviceName = info.getDeviceName();
            }
            catch(IOException ex) {
                Status.show("Error: " + ex.getMessage());
            }

            m_gaugesScreen = new MainScreen() {
                protected void makeMenu(Menu menu, int instance) {
                    menu.add(m_closeItem.toString(), m_closeItem, Menu.UNDEFINED);
        }
    };
    m_gauges = new Vector();
    m_gaugesScreen.setTitle(new LabelField(info.getDeviceName()));
    m_gaugesManager = new FlowFieldManager();
    m_gaugesScreen.add(m_gaugesManager);

    pushScreen(m_gaugesScreen);

    Runnable refreshGauges = new Runnable() {
        public void run() {
            m_gaugesManager.invalidate();
        }
    };
    invokeLater(refreshGauges, 20, true);
}

public void deviceConnected(boolean success)
{
    if (success)
        Status.show("YES");
    else
        Status.show("NO");
}

public void deviceDisconnected()
{
    Status.show("Disconnected from " + m_deviceName);
}

public void dtrStateChange(boolean high)
{
    Status.show("DTR: " + high);
}



private static final int NO_SYNC_YET = 0;
private static final int SAW_SYNC = 1;
private static final int READING_DATA = 2;
private static final int READING_CHECKSUM = 3;
private static final int READING_EOF = 4;
private int m_state;
private int m_rawPos;
private byte[] m_raw;

public void dataReceived(int length)
{
    try {
        for (int i = 0; i < length; ++i) {
            int data = m_port.read();
            switch (m_state) {
            case NO_SYNC_YET:
                if (data == 0x43) {
                    m_state = SAW_SYNC;
                }
                break;
            case SAW_SYNC:
                m_raw = new byte[data];
                m_rawPos = 0;
                m_state = READING_DATA;
                break;
            case READING_DATA:
                m_raw[m_rawPos] = (byte)data;
                ++m_rawPos;
                if (m_rawPos >= m_raw.length) {
                    parseMessage();
                    m_state = READING_CHECKSUM;
                }
                break;
            case READING_CHECKSUM:
                m_state = READING_EOF;
                break;
            case READING_EOF:
                m_state = NO_SYNC_YET;
                break;
            }
        }
    } catch(IOException ioex) {
        //Catch and re-throw the exception.
        throw new RuntimeException(ioex.toString());
    }
}

void parseMessage()
{
    if (m_raw[0] != 0x01) {
        Status.show("Unknown message type " + Integer.toString(m_raw[0], 16));
        return;
    }

    int id = (m_raw[1] << 8) | m_raw[2];
    //Status.show("ID " + Integer.toString(id, 16));
    AwesomoGauge gauge = null;
    for (int i = 0; i < m_gauges.size(); ++i) {
```

```
                AwesomoGauge ith_gauge = (AwesomoGauge)m_gauges.elementAt(i);
                if (ith_gauge.m_id == id) {
                    gauge = ith_gauge;
                }
            }
            if (gauge == null) {
                gauge = new AwesomoGauge("Gauge ", id);
                m_gauges.addElement(gauge);
                synchronized (getEventLock()) {
                    m_gaugesManager.add(gauge);
                }
            }
            gauge.m_value = m_raw[4];
        }

        public void dataSent()
        {
        }
    }
}
```

Appendix F: Expanded Pictures

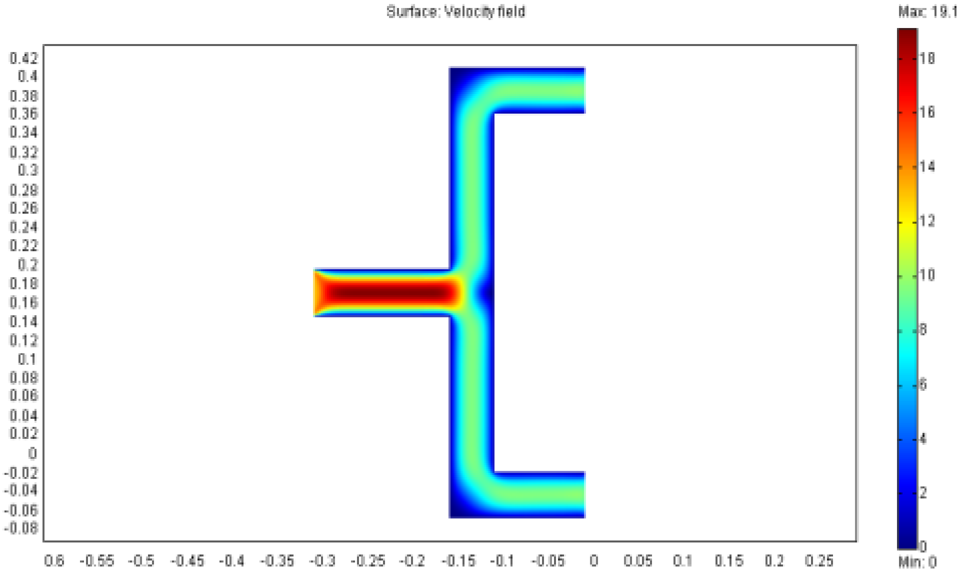

F1: Equal length fuel cell air feed results in 1:1 distribution

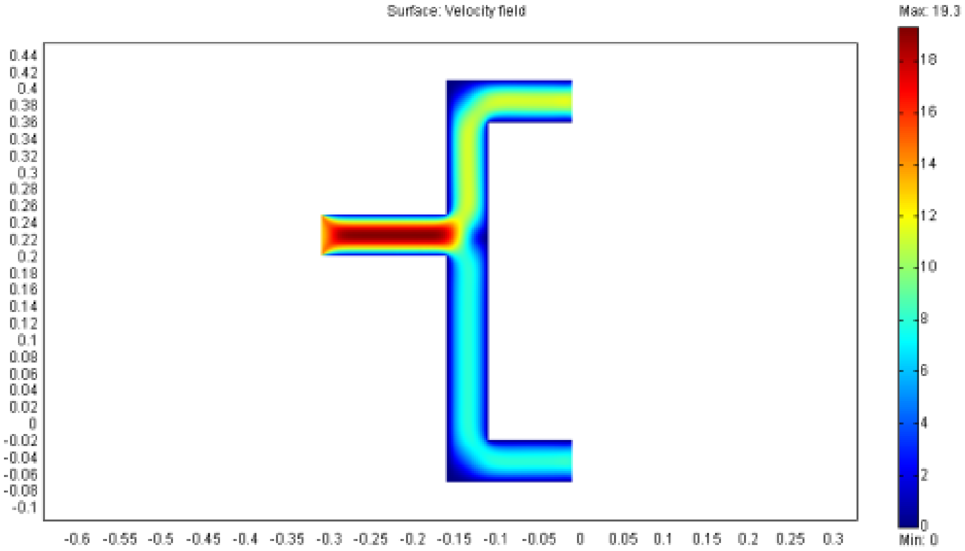

F2: Actual implemented fuel cell air feed results in 1:0.82 distribution

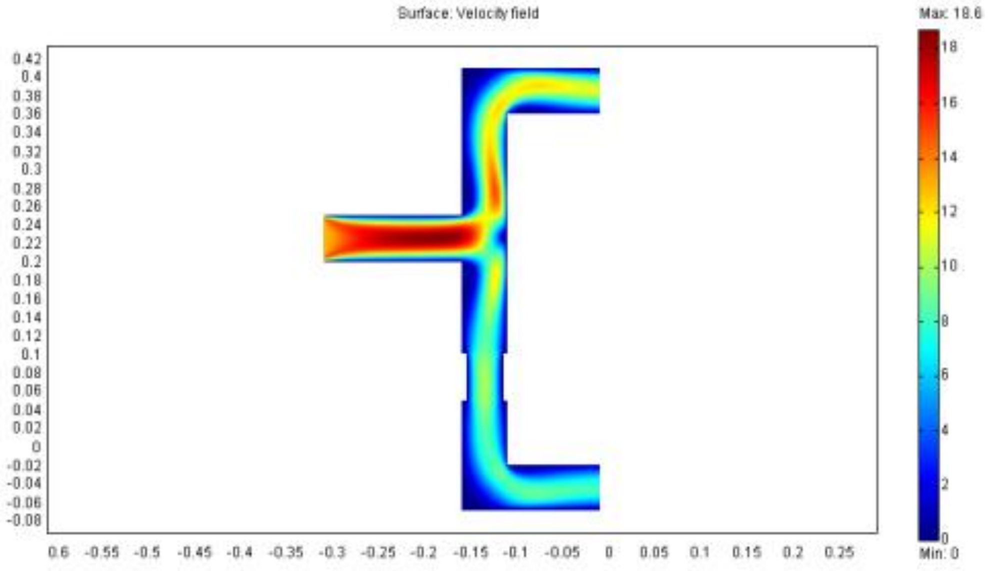

F3: Imposed constriction in air feed results in 1:0.69 distribution

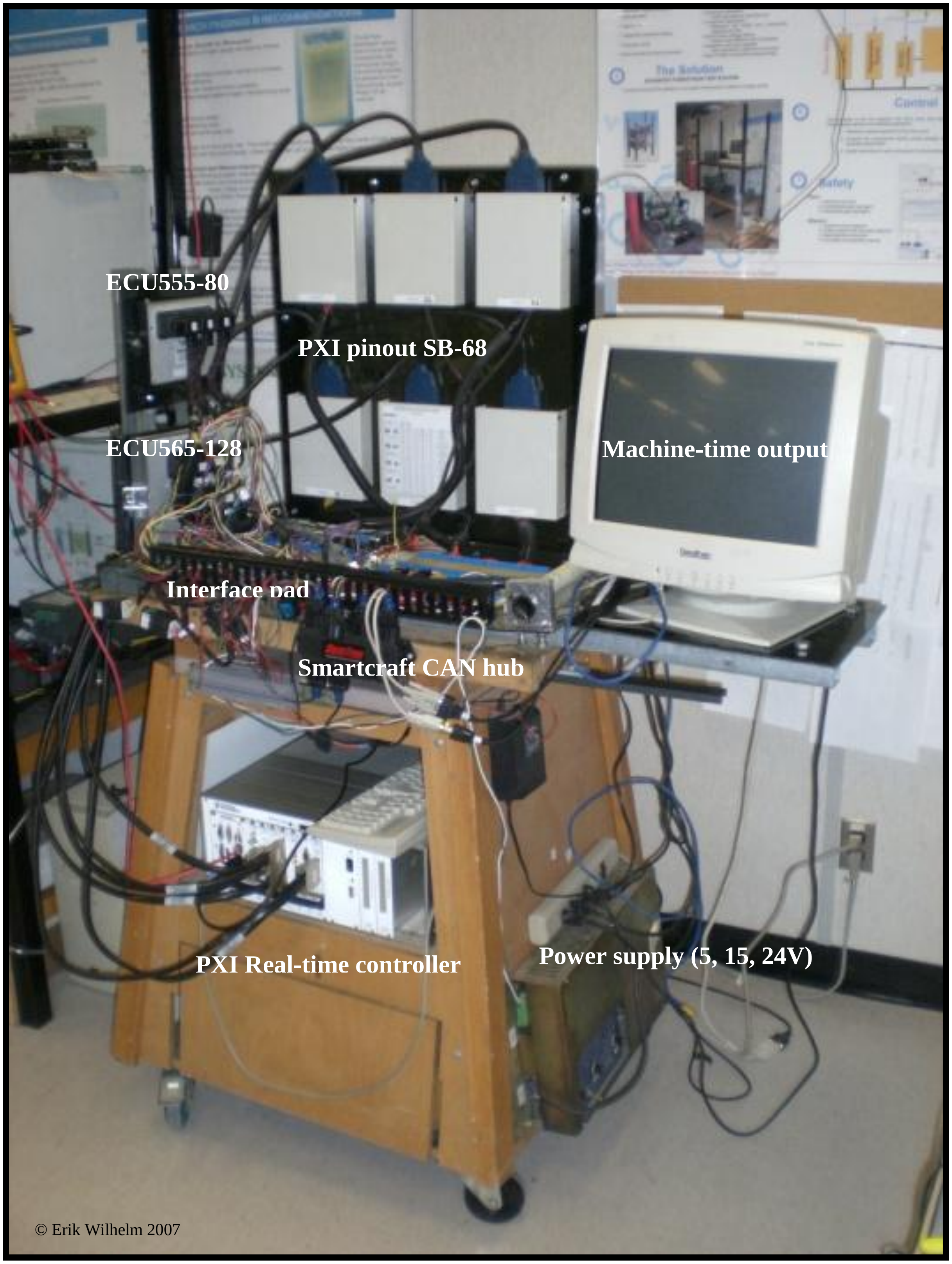

F4: Hardware in the loop simulation system

Appendix G: Scientific contributions

- Refereed Publications

Wilhelm, E., Fowler, M. 2006. "A Technical and Economic Review of Solar Hydrogen Production Technologies". Bulletin of Science Technology and Society. Vol. 26, No. 1, 278-287

- Non-refereed Publications

E. Wilhelm, M. Wahlstrom, M.B. Stevens, C. Mendes, C. Lawrence, D. Sellan, C. Haliburton, Dr. M.W. Fowler, Dr. R.A. Fraser. 2007 "Implementation and Optimization of a Fuel Cell Hybrid Powertrain" SAE World Congress 2007. 07PFL-748.

T.J. Mali, J. Marshall, M.B. Stevens, C. Mendes, D.M. Shilling, K. Tong, **E. Wilhelm**, S. Beckermann, R.A. Fraser, M.W. Fowler 2006. "Fuel Cell Hybrid Powertrain Design Approach for a 2005 Chevrolet Equinox" SAE World Congress 2006. 2006-01-0744

- Selected Presentations

Wilhelm, E., Fowler, M.W. 2007. "A Hardware-in-the-loop Simulation System for Fuel Cell Vehicle Control" Graduate Studies Research Conference, University of Waterloo. April 28th, 2007.

Wilhelm,E., Stevens, M. Mendes,C. Wahlstrom, M. Sellan, D. Marshall, J. Fowler, M. Fraser, R. 2006.„Design Review of a Fuel Cell Hybrid Vehicle for the ChallengeX competition" Conference Proceedings: 2nd International Green Energy Conference. IGEC2-129